NTNU

Norwegian University of
Science and Technology

Modelling Phase Equilibria of CO_2 Hydrates in Aqueous Solutions of Tetrabutylammonium Bromide

Linda Claire Undall

Petroleum Geoscience and Engineering
Submission date: June 2017
Supervisor: Roar Larsen, IGP

Norwegian University of Science and Technology
Department of Geoscience and Petroleum

Preface

This thesis, "Modelling Phase Equilibria of CO_2 Hydrates in Aqueous Solutions of Tetrabutylammonium Bromide", is written as part of the Master of Science degree, Petroleum Geosciences and Engineering at NTNU, during the spring semester of 2017.

The idea for the topic of the thesis was brought up during research of potential hydrate applications, such as hydrate based desalination, which was studied in the specialization project Undall (2016). There are few available hydrate promoter models known to us, encouraging modelling efforts.

Trondheim, 11.06.17

Linda C. Undall

Acknowledgment

I would like to thank my supervisor, Professor Roar Larsen, Norwegian University of Science and Technology, for helpful suggestions, guidance and feedback, throughout the completion of this master thesis.

L.C.U.

Abstract

The oil and gas industry's increased focus on efficiency in recent times, encourages development of new technologies. Technologies such as; hydrate based desalination, hydrate based gas capture, hydrate based gas transport and hydrate based gas storage, are proposed to have the potential to reduce costs and improve safety, compared to conventional alternatives. Hydrate phase equilibria models for hydrate promoters (additives that promote hydrate formation) are believed to be a useful tool for hydrate based technologies. There are few available hydrate promoter models known to us. Development of hydrate inhibitor models have had great success for their use, and it is believed that the development of hydrate promoter models may have the same.

A model for phase equilibria of CO_2 hydrates in aqueous solutions of tetrabutylammonium bromide (TBAB) has been developed. TBAB is a hydrate promoter. Experimental CO_2/ TBAB hydrate phase equilibria data and CSMGem simulation data for pure CO_2, were the basis for modelling. The starting point was the hypothesis that CO_2/ TBAB phase equilibria is a horizontal shift of CO_2 phase equilibria. This resulted in the development of Model 1. Model 1 is implicit and inaccurate, meaning that a horizontal shift is not a valid approximation. Further modelling resulted in an explicit model, Model 2, which modelled a more complex shift by expressing the promotion temperature (ΔT) as a function of temperature and TBAB concentration. The accuracy of Model 2 was satisfactory. With the development of Model 2 the aim of this master thesis had been reached. The developed models and experimental data show that maximum promotion effect occurs at 25 weight% TBAB, and not at the concentration corresponding to maximum cavity occupation ($\approx$40 weight% TBAB).

Model 2, an explicit model for CO_2/ TBAB hydrate phase equilibria, may be seen as a small step towards commercialization of hydrate based technologies. Development of phase equilibria models for other hydrate promoters, and later software, is strongly encouraged.

Sammendrag

Det økende fokuset på effektivisering i olje- og gassindustrien, oppfordrer til utvikling av ny teknologi. Eksempelvis; hydratbasert avsalting, hydratbasert gassfangst, hydratbasert gasstransport og hydratbasert gasslagring. Hydrat-teknologi kan blant annet senke kostnader og øke sikkerhet, i forhold til konvensjonelle alternativer.

En hydratpromotør er et stoff som fremmer hydratdannelse, og dermed kan anvendes i hydratbaserte teknologier. Det finnes svært få hydratpromotørmodeller, til forskjell fra de mer kjente inhibitormodellene. Arbeidet med denne masteroppgaven har resultert i en faselikevektsmodell for hydrater av CO_2 i vandige løsninger av tetrabutylammonium bromid (TBAB). TBAB er en hydratpromotør. Utgangspunktet for modelleringen var en hypotese om at CO_2/ TBAB faselikevekt er en horisontal forskyvning av CO_2 faselikevekt, noe som førte til en implisitt modell (Modell 1). Nøyaktigheten av den implisitte modellen er ikke tilstrekkelig, den klarer ikke å modellere både CO_2 and CO_2/ TBAB faselikevekt. Videre arbeid resulterte i en eksplisitt modell (Modell 2), med økt nøyaktighet. Modell 2 modellerer en mer kompleks forskyvning ved å utrykke promoteringstemperaturen (ΔT) som en funksjon av temperatur og TBAB konsentrasjon. Eksperimentelldata og modellene viser at maksimal promoteringeffekt er ved 25 vekt% TBAB, noe som er lavere enn konsentrasjonen som fører til maksimal hullromsfylling ($\approx$40 vekt%).

Den eksplisitte modellen for CO_2/ TBAB faselikevekt, Model 2, kan sees på som et lite steg mot kommersialisering av hydratbaserte teknologier. Utvikling av faselikevekt modeller for andre hydrat promotører, og senere programmer, oppfordres på det sterkeste.

Contents

List of Equations

Chapter 1

Introduction

"Natural gas hydrates are usually considered as possible nuisances in the development of oil and gas fields, mainly in deep-water drilling operations and if multiphase transport technologies are to be examined." (Lachet and Béhar, 2000). The upstream and downstream oil and gas industry has experienced significant problems due to formation of gas hydrates: "they clog pipelines, valves, wellheads and processing facilities, thus reducing production and causing safety problems." (Dashti et al., 2015). When it comes to drilling, many severe problems are encountered due to drilling through hydrate zones, either for production directly from the hydrate zone or for oil and gas production below the in-situ hydrate zone.

Although hydrates have a stigma based on several related issues, gas production from naturally occurring methane hydrates in the earth's crust is known to hold great potential value in terms of energy and economy. "Such gas resources are regarded as the energy of the future ("white coal") provided economic recovery schemes are found." (Lachet and Béhar, 2000). Current technologies do not allow for economic recovery schemes.

Apart from gas production from naturally occurring hydrates, there are other examples of means of utilizing hydrates that may benefit the oil and gas industry. Looking into this gave the idea for the master thesis. Many of the means of utilizing hydrates are related to carbon capture and storage (CCS). Gas transport and desalination are other examples. Common for the technologies are that they utilize the separation mechanism of gas hydrate formation (gas molecules are entrapped in the cavities of a hydrate structure and thereby separated from a solution). Hydrate based technologies can reduces costs and improve safety compared to more

conventional alternatives. One reason being that "(...) volumetric gains can reach almost 155, meaning the hydrate volume can be about 155 times smaller than the corresponding gas volume under standard conditions." (Lachet and Béhar, 2000).

There has been a growing interest in additives that promote hydrate growth in recent times, but few known models have been developed. Additives of this kind are termed hydrate promoters in this thesis. Note that a hydrate promoter may be either mechanical or chemical. Hydrate promoters have the potential to increase the efficiency of hydrate based technolgies. Models for hydrate inhibitors (chemical) are widespread and commonly used, and with the growing interest in hydrate based technologies, models for hydrate promoters should be developed. Such models may be a step towards successful development of hydrate based technologies. Chemical inhibitors are often referred to as inhibitors, and throughout this thesis chemical promoters are most commonly referred to as promoters.

This master thesis will cover gas hydrate theory, especially hydrate kinetics. A discussion of hydrate based technologies with a focus on CO_2 capture will follow, to provide motivation for modelling. The chapter about CO_2 capture introduces common hydrate promoters. The main objective and aim of this master thesis is to develop a phase equilibria model for CO_2 hydrates in aqueous solutions of tetrabutylammonium bromide (TBAB). Modelling was carried out in Matlab, attempting to develop an explicit model. The model for phase equilibria of pure CO_2 hydrates was based on CSMGem simulation results. To model CO_2 hydrates was a natural choice considering CCS, and TBAB was chosen due to its known benefits and available experimental data. When adding TBAB, hydrate phase equilibria occurs at lower pressures and higher temperatures than before adding TBAB. This is related to an increase in stability meaning that "(...) TBAB has the potential to reduce the formation pressure of CO_2 hydrates by up to over 90% at concentration as low as 29 mol%" (Li et al., 2010). Note that CO_2/ TBAB form semiclathrates (SC), which have a slightly different structure to conventional hydrates. The modelling procedure presented in this thesis has resulted in an explicit phase equilibria model for hydrates of CO_2 in aqueous solutions of TBAB. Throughout the thesis phase equilibria refers to hydrate phase equilibria.

Chapter 2

Clathrate Hydrates

For hydrate utilization, the nature of clathrate hydrates must be understood to a large extent. Due to the stochastic nature of hydrates, they are in some sense still a mystery. The kinetics (time dependent properties), such as hydrate formation, are especially of interest for the topic of this thesis. This chapter will provide a thorough theoretical background to clathrate hydrates. The theoretical background is based on Sloan and Koh (2008). This chapter is modified from Undall (2016), which led up to this master thesis. Note that some sections have been directly copied.

2.1 Introduction to and Brief History of Hydrates

Clathrate hydrates are crystalline solids composed of water and gas. They resemble ice, as their structure consists of hydrogen bonded water molecules, the difference being the gas molecules that occupy the cavities. The water molecules are termed the "host" molecules, whereas the gas molecules are termed the "guest" molecules, as they occupy the cavity spaces. The term hydrate may in simple terms be defined as “a chemical that contains water” (Cambridge Dictionary), and clathrate means to encage. In this thesis the term hydrate refers to clathrate hydrate, and the terms may be used interchangeably.

Hydrates have been an area of interest since the 19th century. Sloan and Koh (2008) propose three major landmarks of clathrate hydrate research, which will be briefly discussed, serving as an introduction to clathrate hydrates.

The "Scientific Curiosity" (1810 – today)

The goal of the "scientific curiosity" was to identify which compounds formed hydrates, and to quantitatively describe these compounds in terms of composition and physical properties. It soon proved challenging to perform a direct measurement of the water-to-gas ratio. However, as discussed by Sloan and Koh (2008), Circone et al. (2005) proposed to able to quantify the hydration number (number of water molecules per guest molecule) by measuring the amount of gas released during dissociation. Prior to this Roozeboom (1884) and Roozeboom (1885) proposed the first pressure-temperature plot diagrams involving hydrates. For direct determination of hydrate phase properties, statistical thermodynamics must be applied.

Discovery of Man-made Hydrates (1934 – today)

Man-made hydrates are first and foremost associated with the oil and gas industry. Hydrates were early on seen as a challenge in the oil and gas industry, as they were known to cause potential blockage of pipelines. Blockage was observed above ice point, meaning that ice could not be the reason for the blockage. Realization of the challenges man made hydrates brought with them lead to an explosion of hydrate research.

The results of diffraction experiments showed two types of hydrate crystals; structure I (sI) and structure II (sII). A third hydrate structure, structure H (sH) was later discovered. sH will not be discussed in this paper as it is rare and highly unlikely to host natural gases. Common for all hydrate structures is that they have repetitive crystal units that are asymmetric, spherical-like cages (see fig. 2.1). The cages are hydrogen-bonded water molecules. Hydrate structures will be covered more in depth in section 2.3: Structure. (Sloan and Koh, 2008)

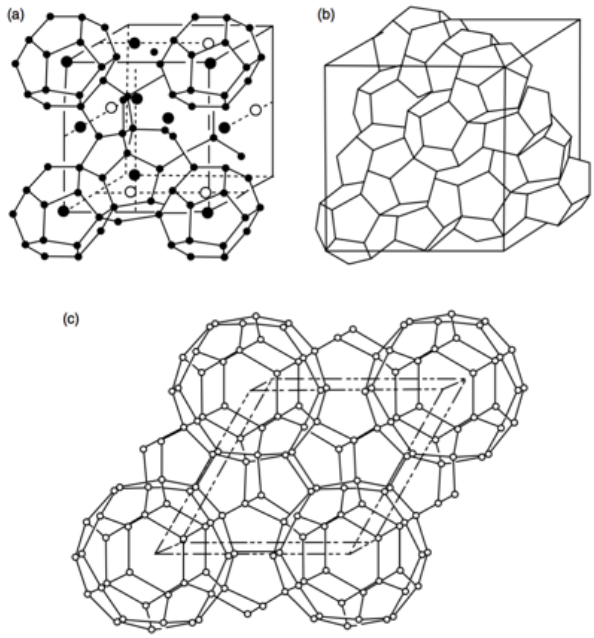

Figure 2.1: Crystal structure of hydrates. From top left; sI (a), sII (b) and sH (c). Each of the three figures represent a unit structure (Sloan and Koh (2008), p.9).

Efforts have been put into enabling gas production, transport and processing - where hydrates may otherwise have stopped this - by applying knowledge about hydrate phase equilibria. This has led to the development of hydrate inhibitors, additives to prevent hydrate formation. Hydrate promoters work in the opposite way of hydrate inhibitors. Hydrocarbon production is subject to challenging conditions such as those found in the Arctic and in subsea pipelines. This has led to the development of new types of inhibitors known as kinetic inhibitors and anti-agglomerates.

When it comes to the research behind this, large corporations such as ExxonMobil have constructed large scale pilot flow loops, in order to study hydrate nucleation, growth and dissociation in flow lines. Rigorous methods for prediction of thermodynamic properties of hydrates have been proposed. It is worth noting that the physics of hydrate formation is the same in situ and in pipelines- (Sloan and Koh, 2008)

A well-known name in the world of hydrate research is Yuri F. Makogon. Makogon lead a research group motivated by the fact that natural gas hydrates could serve to be a great resource in the Union of Soviet Socialist Republics (USSR). The resulting studies, carried out in the 1960s, are the first to consider hydrate kinetics (Sloan and Koh, 2008). Time dependent studies have

had a growing interest, but up until the 1990s research was very limited. The relatively recent and important concept of flow assurance has led to an explosion of time dependent studies. The shift from hydrate avoidance to hydrate "acceptance" (learning to live with hydrates under risk management) is a result of this. Time dependent properties are more challenging to study than time independent properties, leaving many gaps to be filled. Techniques used to study hydrates today - which in the future hopefully will allow us to fill several gaps in our knowledge - include light scattering (used to measure hydrate particle size distribution) and mesoscale imaging (used to measure hydrate formation, nucleation and dissociation). (Sloan and Koh, 2008)

Acknowledgement of Hydrates as a Major Resource (mid 1960s – today)

Today, clathrate hydrates are considered a potential, unconventional resource, with extremely high energy as hydrates are compressed by a factor of 184 (1 Sm^3 of hydrate contains up to 184 Sm3 of gas at standard conditions) (Sloan and Koh, 2008). Note that the exact compression factor may vary from source to source. Naturally existing hydrates commonly occur at depths where organic carbon accumulates rapidly; 300-800 m below sea level, and are mainly biogenic. Other potential means of utilizing hydrates have also received interest in recent times. These include the technologies to be discussed in thesis; desalination, gas capture, gas transport, and gas storage.

Research in the areas presented in these three chapters continues today. Considering the challenging times the oil and gas industry is facing, further research within the field of hydrate based technologies is strongly encouraged.

2.2 Environmental Aspects

Hydrates are not limited to this earth; Mars and E rings of Saturn - as well as comets - are comprised of among other components hydrates. When it comes to hydrates on earth they are believed to be of large extent; hydrate methane resources are believed to surpass conventional gas reserves, and be twice that of other fossil fuels. (Sloan and Koh, 2008)

It has been proposed that hydrates have contributed to global warming, but there is a lot of uncertainty linked to this, and people are currently investigating the role of gas hydrates in the carbon cycle. Sloan and Koh (2008) present a theory by Henriet (1998) that states that the uncertainty is greater than the likelihood of existing models. An example of a recent and controversial hypothesis is "the clathrate gun hypothesis", which suggests that the gas released from methane hydrates increases the earth's temperature. The clathrate gun hypothesis is presented by Sloan and Koh (2008) and originates from Kennett et al. (2003). It could serve as an explanation of the "late quaternary climate change", which led to a dramatic increase in the earth's temperature. Such a climate change may also occur in the future, meaning that if the hypothesis is correct, it is a past and future problem.

On a more positive note the idea of producing naturally occurring hydrates to meet energy demands has been explored in recent times. The energy density of clathrate hydrates is high. Today, these hydrates cannot be termed reserves as they are currently not economically recoverable. The reason for this is mainly that; they are too dispersed (typically occupying less than 3.5% of the total pore volume) and too deep (occurring at depths greater than 500m below sea level), for the technology of today to allow for recovery. However, in the future this may not be the case, providing a lot of net energy as less than 15% of the hydrate energy is required for dissociation. When it comes to potential environmental benefits of hydrates, hydrate based technologies must not be forgotten. Hydrate based technologies are discussed in chapter 3. (Sloan and Koh, 2008)

2.3 Structure

There are three types of hydrate structure: cubic structure I (sI), cubic structure II (sII) and hexagonal structure (sH) (see figure 2.1). This thesis will, as mentioned, focus on sI and sII. Hydrates of sI are found naturally occurring at the seafloor, in permafrost regions, and in subsea sediments, whereas sII are known to form in pipelines, causing challenges in the oil and gas industry. The comparison of hydrates and ice is the basis for this chapter.

Although hydrates are similar to hexagonal ice structure-wise, there are some significant differences, such as the fact that hydrates need guest molecules to occupy the structure of hydrogen bonded water molecules. Common guest molecules of sI include: methane (CH_4), ethane (C_2H_6), carbon dioxide (CO_2) and hydrogen sulphide (H_2S). Whereas common guest molecules of sII include: nitrogen (N_2), propane (C_3H_8) and isobutane (C_4H_{10}). It is common to have one guest molecule per cavity, and it is not a criterion that all cavities must be filled for a hydrate to remain stable. This makes it challenging to determine the degree of cavity filling. The type of guest molecule, and the guest-to-host ratio will affect the chemical nature of the hydrate. Under extremely high pressures one cavity can have several guest molecules. (Sloan and Koh, 2008)

Other differences between hydrates and ice include; thermal conductivity, melting and freezing point, diffusion (the diffusion of water molecules is orders of magnitude faster in ice than in hydrates) and some mechanical properties such as yield strength. Melting and freezing point of hydrates need to be distinguished. The melting point of a hydrate is the highest possible temperature where melting will occur, whereas freezing may occur at this point or at a lower temperature. Freezing and melting do not necessarily occur at the same temperature, and hydrates can form at temperatures well above the melting point of ice (Qi et al., 2012). Regardless of the differences, the hydrate structures consist of 85% water, meaning that many of the hydrate properties are the same as those of ice. (Sloan and Koh, 2008)

In order to understand the behaviour of hydrates or ice, chemical bonding must be considered. In ice each water molecule is hydrogen bonded to four others (structure Ih, hexagonal ice), sharing the tetrahedral angle of 109°, where the structure is the most stable. A hydrogen bond is relatively weak and can only exist between neighbouring molecules. The more stretched the tetrahedral angle, the less stable the structure. Hydrogen bonds are also found in hydrates,

but the tetrahedral angel is less stretched, making hydrates more stable. Other kinds of bonds present are Van der Waals (very weak bond between guest and host molecules in hydrates) and covalent (between hydrogen and oxygen within a single water molecule.)

Chemical bonding results in structure. Hexagonal ice consists of solely hexagons whereas the structure of hydrates is more complex. Considering the numbering system in figure 2.2. The exponent of a number indicates the number of given polygon, whereas the base indicates the number of faces of the polygons in question. sI and sII consists of pentagons and hexagons. One cavity (typically 5^{12}) goes together with other cavities to form a unit structure (a repeatable hydrate unit). The unit structure of structure I hydrates is put together by two 5^{12} and six $5^{12}6^2$, whereas the unit structure of structure II hydrates is composed of sixteen 5^{12} and eight $5^{12}6^4$. Different structures give different chemical properties.

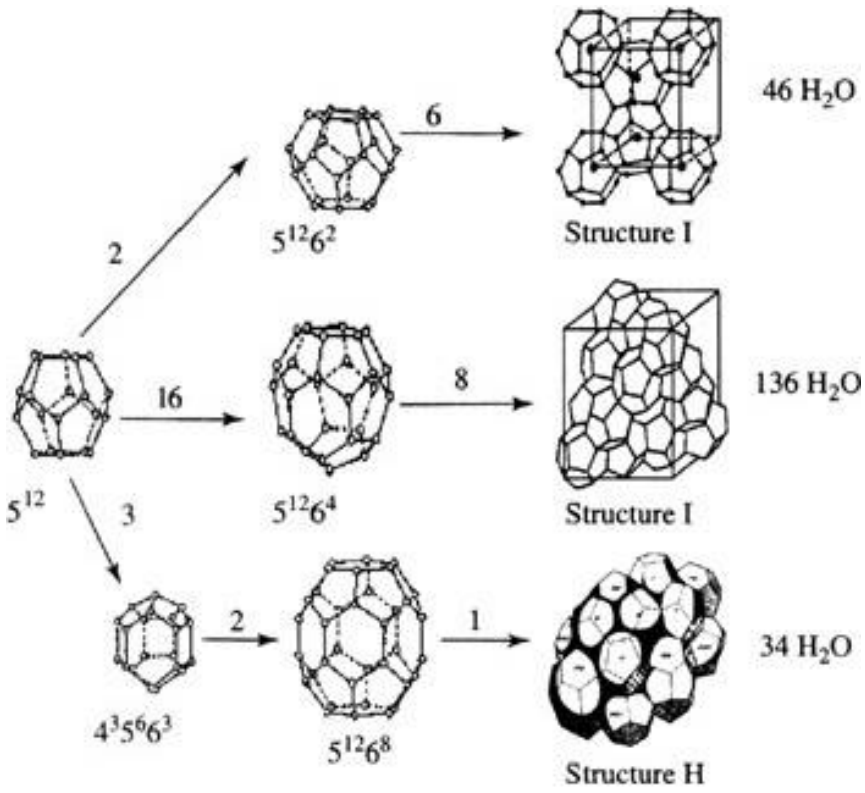

Figure 2.2: Clathrate hydrate structures. The total number of water molecules in a unit structure is also indicated (Letcher).

2.4 Kinetic Processes

This chapter will consider the time dependant processes; nucleation, growth and dissociation. The challenges with quantifying time dependent properties has led to that most of the knowledge regarding hydrate kinetics is based on laboratory experiments. Note that the processes are both stochastic and apparatus dependent, so they are difficult to measure and model, which brings many challenges and uncertainties.

Modelling tools and experiments have been used to study hydrate formation for decades. It has been suggested that the rate of consumption of hydrate former in a solution is a measure of the hydrate formation rate, but the correlation is not so simple. The consumption of gas *does* cause a decrease in pressure of the solution which can be quantified, but the amount of hydrate formed cannot be found directly from this change in pressure. By applying the ideal gas law (or a suitable modified version) the number of moles associated with a given pressure change, can be found. Knowing the number of moles is not enough. This is because the degree of cavity filling is not known, and there is essentially no easy way of knowing this. If the number of moles is known and the degree of cavity filling is not known, the amount of hydrate formed can not be found with certainty. It can only be found within an upper and lower boundary. In research, the degree of cavity filling is often estimated or found by accompanying simulations. Estimation of the degree of cavity filling (often estimated as ideal) or using simulation results will affect the accuracy of the obtained hydrate formation rate. As there is presently no simple way of knowing the degree of cavity filling, experiments suffer from uncertainties. There are some current methods for determining degree of cavity filling, such as spectroscopy, but they are hard to incorporate in small scale laboratory experiments.

Another factor to consider, when it comes to the correlation between gas consumption and hydrate formation is that hydrate former may be consumed in other ways than cavity occupation. If the particles are large, small volumes of hydrate former may be trapped in “pockets” between the particles instead of inside cavities. Lastly, as a change in pressure is also associated with a change in temperature, the temperature change should also be considered before drawing conclusions regarding hydrate formation. By the ideal gas low pressure and temperature change is proportional.

Hydrate formation (and dissociation) may occur at the hydrate equilibria curve (see figure 2.3), the hydrate region being on the left side of the curve. At each point on the equilibria curve, the corresponding equilibria pressure and equilibria temperature is the lowest possible pressure and highest possible temperature for hydrate formation. (Sloan and Koh, 2008)

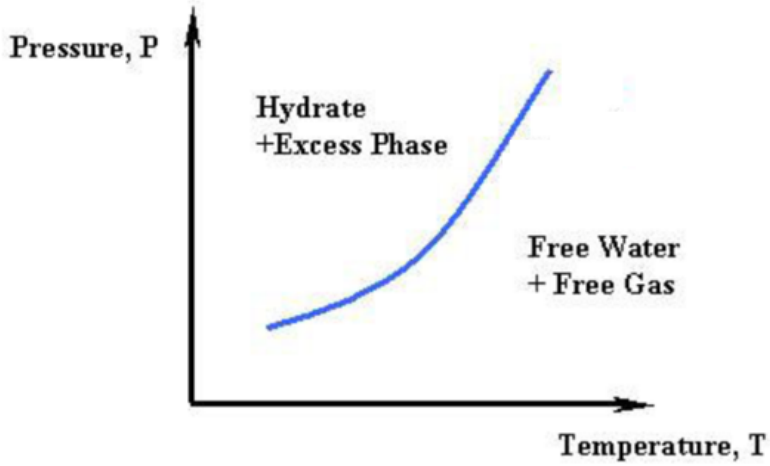

Figure 2.3: Phase diagram of a water-hydrocarbon system indicating the hydrate and the water + free gas region, separated by the hydrate phase equilibria curve. Modified from Adewumi (2017).

Nucleation

Hydrate formation starts with nucleation and the "induction time". It is a stochastic process which occurs when the conditions (pressure and temperature) are within the hydrate stability region. Hydrates do not form immediately due to metastability (a non-equilibrium state is enabled to persist for a significant time). During induction, there is no detectable hydrate (it cannot be seen by a microscope), and no detectable gas consumption, so induction is hard to measure and control. Next the hydrate grows to a detectable size, and lastly it enters the growth period, during which gas is being concentrated in the cavities. (Sloan and Koh, 2008)

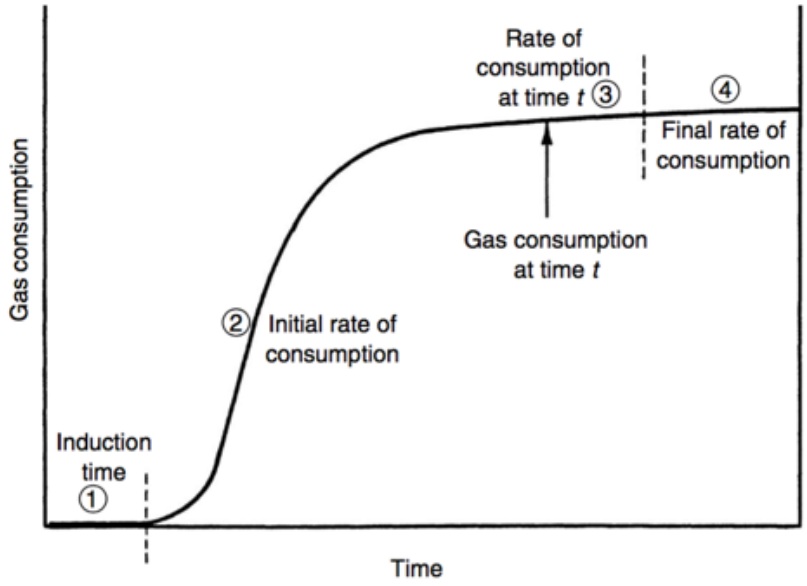

Figure 2.4: Gas consumption vs. time. As gas starts to be noticeably consumed by hydrate formation the slope decreases (Sloan and Koh (2008), p. 115).

At the start of nucleation small clusters of water and gas, grow and disperse to achieve critical size. Achieving the critical size is a necessity for hydrate formation, and experiments have shown that hydrate nucleation taking place is statistically probable (Sloan and Koh, 2008). For a critical cluster size to be reached, the related Gibbs free energy must be overcome (ΔG_{crit}) (see fig. 2.5). Surface Gibbs free energy (ΔG_s) is positive, where as volume provides excess Gibbs free energy, and is seen as negative. The line in between the line representing the surface Gibbs free energy (ΔG_s) and the volume Gibbs free energy (ΔG_v) is simply the sum, and the Gibbs free energy (ΔG) associated with a given cluster size. The time it takes for a cluster to reach the critical radius (r_C), is the induction time, during which the process is endothermic. Once the critical size is reached

the process becomes exothermic. The energy required for critical cluster size to be reached is something that is given by natural fluctuations or provided externally, the last being the case for artificially made hydrates for hydrate based technologies.

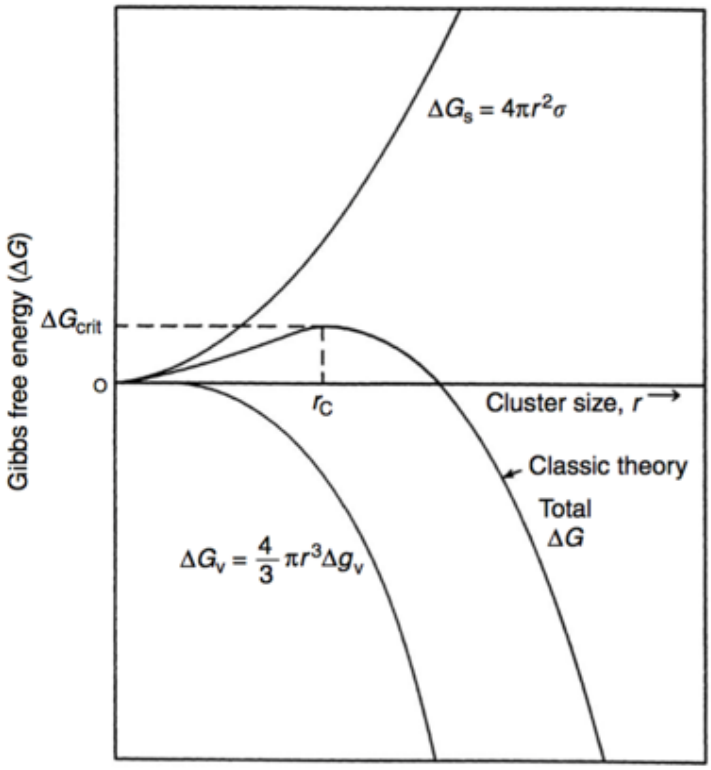

Figure 2.5: Gibbs free energy as a function of cluster size. Gibbs free energy consists of surface free energy (ΔG_s) and volume free energy (ΔG_v) (Sloan and Koh (2008), p. 126).

Gibbs free energy is defined as:

$$\Delta G = \Delta H - T\Delta S \tag{2.1}$$

where ΔG is the Gibbs free energy, ΔH is the enthalpy, T is the temperature and ΔS is the entropy of the system. When positive Gibbs free energy is maintained it means that the large negative entropy of the solution (unfavourable) overcomes the negative enthalpy of the solution (favourable). Large negative entropy changes are unique to aqueous solutions of non-polar gases, and are associated with the creation of structure. (Sloan and Koh, 2008)

The study of liquid water, in some cases supercooled (liquid water that exists below the freezing point of water), has resulted in models for hydrate nucleation such as the “The hydrogen-bonded network” and “The flickering ice berg theory”. In “The hydrogen-bonded network” there is a random network of hydrogen bonds, frequently undergoing strain and breakage, whereas in “The flickering ice berg theory” there are hydrogen-bonded clusters with a non-hydrogen bonded dense phase. Both these models are presented by Sloan and Koh (2008).

Models have also been developed to describe hydrate nucleation on a molecular level. Examples being “The labile cluster model” and “The local structuring model”. In “The labile cluster model” the formed clusters are seen as unstable (clusters form and then they may dissociate) whereas in “The local structuring model” guest molecules are arranged in configurations. “The local structuring model” is an opposition to “The labile cluster model”, however evidence has shown that it is thermodynamically favourable for clusters to disintegrate, which is the case for the unstable labile cluster model (Sloan and Koh, 2008). Although hydrate nucleation is stochastic and more experimental evidence regarding its nature is desired, there is evidence that the higher the driving force (ΔT), the less stochastic nucleation is. If nucleation is desired, one should therefor apply a high driving force. The driving force is often defined as ΔT. Adding a hydrate promoter can be seen as adding a driving force as it promotes hydrate nucleation.

Growth

Sloan and Koh (2008) present a hypothesis for hydrate growth in figure 2.6. The cluster at location (i), a guest molecule with surrounding hydrogen bonded water molecules, is attracted to the hydrate surface. The movement is driven by lower Gibbs free energy at the surface, and the driving force is in principle "gas concentration gradients". When gas molecules are "removed" from the solution close to the hydrate crystal (to occupy cavities), an imbalance appears that must be balanced out. This happens by drawing new gas molecules to the location that experiences imbalance. On absorption, a few water molecules are released. The remaining cluster at location (ii) experiences an even stronger attraction at "steps", as the force field is exerted from two surfaces. The concentration gradients are what leads to a force field. Again, on absorption water molecules are released as there is not space for them. The ultimate location for the cluster is a "kink" site, where the sum of the force field is the strongest. The cluster can no longer move, and the hydrate structure has grown. As a hydrate is growing this procedure is repeated for other clusters. It should be noted that there is little experimental evidence for this hypothesis.

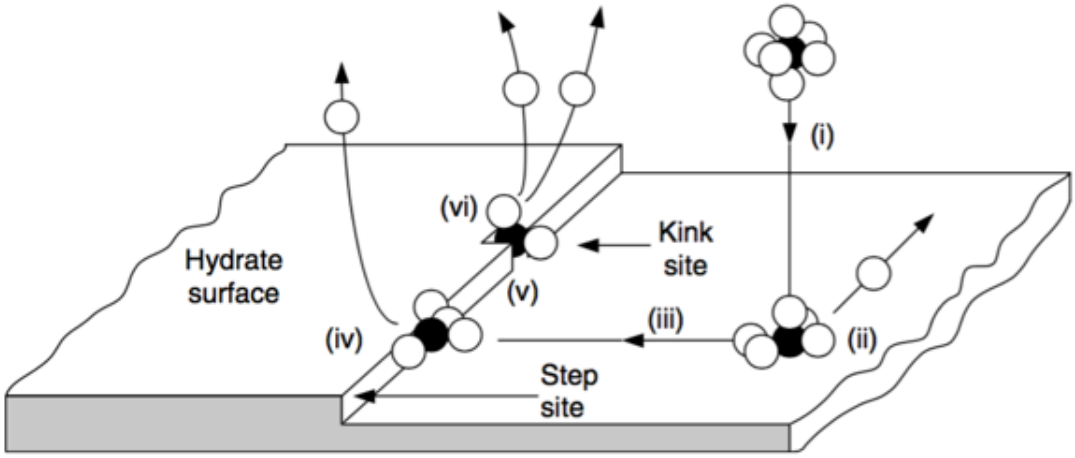

Figure 2.6: Hydrate growth hypothesis (Sloan and Koh (2008), p.151).

Dissociation

Hydrate dissociation may occur when phase equilibria is no longer maintained. Hydrate dissociation leads to gas release, examples being production from naturally occurring hydrate reservoirs and in pipeline plug remediation. Hydrate dissociation is an endothermic process, meaning that energy must be provided for it to occur. Energy is required to break hydrogen bonds between water molecules and the Van der Waals force between the guest and host molecules. Dissociation methods include thermodynamic inhibitor injection, thermal stimulation (heating) and depressurization. As the occurrence of hydrate plugs in pipelines may have fatal consequences, many people have studied hydrate avoidance and dissociation. This means that there is more available knowledge regarding dissociation than nucleation and growth, allowing dissociation to be predicted more accurately.

Chapter 3

Hydrate Based Technologies

Hydrate based technologies refer to technologies that utilize hydrates. The technologies to be discussed are; hydrate based desalination, hydrate based CO_2 capture (note that the principle is the same for capture of any gas) and hydrate based transport and storage of gas. The section about CO_2 capture (section 3.2) also includes an introduction to hydrate promoters. Technologies that utilize hydrates are concerned with the kinetics of hydrates. Common for all the technologies is that they rely on hydrate phase equilibria.

The time dependant properties of hydrates can be better understood by phase equilibria models. Because of the known consequences of hydrates in the oil and gas industry, there has been a lot of interest in hydrate avoidance. Study has, as mentioned, led to the development of phase equilibria models for common hydrates, and later for hydrate inhibitors. Hydrate inhibitor models are well recognized. Common inhibitor models include models for salt (NaCl), methanol (MeOH) and mono-ethylenglycol (MEG), examples are consequently shown in equations 3.1, 3.2 and 3.3. The models are by Kamath and Patil (1994).

$$\Delta T = 0.42x + 0.0202x^2 \tag{3.1}$$

$$\Delta T = 0.3938x + 0.0006166x^2 \tag{3.2}$$

$$\Delta T = 0.1721x + 0.004466x^2 \tag{3.3}$$

where ΔT is the temperature shift (protection) and x is the weight% inhibitor in the water phase. Software incorporating phase equilibriam models, for pure hydrates and hydrates inhibitors, have been developed and are widely used today. An example of such a software is CSMGem. There are currently few available models for prediction of phase equilibria of hydrate promoters. Development of hydrate promoter models is believed to benefit hydrate based technologies. The objective of this chapter is to provide motivation for hydrate promoter modelling.

3.1 Desalination

Hydrate based desalination can be summarized as: “to recover water from an aqueous solution by forming hydrates, separating the crystals from the concentrated solution and then decomposing the hydrates.” (Lachet and Béhar, 2000). Hydrate conditions are created, and later removed. Hydrate based desalination was the topic of Undall (2016) leading up to this master thesis. This chapter is based on Undall (2016), with a focus on the conclusion and the discussion. Smaller sections have been directly copied.

As an introduction to the general method “The 2014 Offshore Technology Conference” will be considered. The process that was presented at the conference had three main components: crystallizer, wash column and melter (see figure 3.1). This process is essentially common for all hydrate methods, although the processing terminology may vary. Most processing diagrams will include a “separator”. Hydrates are formed in the crystallizer and dissociated in the melter. The wash column or separator is where the formed hydrates are separated from the brine. (Anres et al., 2014)

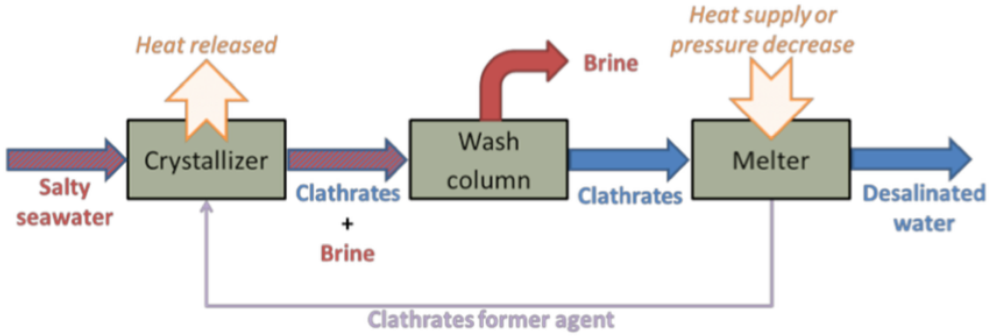

Figure 3.1: Desalination utilizing clathrate hydrates as presented by "The 2014 Offshore Technology Conference" (Anres et al., 2014).

The technology was first proposed in the 1940s, and interest grew in the 1960s and 1970s (Corak et al., 2011). Several hydrate desalination processes have been developed, but they have not replaced more traditional alternatives such as; reverse osmosis (RO) and multi-stage flash distillation (MSF). The reasons for this are related to the energy efficiency of the hydrate methods, which currently are too low (Anres et al., 2014). According to Tretyakov, the energy efficiency of distillation technologies is however even lower. Considering this, and the fact that RO

requires preliminary water treatment (adding to costs), the hydrate method holds great potential.

Early contributions to the hydrate based desalination technology were based on the mixing of seawater with gas, the aim being to consume all the gas in the brine by hydrate formation. The result of the mixing of seawater and gas was a "hydrate brine slurry", which caused challenges. The hydrate brine slurry was unwashable, meaning that a lot of the brine was stored within the hydrate mass (Sloan and Koh, 2008). When the hydrate structure was dissociated, the solution would not be desalinated to an acceptable extent. More recent methods propose solutions where a hydrate brine slurry is avoided. Significant contributions are by the companies Ecowat and Marine Desalination Systems. Ecowat proposed a method where the hydrate structure would grow by first forming a small hydrate and then growing outwards, avoiding unnecessary stored brine. In addition to this Ecowat handled the problems related to brine being stored in "pockets" between particles by working with larger particles. The slurry that still formed, was attempted separated by centrifugation. The approach used by Marine Desalination Systems involved attempting to increase the mass to surface area of the formed hydrate crystallites, as this allows for the absorption of the salt to become insignificant. (Sloan and Koh, 2008)

In the early 2000s there was a lot of interest in developing improved hydrate desalination methods with an increased efficiency. Nowadays, there seems to be a decreasing interest in the technology as there are significantly fewer published papers. The energy efficiency issues have still not been solved. Ecowat was close to reaching a breakthrough as they were able to desalinate water to a significant extent with just one step (repeating the process would lead to "ultra-clean" water), but the energy consumption was too high, and the Trondheim-based company was liquidated in 2014.

Anres et al. (2014) presents the technical gaps to be: selection of hydrate former and control and efficiency of each process step. Selection of hydrate former and control and efficiency of each process step - as well as other parameters that affect the efficiency of the technology - were identified in the specialization project Undall (2016). Addition of hydrate promoters was not part of the discussion by Undall (2016). Adding a hydrate promoter is believed to cause an increase in energy efficiency, much because of an increase in hydration speed. A short discussion of the parameters identified by Undall (2016) follows:

- ***Selection of hydrate former.*** Different hydrate formers have different effects on hydrate desalination. CO_2 has been widely tested (Ecowat, Park et al. (2011) and Corak (2011)) and has allowed for up to ultra clean water. Corak (2011) worked with different hydrate formers and was most successful with natural gas (rapid growth was one of the deciding factors), which is convenient for the oil and gas industry as it is easily accessible during oil and gas production. Certain hydrate formers are known to form hydrates at lower pressure and higher temperature than the most common hydrate conditions, something that can reduce energy consumption. Corak (2011) worked with cyclopentane (C_5H_{10}) which forms at atmospheric pressure.

- ***Subcooling.*** Subcooling is when a liquid exists at a temperature below its boiling point. Experimental results suggest that desalination is significantly affected by subcooling, and desalination was most effective for high subcooling. Subcooling was found to affect hydrate growth, and evidence for a correlation between hydrate number and subcooling was found. More data from a wider subcooling range is desired to verify this. (Park et al., 2011)

- ***Amount of hydrate former.*** The concentration of the hydrate former was found to affect desalination less than subcooling. Increased amount of hydrate former does not necessarily mean increased purity.

- ***Separation.*** Separation is related to successfully extracting hydrates from a hydrate brine slurry, increasing the purity of the remaining phase. This was the major challenge of early methods, but advances have been made. Such as by centrifugation and a vacuum suction (Ecowat and Corak (2011)), and by use of a pelletizing process (Park et al., 2011). In the pelletizing process the remaining liquid phase is “squeezed out” in the process of forming pellets from slurry. In theory, complete separation should result in salt free water, but there has been discussions whether hydrates can be salt free (Qi et al., 2012). The conclusion by molecular simulation is that hydrates could not be salt free to a degree less than 0.07 weight% (Qi et al., 2012). Questions regarding the extent to which hydrate formers can be removed once hydrates have dissociated, should also be lifted for future development. Big quantities of hydrates may have larger amounts of impurities due to the complexity of the crystallization process.

- ***Water composition.*** Regarding the effect of dissolved minerals in water, ionic radius was found to be proportional to removal efficiency, whereas ionic charge was inversely proportional to removal efficiency for common minerals, with an exception of Ca2+ (Park et al., 2011). These results suggest that there is a size effect or electrostatic adhesion between particles during hydrate desalination. The pelletizing method showed that up to 80% of minerals were removed (Park et al., 2011), and Ecowat claim close to no contamination (salts, minerals and chemicals) and less than 1ppm remaining oil. Further studies such as hydrate-ion interaction and surface analysis (e.g. x-ray) are encouraged to gain knowledge regarding removal of dissolved ions.

- ***Cavity filling.*** The degree of cavity filling is important to quantify when performing hydrate desalination experiments, however this is challenge with today's technology such as spectroscopy. Cavity filling is important to know as change in pressure (due to gas consumption) cannot be directly converted to hydrate formation. Both hydrate formation rate and volume of hydrate formed is hard to quantify when degree of cavity filling is not known.

- ***Process efficiency.*** This is related to preserving energy in the process, and an increase of the efficiency of the various processing steps is desired. Ecowat was successful with preserving energy at small scale, but not when upscaling. Solutions may involve utilizing the heat from hydrate formation (an exothermic process) for the endothermic process of dissociating hydrates further down the line in the process.

Further research regarding the listed parameters and increased understanding of hydrate kinetics, will help towards commercialization of the process. Even though varying parameters such as; subcooling, amount of hydrate former and type of hydrate former, may be part of the solution, it is still believed that a breakthrough must be reached. Addition of hydrate promoters may be part of the solution, encouraging the development of hydrate promoter models.

3.2 CO_2 Capture

As gas hydrates are composed of both guest and host molecules, they can be used for gas capture, the gas being the guest molecule. The principle of hydrate based CO_2 capture (HBCC) is the same as the principle of hydrate based capture of other gases. Considering today's interest in and importance of carbon capture and storage (CCS) – and that CO_2 is ideal for hydrate based capture – this chapter will look at CO_2 capture. An introduction to hydrate promoters is part of the discussion, considering their effect on parameters such as induction time and equilibria pressure. This will provide justification for the choice to model CO_2/ TBAB hydrates. HBCC will also be briefly compared to more conventional methods of CO_2 capture. The main part of the discussion carried out in this chapter is based on Dashti et al. (2015), a review study on hydrate based CO_2 capture.

"CO_2, as a small nonpolar hydrocarbon, forms SI hydrates with the formula $CO_2 \cdot nH_2O$ (n = 5.75) when coming into contact with water molecules below the equilibrium temperature and above the equilibrium pressure." (Sloan and Koh, 2008). Due to the great concentration of gas in hydrates, dissociation causes release of great amounts of CO_2 gas (Dashti et al., 2015). CO_2 hydrates have mild phase equilibrium conditions (see fig. 3.2), are easy to regenerate and have a unique separation mechanism (Dashti et al., 2015). Of the components of flue gas (CO_2, N_2, O_2), CO_2 has the lowest hydrate forming pressure. This and the fact that the hydrate forming pressure is significantly different from that of N_2 and O_2 is ideal for sequestering CO_2. Forming a solid hydrate phase enriched with CO_2 has been shown to increase the concentration of CO_2 by up to four times. (Dashti et al., 2015)

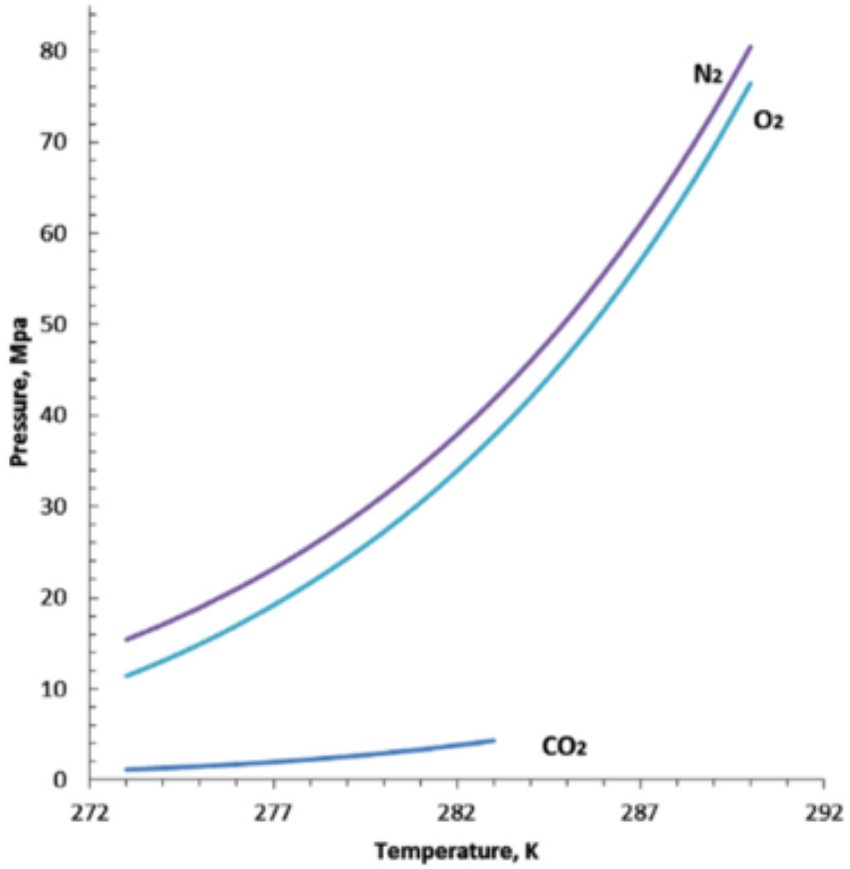

Figure 3.2: Phase equilibria diagram of hydrate formers CO_2, N_2 and O_2. Modified from Dashti et al. (2015).

All technology is concerned with energy efficiency. When it comes to CCS, the energy consumption is the greatest from capture, meaning that improving capture technology can have great benefits (Dashti et al., 2015). Current and conventional capture methods include absorption and membrane technologies. The use of membrane technology is also found in conventional desalination technologies. Hydrates as a means of desalination is discussed in in the previous section (section 3.1). The efficiency of conventional capture methods is low, as multiple stages are often required, suggesting that new technologies should be developed.

The processing unit of a standard HBCC plant includes a hydrate formation reactor, a separator and a dissociation reactor. A simplified flow chart of the processing unit is displayed in figure 3.3. Purified CO_2 is released when the hydrate slurry in the last reactor is dissociated, whereas CO_2 rich gas is recycled for further purification. In the first reactor hydrates are formed.

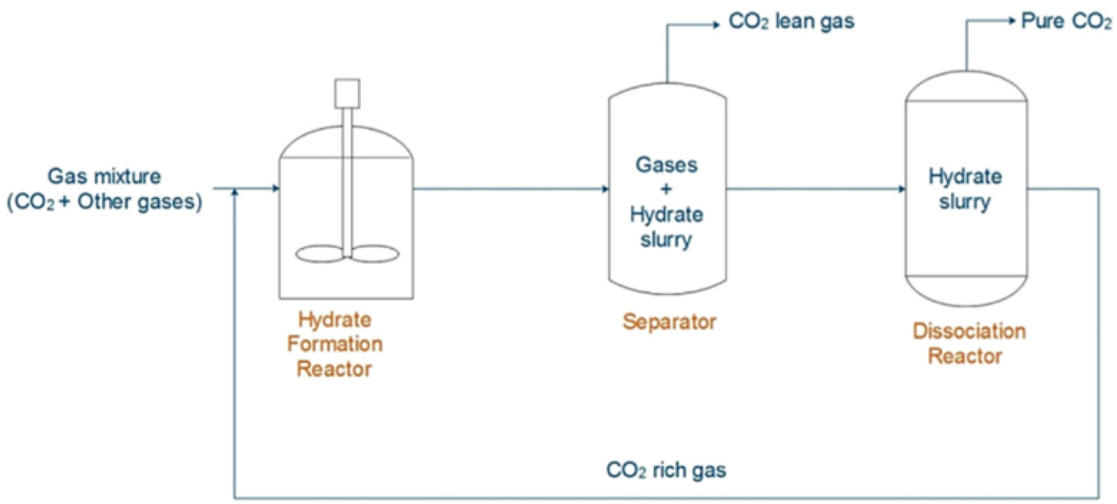

Figure 3.3: HBCC processing unit (Dashti et al., 2015).

The main advantages of hydrate based CO_2 capture are related to cost and energy consumption. By considering HBCC technology in an integrated gasification combined cycle the cost is low compared to CO_2 capture by conventional amine-based absorption and absorption using zeolite (Dashti et al., 2015). The prices are commonly given in in USD per ton CO_2 captured. In terms of energy consumption (MJ/ kg CO_2) HBCC is comparable or more efficient than absorption. Membrane technology has the lowest energy consumption, but membrane technology is sensitive to high temperatures and is only suitable for CO_2 concentrations > 20%. In addition to this its removal efficiency is low, which is a major disadvantage. More stages would be required for the same removal efficiency as achieved by one stage of HBCC.

Dashti et al. (2015) highlight the following advantages: moderate operational temperature range, relatively low energy consumption in hydrate dissociation/ regeneration and capability of continuous operation. Concerning disadvantages, they are related to the practical applications of HBCC. High pressure operating conditions (compared to conventional technologies) as well as large footprint make practical applications challenging. In terms of energy penalty HBCC is not comparable to conventional methods. (Dashti et al., 2015)

There has been an increasing interest in HBCC and it has been claimed to be capable of separating gas mixtures that might not be possible with conventional technologies. Early research was focused on pure CO_2 (studies of phase equilibria of pure CO_2 hydrates), whereas later studies have considered the use of various additives to increase efficiency. Chemical additives and

different mechanical approaches have been found to improve the selectivity, efficiency and kinetics of this technology (Dashti et al., 2015). Additives affect parameters such as: induction time, gas consumption, split fraction (S.Fr) and separation factor (S.F.). Split fraction (the percentage recovery of CO_2) is defined in eq. 3.4 and separation factor is defined in eq. 3.5.

$$S.Fr = \frac{n^H_{CO_2}}{n^{feed}_{CO_2}} \tag{3.4}$$

where $n^H_{CO_2}$ is the number of CO_2 moles in the hydrate phase, and $n^{feed}_{CO_2}$ is the number of CO_2 moles in the feed gas.

$$S.F. = \frac{n^H_{CO_2} \times n^{gas}_A}{n^{gas}_{CO_2} \times n^H_A} \tag{3.5}$$

where $n^H_{CO_2}$ is the number of moles of CO_2 in the hydrate phase, n^H_A is the number of moles of another gas (A) in the hydrate phase and $n^{gas}_{CO_2}$/ n^{gas}_A is the number of moles of CO_2/ A in the residul gas phase.

"For CO_2 capture, a short induction time and high gas consumption, combined with high separation factor, are highly desirable." (Dashti et al., 2015). Although ideal, it is challenging to meet these criteria simultaneously. Higher operating pressure leads to fast and high gas consumption. However, it does not guarantee a high CO_2 separation factor, since other gases may form hydrates at the same time. In addition to this, the high pressure requirement leads to an increase in compression costs due to the high energy consumption (Dashti et al., 2015). Lowering the operating pressure, while at the same time increasing the hydrate formation rate and the selectivity of the CO_2 is difficult and still under much research. Chemical additives (to improve CO_2 capture/ separation efficiency) and mechanical methods (to improve contact area and mass transfer between gas and water) have been researched with this in mind. It is known that an increased mass transfer between gas and water would increase gas consumption and decrease induction time (Dashti et al., 2015). The chemical additives aim to: shorten the induction time, reduce hydrate equilibria formation pressure, increase the hydration rate, enhance gas uptake and improve the selectivity of CO_2 in the hydrate cages. The different chemical ad-

ditives are divided into two categories; “kinetic promoters” and “thermodynamic promoters”. Corresponding to the more well-known hydrate inhibitor categories of “kinetic inhibitors” and “thermodynamic inhibitors”. The kinetic promoters are mostly surfactants, increasing the rate of hydrate formation without taking part in it, whereas thermodynamic promoters actively take part in hydrate formation. Hydrate promoters work in the opposite way of hydrate inhibitors. Common for all thermodynamic promoters are that they consist of small molecules.

Examples of researched kinetic promoters include; sodium dodecyl sulphate (SDS), tween-80 (T-80) and dodecyl-trimethyl-ammonium chloride (DTAC). Whereas examples of researched thermodynamic promoters include; tetrahydrofuran (THF), cyclopentane (CP), propane (C_3H_8) and tetra-n-butyl ammonium bromide (TBAB). The effects of some chemical additives, on parameters affecting the efficiency of hydrate based technologies, have been summarized in table 3.1. Table 3.1 displays the general trends form a collection of experimental results presented by Dashti et al. (2015). The information in the table and the discussion that follows will help justify the choice to model TBAB.

Table 3.1: Effects of chemical additives.

Chemical additive/ Parameter	**THF $(CH_2)_4O$**	**Cyclopentane C_5H_{10}**	**Propane C_3H_8**	**TBAB $C_{16}H_{36}BrN$**	**Surfactants**
Induction time	Reduced	Reduced	Reduced	Reduced	Reduced
Hydrate formation rate/ nucleation rate			Reduced	Increased	Not sacrificed
Hydrate growth rate	Reduced		Reduced		
Gas consumption		Reduced			Not sacrificed
Hydrate equilibrium pressure	Reduced	Reduced	Reduced	Reduced	No effect
Split fraction fraction (S.Fr)	May increase		Little effect		
Separation factor (S.F.)	May decrease		Slight decrease		Not sacrificed
Hydrate structure (with CO_2 as guest)	sII	sII	sII	Semi-clathrate	
Phase equilibrium conditions	0.1 MPa, 277.6 K	0.1013 MPa, 280 K	0.36 MPa – 0.48 MPa, 275 K	0.25 MPa – 4.09 MPa, 273.15 K – 291.15 K	No change

Blank fields indicate lack of information, not that there is no effect.

It should be noted that most of the information/ results presented in table 3.1 are obtained from lab experiments using a stirred tank reactor. This brings an inevitable inconvenience; "In stirred tank reactors, the agglomeration of hydrate crystals becomes an obstacle to reducing the gas/water interface area and, consequently, the rate of hydrate formation and conversion of water." (Dashti et al., 2015). As an increased contact area increases efficiency, the results may be more desirable in a different environment.

The most commonly studied chemical additive in HBCC is THF. THF causes a drastic reduction of hydration pressure and induction time, causing large amount of hydrates to form. THF molecules occupy large cavities, meaning that high concentrations of THF can lead to reduced number of cavities available for CO_2 capture (Dashti et al., 2015). This would reduce the separation factor of CO_2. Cyclopentane (CP) also reduces hydration pressure as well as induction time.

When it comes to TBAB an important point to note is the increased hydrate formation rate for CO_2 and N_2 hydrates. Increased formation rate for pure $CO_2$when adding TBAB is especially interesting considering the benefits of CCS. There is a significant amount of available experimental data for CO_2/ TBAB hydrate phase equilibria, which is a good starting point for modelling. Other advantages of TBAB include; that it mainly consists of environmentally friendly TBA+ ionic liquid, that it allows for greater gas capacity in water cages and that it causes better stability at atmospheric pressure. Greater gas capacity and better stability are features of semi-clathrate (SC) hydrates. In CO_2/ TBAB SC the host molecules are water and bromide anions bonded together, and the guest molecules are cations (Dashti et al., 2015). For more information about SC, see section 4.1: TBAB. It should also be noted that TBAB has more desirable behaviour than many other known hydrate promoters in the sense that an increased amount of the promoter reduces hydrate forming pressure and increases hydrate forming temperature. This is related to the increased stability at low pressures. The promoters THF and cyclopentane (CP) do not have this effect. The low pressure values for hydrate formation with TBAB is especially low for low temperatures, this statement is backed up by experimental data and the developed model.

Regardless of its benefits, the phase behaviour of TBAB is challenging to work with and study as TBAB hydrates have two different structures that vary in dominance. Which of the

two structures that is dominant is a function of the concentration of TBAB. The structures may also be referred to as types, the two types being type A and type B. Note that the structures/ types should not be confused with the more common structure classification system where a hydrate structure is either known as structure I (sI) or structure II (sII.) The two types A and B vary in hydration number and shape; hydration number is either 26 (A) or 38 (B), and the shape is cylindrical (A) or irregular and composed of several crystals (B). Different hydration number and shape gives different properties. (Dashti et al., 2015)

Although this makes TBAB hydrates hard to analyse in theory, it does not complicate the modelling of the CO_2/ TBAB phase equilibria in this master thesis. The concentration range of the final model is seen as to corresponds to one type (type A). Note that the upper limit of the concentration range (for convenience set to 40 weight%) does not exceed the concentration leading to maximum cavity occupation. Type A has a hydration number of 26 meaning that maximum cavity occupation is at 41 weight% TBAB. This was calculated by dividing the mol weight of TBAB by the total mol weight. The total mol weight is the sum of the mol weight of TBAB and the mol weight of water multiplied by the hydration number. A higher concentration than 41 weight% is believed to have a negative effect as maximum cavity occupation has been reached. At weight% 41 there are no more available water molecules, meaning that adding more TBAB could harm the diffusion of CO_2, thereby inhibiting hydrate formation.

The model does not specify the lower boundary, as it is very low. The theoretical lower boundary can be estimated. Estimation is based on the statement presented by Dashti et al. (2015) that above 0.014mol% type A is the most stable, whereas at 0.014 mol% and below type B is the most stable. 0.014 mol% corresponds to 0.25 weight% ($\approx$ 0 weight %), so the simplification that the concentration range of the final model corresponds to type A is reasonable. The weight% was obtained by simple conversion calculation. The statement by (Dashti et al., 2015) is for pure TBAB hydrate systems, but it is reasonable to assume a similar value for TBAB/ CO_2 systems. It should be noted that other TBA^+ salts are also able to form SC hydrates, but TBAB is the most widely researched, and thereby modelled. Other TBA^+ salts have been proposed to have greater potential (lower pressure and greater gas uptake than TBAB), and may replace TBAB in the near future. (Dashti et al., 2015)

When it comes to surfactants, they do not cause a change in the thermodynamic conditions for hydrate nucleation. The fact that gas consumption and separation factor is not sacrificed is because surfactants do not take part in the enclathration process. The hydrophobic and hydrophilic end of surfactants do however lead to reduced induction time and faster formation rate. A higher formation rate is related to the fact that: "The presence of surfactants improves the gas diffusion through the gas/ water and gas/ hydrates interfaces, leading to enhanced inward and outward growth of hydrates." (Dashti et al., 2015). Except for surfactants, all chemical additives cause a reduction of hydrate equilibrium pressure. The lowest hydrate equilibrium pressure is found for THF and CP (~ atmospheric pressure). Low hydrate equilibrium pressure is ideal as less energy is required for compression, which reduces costs.

"Mechanical methods" involve hydration methods that include a reactor. Various reactors and varying reactor conditions have been subject to experimental research. Regarding the disadvantages of laboratory experiments using a stirred tank reactor (hydrate agglomeration becomes an obstacle for growth), the mechanical method "fixed bed crystallizer" avoids it. The fixed bed crystallizer incorporates a porous silica gel which enhances the contact area of gas and water. This would improve the total gas uptake, as it would allow for more gas to be enclathrated. Kang et al. (2013) found that over 93% of small cages and 100% of large cages were occupied by CO_2 if porous silica gels were used. Silica is cheap, and therefor ideal for large scale CO_2 capture. Other studies show that temperature fluctuations can be used to increase hydrate formation. Temperature fluctuations can be applied by vibration. Results have shown that pressure drop could increase by up to 30% as a result of this. (Dashti et al., 2015)

There are many suggested ways of improving the efficiency of HBCC. These may also be seen as potential ways of improving hydrate based technologies in general. Chemical additives, which has been in focus, is a diverse field of research. A possible reason for this being that the chemical stirred reactor (commonly used in experiments with chemical additives) is cheap and few modifications are required from one experiment to the next. From the discussion carried out, it becomes clear that different chemical additives will benefit the CO_2 capture process in different ways. The concentrations required of the different chemical additives need to be taken into account when evaluating economic feasibility, and should be included in further evaluation. This would be easier if hydrate promoter models were available. Note that this is not the

case of CP, as its equilibrium conditions is independent of concentration. The combinations of different chemical additives is also something that should studied in future work. Research has shown that combinations of different chemical additives can produce desirable outcomes. "SDS/ THF additive mixture has been proven to double the gas uptake, compared with the case of using THF alone." (Dashti et al., 2015). SDS refers to sodium dodecyl sulphate. A combination of SDS and THF is an example of combining a kinetic promoter with a thermodynamic promoter. Although HBCC has not yet been commercialized, it is a novel technology with great potential. As a step towards commercialization, hydrate promoter models should be developed.

3.3 Transport and Storage of Natural Gas

Transport and storage of gas in hydrate form is concerned with maintaining hydrate phase equilibria (assuming hydrates already have been created). Less space, lower cost and improved safety are examples of benefits of this.Lachet and Béhar (2000) state that transport of gas in hydrate form is an economic alternative to the processes based on liquefaction and compression. This view is also presented in relation to storage by Kelland (1994). This chapter will discuss both gas storage and transport, as they are linked. In order to store gas, it must be transported to the storage location. In relation to the previous section (3.2: CO_2 capture), this section is about the next step in CCS if the gas in question is CO_2.

When it comes to the advantage; less space, this is a result of the high gas concentration of hydrates. Gas storage capacity has been estimated. "The theoretical storage capacity of Structure II hydrate crystals, with complete filling of all cavities, and with no impurities nor inclusions is approximately 191 m^3 of gas per 1 m^3 of hydrates. 5 volume% of impurities or inclusions within the crystals together with 96% occupation of cavities will result in an effective storage capacity of approximately 174 m^3 of gas per 1m^3 of hydrate crystals." (Lachet and Béhar, 2000).

Transportation and storage of gas in hydrate from has a high level of stability. High stability means high safety. There is some stigma against the stability of hydrates, this may be because of speculations in regards to naturally occurring hydrates and global warming, as well as the consequences seen in the oil and gas industry. When it comes to hydrates that are artificially made for transport and storage purposes they are kept within the stability region, meaning that

hydrates as a means of natural gas transport and storage is considered to be safe. Studies from Norway and Russia have shown hydrate stability for up to two years at -5 to -15 °C at atmospheric pressure (Lachet and Béhar, 2000). In order to improve the hydrate stability even more "help" gases may be added to improve the hydrate stability. "Help" gases are referred to as "hilfgases" by Sloan and Koh (2008). Their effect are milder hydrate forming conditions, making hydrate phase equilibria easier to maintain. Help gases are thereby hydrate promoters.

Regardless of adding a hydrate promoter or not, the chemical nature of hydrates make them a safer means of storing (and transporting) natural gas compared to the more conventional liquefied natural gas (LNG) and compressed natural gas (CNG). The crystal matrix of a hydrate must melt before gases are released, meaning that an explosive release of gas is inhibited. The latent energy of the crystal matrix, that must be overcome, is high. This means that if a hydrate mass is ignited it will burn slowly and not explode. Explosion risks are higher in the case of LNG and CNG. In terms of transportation, gas hydrates will not be "lost" by flowing out of a ship or a pipeline if a hole appears as a result of damage. (Lachet and Béhar, 2000)

When it comes to costs, the operating conditions for generating hydrates, which are close to ambient, bring low costs compared to LNG and CNG. LNG requires very low temperatures, whereas CNG requires very high pressure. Both these extremes require extra energy. A comparison between LNG, CNG and natural gas in hydrate form in terms of operating conditions is displayed in figure 3.4. Gudmundsson and Borrehaug (1996)

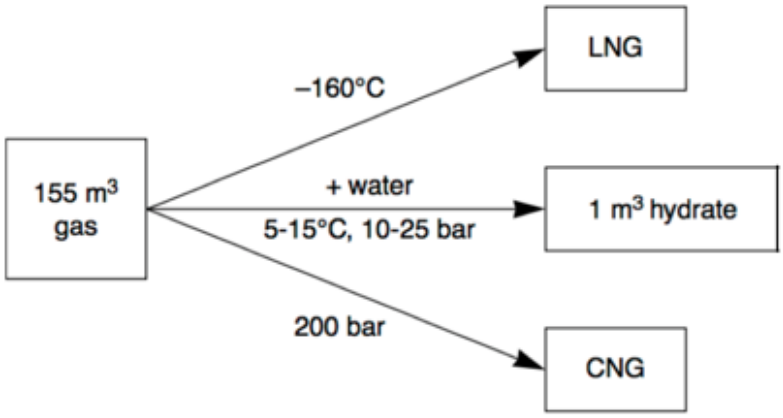

Figure 3.4: Comparison of gas hydrates, LNG and CNG (Lachet and Béhar (2000), based on Kelland (1994).

Gudmundsson and Borrehaug (1996) were influential in showing that gas transport in hydrate form has advantages, estimating that the capitol cost of natural gas hydrates technology could be less than that of LNG. The estimate incorporated production/liquefaction, shipping and regasification costs. The discussion of whether transporting natural gas hydrates in pipelines or ships is economical is highly relevant today, as it is stated to be especially cost effective for scattered, remote and limited high well-pressure gas field (Sun, 2009). Such challenging fields are of growing interest. The technology for natural gas to be transported and stored in hydrate form has not yet been fully developed, bringing challenges. The fact that current large LNG projects typically have contracts for up to 20 years, does not help (Dawe, 2003). The transport of natural gas in slurry pipelines or in a pelletized form are suggestions of means of realizing the technology. Together with the addition of hydrate promoters, efficiency is believed to be increased significantly.

Chapter 4

Predicting Hydrate Phase Equilibria

All hydrate based technology requires hydrate formation to occur. Being able to predict hydrate phase equilibria is thereby crucial. As mentioned, the interest in hydrate avoidance has led to development of phase equilibria models for pure hydrates, and later also for hydrates with added inhibitors. The development of phase equilibria models has resulted in the development of software used in the industry today. Petrowiki (2015b) presents two types of commercial software:

- "Those which enable the prediction of the pressure and temperature at which hydrates begin to form (incipient hydrate formation programs)."
- "Those which predict all phases and amounts at higher pressures and lower temperatures than the incipient hydrate formation point (flash programs, or Gibbs energy minimization programs)."

The aim of the modelling presented in this thesis is to develop a simple model of the first kind, an incipient hydrate formation program, for a hydrate promoter. Note that a model is to be developed and not a software. "The hydrate flash program usually is so complex as to require two or more man-years of single-minded effort to construct a robust version of the program" (Petrowiki, 2015b), meaning that it is not within the scope of a master thesis. Both types of models are based on a hydrate equation of state (EOS). An EOS is a simplified mathematical model that calculates thermodynamic properties and the equilibria state (Petrowiki, 2015a). The starting point for the developed model, a CO_2 equilibria curve by the software CSMGem, is based on

an EOS. The final model for CO_2/ TBAB phase equilibria is purely based purely on experimental data.

Considering the large effort required (especially with the second type) readily available commercial software is often used for phase equilibria prediction. In 1959 the first statistical model for phase equilibria of hydrates was developed. It included many assumptions such as constant volume. The software was to be used in the oil and gas industry, and it worked reasonably well for predicting hydrate formation temperatures near the ice point and at low pressures. With the development of the industry to drill in deeper waters, an improved software was however needed. CSMGem, which has been used for CO_2/ TBAB modelling purposes, became a solution. "CSMGem is a program written for the prediction of the thermodynamically stable hydrate structures and cage occupancy at given pressure, temperature and composition conditions by minimization of the Gibbs free energy of the specified system" (Center for Hydrate Research CSM, 2015). CSMGem is developed at The Colorado School of Mines. It relaxes the constant volume assumption, and is tailor made to cover a range of situations that occur in the oil and gas industry today, as its pressure and temperature range corresponds to that found in subsea pipelines (temperatures above ice-point and pressures up to approximately 100MPa). (Center for Hydrate Research CSM, 2006)

There is no known available software and few available models for determining phase equilibria when adding hydrate promoters, suggesting that modelling efforts should be made. The work in relation to this master thesis has resulted in the development of a model for phase equilibria of CO_2 hydrates in aqueous solutions of TBAB. Modelling was carried out in Matlab. This chapter will present the modelling procedure, including results and discussion. The aim and the hypothesis of the model is presented and commented on throughout the discussion. The hydrate promoter to be modelled, TBAB, will be briefly presented prior to this. Experimental data and a collection of scripts that show the modelling procedure, are found in the appendices, in addition to some plots that are not included in the thesis itself. Small extracts of code are found in the thesis. Throughout the thesis four decimals figures are most frequently used, as the final model has four decimals. In Matlab the exact values are used, for increased accuracy.

4.1 TBAB

Before going on to the modelling procedure, the hydrate promoter that has been modelled, will be briefly presented. Tetrabutylammonium bromide (TBAB) is a quaternary ammonium compound with the molecular formula $C_{16}H_{36}BrN$ and the molecular weight 322.375 g/mol (PubChem, 2005). TBAB's 2D chemical structure is displayed in 4.1. Note that each discontinuity in the line between N^+ and H_3C corresponds to a carbon (C) atom bonded to the associated hydrogen (H) atoms of a hydrocarbon structure. Figure 4.1 gives a visual representation of TBAB's linear formula $(CH_3CH_2CH_2CH_2)_4N(Br)$. TBAB has a range of industry uses, for example agricultural chemicals (non-pesticidal) and process regulators, as well as hydrate promotion which the developed model will justify.

TBAB takes part in hydrate formation, in the sense that semi-clathrate (SC) hydrates are formed. "Semi-clathrates compounds are formed in the presence of tetra-n- alkyl ammonium halides (bromide, TBAB; chloride, TBAC; or fluoride, TBAF) in the system and are not exactly similar to gas hydrates structures but share many of the physical and structural properties as true clathrate hydrates." (Joshi et al., 2012). Halide ions form hydrogen bonds with water molecules, forming cages. The cages are partly occupied by the tetra-n- alkyl cation (4 cages) and the rest by the guest gas. (Joshi et al., 2012)

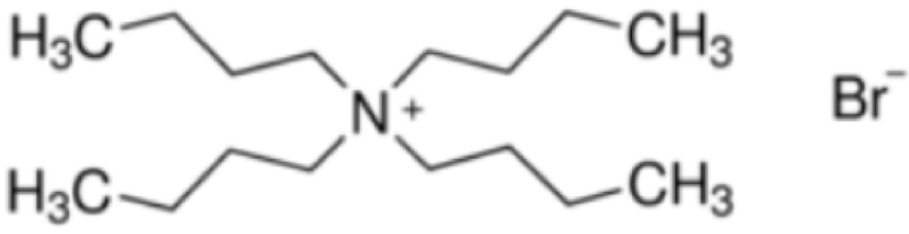

Figure 4.1: TBAB's 2D chemical structure (Sigma-Aldrich).

4.2 Selecting a CO_2 Hydrate Phase Equilibria Model

Selecting a CO_2 hydrate phase equilibria model was the first step of the modelling procedure. The selected model was obtained by an exponential fit of the data points from a CSMGem simulation. CSMGem is simple to use, and does not require a lot of inputs. It is known to produce reasonably accurate results, and it is widely used in the oil and gas industry today. For convenience CSMGem will be referred to as CSM. Phase equilibria was calculated for the condition: "incipient hydrate formation pressure at fixed temperature", with the inputs displayed in table 4.1. The opposite is also possible (specifying the pressure). The software interface is displayed in fig. 4.2, where a simulation for pure CO_2 has been carried out.

Table 4.1: CSM inputs for generation of CO_2 phase equilibria curve.

T [K]	275
Mol%feed+water	10
Plot	Specify phase boundary-sI hydrate
Pressure [MPa]	0.5 (lower), 80 (upper)
# of intervals	100

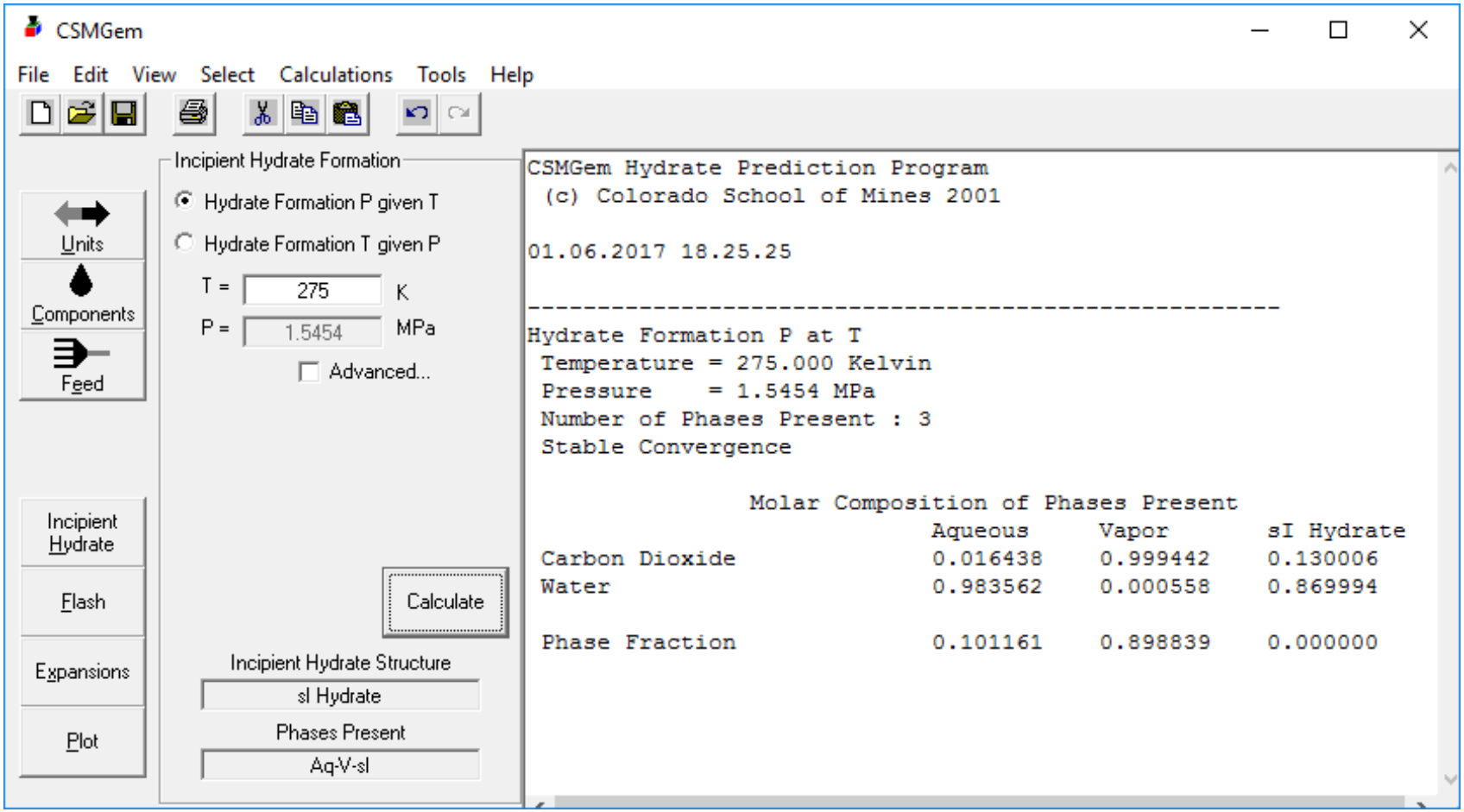

Figure 4.2: CSM interface.

CSM can be used in conjunction with MSExcel, automatically producing plots in MSExcel when a simulation is run. For convenience regarding further modelling all plotting was done is Matlab. The CSM data was saved as comma separated value (CSV) files, which can be loaded in Matlab. Matlab reads CSV files as matrices. The matrices from the loaded data had two columns (temperature, pressure). The CSM simulation results are displayed in Appendix A, and a graphical representation is seen is fig. 4.3.

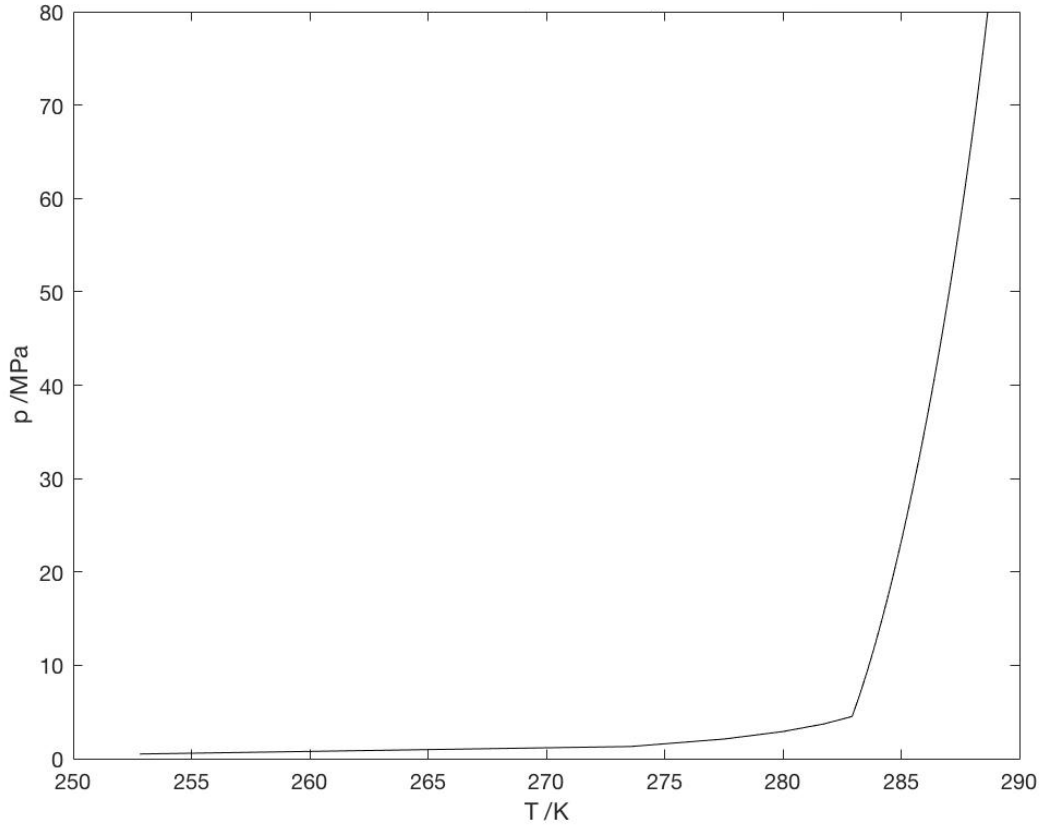

Figure 4.3: CO_2 phase equilibria by CSM.

Considering the pressure range of the collected experimental CO_2/ TBAB phase equilibria data (see appendix A), the upper limit of the pressure range was changed to 5 MPa. A new simulation was done in CSM, the input values (table 4.1) were the same except for the upper pressure limit.

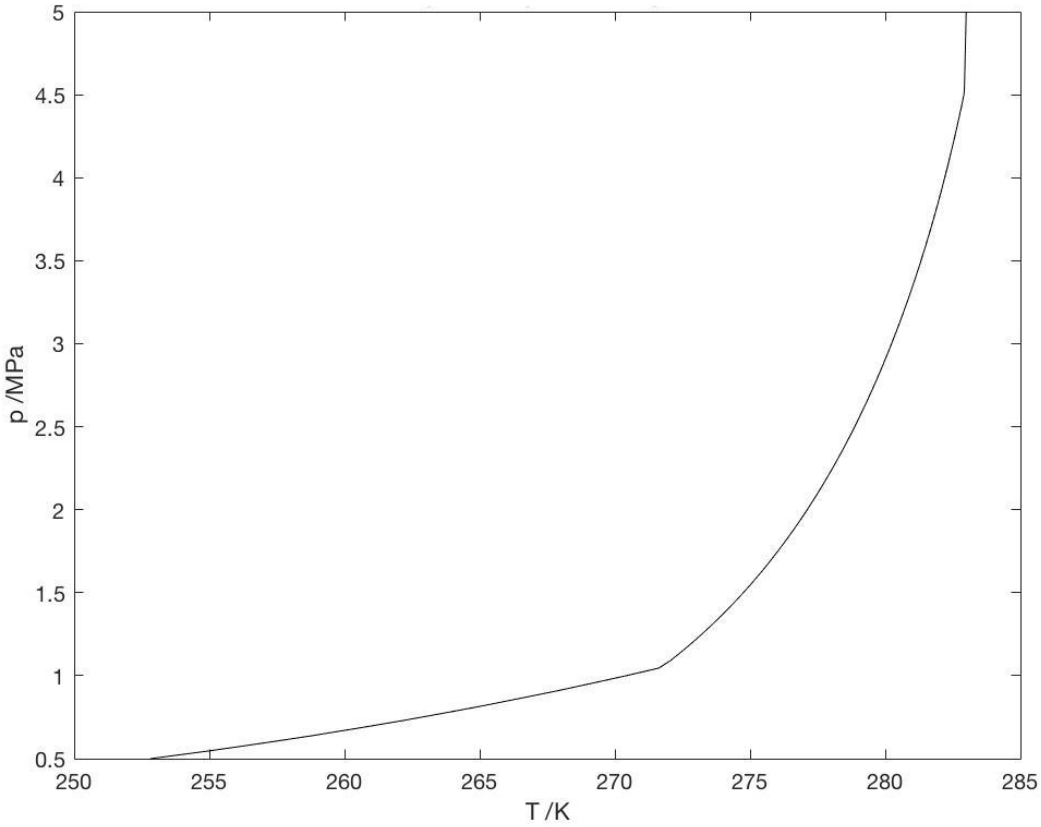

Figure 4.4: CO_2 phase equilibria by CSM with upper pressure limit 5 MPa.

Two clear discontinuities are observed, one at approximately T=272 K and one at approximately T=283 K. The discontinuities suggest phase change; Q_1 at T≈ 272 K and Q_2 at T≈ 283 K. Q_1 is the lower quadruple point (the boundary between I-H-V and L_W-H-V) and Q_2 is the upper quadruple point (the boundary between L_W-H-V and L_W-H-L_{HC}) (Sloan and Koh, 2008). $L_{W/\ HC}$ stands for liquid water/ hydrocarbon, H stands for hydrate and I stands for ice. The main area of interest for modelling of CO_2/ TBAB phase equilibria is the area between Q_1 and Q_2. The x-coordinates of Q_1 and Q_2, were found by plotting the CSM results in MSExcel and moving the cursor along the curve. The accuracy of this method is satisfactory. The obtained results are T=271.622 K Q_1 and T=282.911 K Q_2. The equilibria curve was plotted again for the range between Q_1 and Q_2.

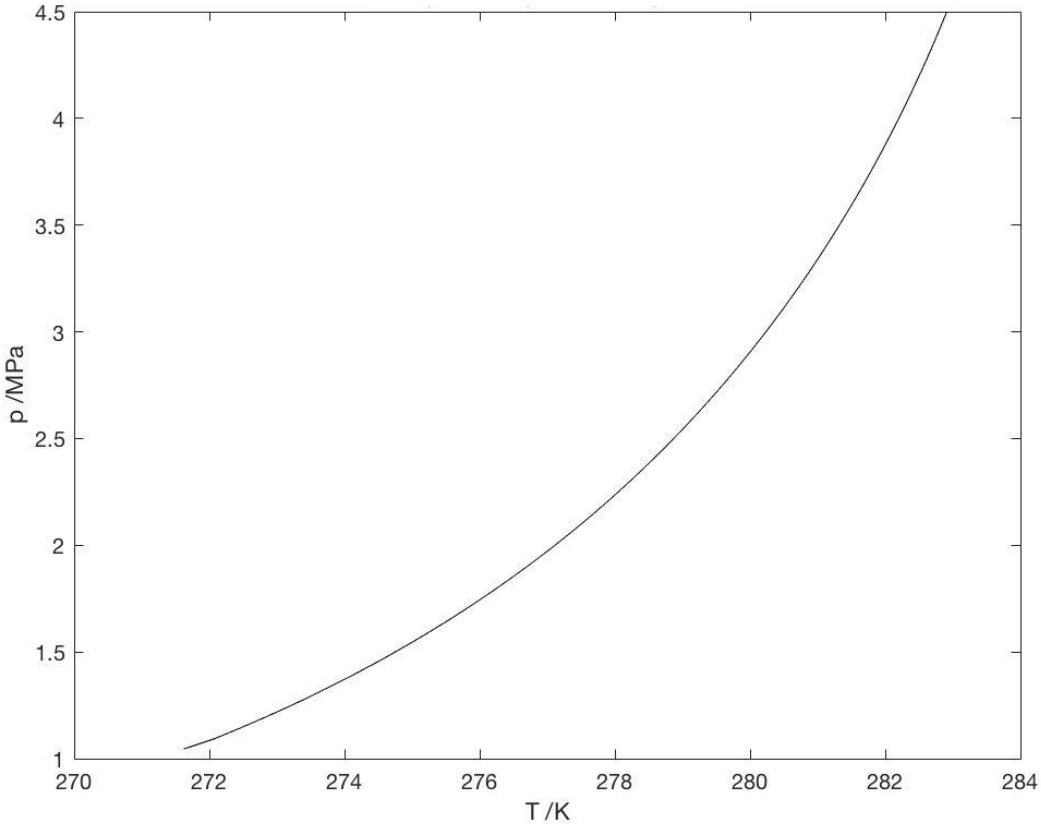

Figure 4.5: CO_2 phase equilibria between Q_1 and Q_2.

Further work required a model for the CO_2 phase equilibria curve. A polynomial and an exponential fit was tested. The choice to test polynomial and exponential fits was based on visual observation. The fits were generated in Matlab.

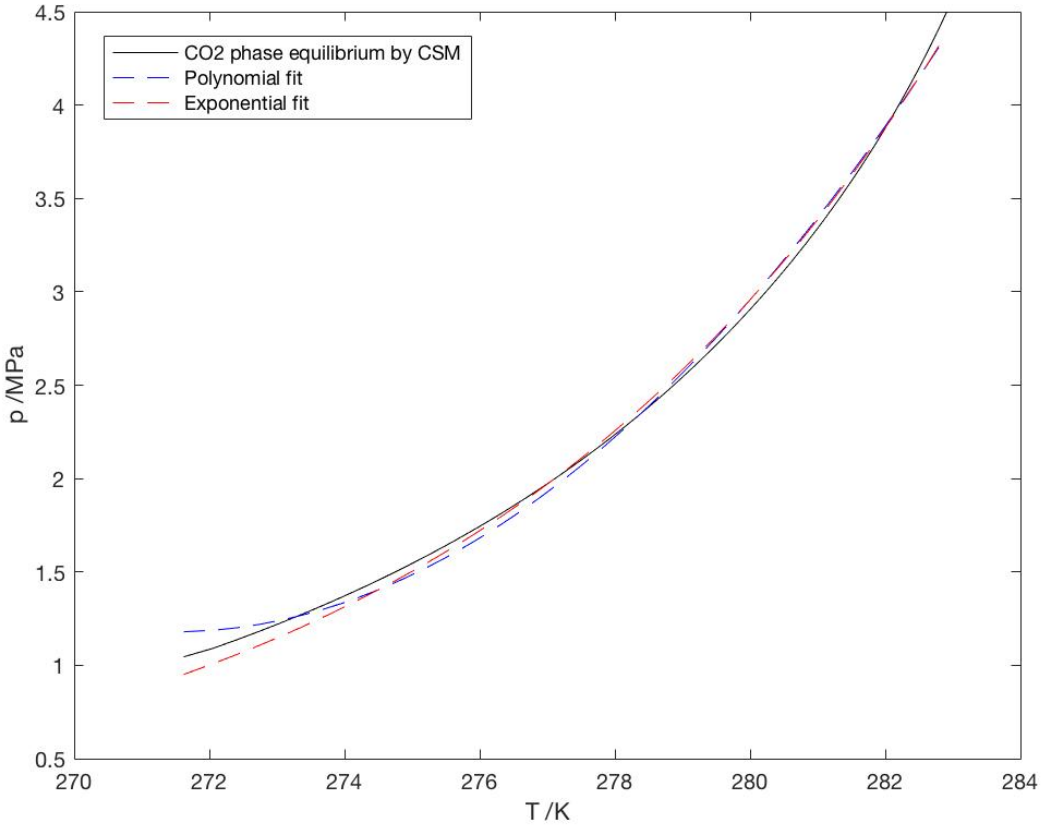

Figure 4.6: CO_2 phase equilibria with fits.

Running the script CO2_phase_eq_with_fits.m (see appendix B) gives the fit coefficients, R^2 and the "root mean square error", as well as a table with the columns: temperature, pressure, fit pressure and the fit error. R^2 (the coefficient of determination) is a measurement of how close the data is to the fitted curve, and is a commonly used variable in statistics. The code for R^2 was taken from an example code (Wells, 2012). The example code is displayed in appendix B.

Considering the R^2 values: $R^2_{polynomial}$= 0.9973 and, $R^2_{exponential}$=0.9977 it becomes clear that both fits are accurate. As the exponential fit was the best fit it was selected as the CO_2 phase equilibria model to be used for further modelling. The exponential fit was found by the Matlab function "fit", which requires specification of function and degree (exponential, first). Matlab provides the coefficients with 95% confidence bounds. The output is displayed:

```
exp_fit =

     General model Exp1:
     exp_fit(x) = a*exp(b*x)
     Coefficients (with 95% confidence bounds):
       a =   1.015e-16  (5.086e-17, 1.521e-16)
       b =      0.1354  (0.1336, 0.1372)
```

From this, the CO_2 phase equilibria model to be used as the starting point for CO_2/ TBAB phase equilibria modelling is defined as:

$$p(T) = (1.015 \times 10^{-16}) e^{0.1354T} \tag{4.1}$$

where p is pressure and T is temperature. Note that the CO_2 phase equilibria data generated by CSM was checked against tabulated data in Sloan and Koh (2008), before proceeding. See fig. 4.7. The CSM simulation result is accurate (the experimental data points are close to the CSM curve), providing validity for the CO_2 model (eq. 4.1).

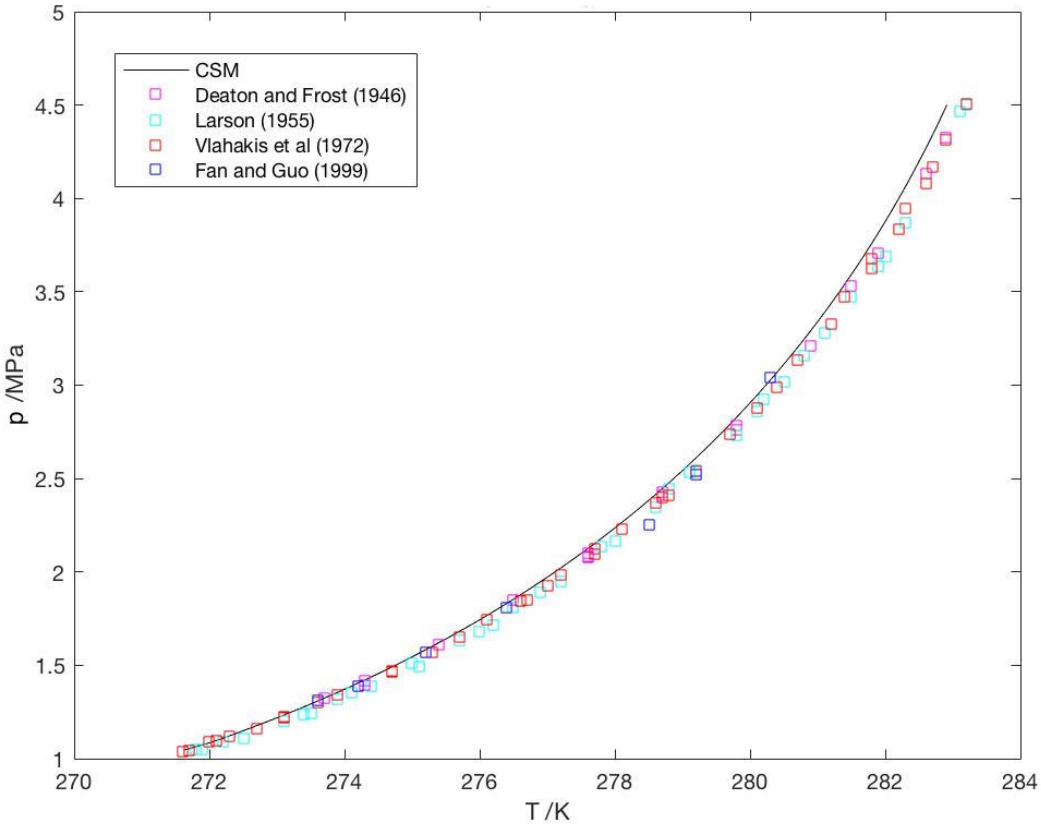

Figure 4.7: CO_2 phase equilibria by CSM and experimental data tabulated in (Sloan and Koh, 2008).

4.3 Data Collection and Processing

The next step was to collect experimental CO_2/ TBAB hydrate phase equilibria data. Dashti et al. (2015) refers to several relevant papers. Such as Mohammadi et al. (2011). Mohammadi et al. (2011) presents a catalogue of some available experimental data for CO_2/ TBAB hydrates. The collected data is presented in table 4.2 and fig. 4.8. Considering figure 4.8 modelling seems reasonable, as trends are apparent. Note that uncertainties are not listed for most of the papers, and will not be a large part of the discussion as only the results of the experiments and not the experiments themselves, have been considered. Another reason is that the different uncertainties from the different experiments are likely to cancel each other out. The abbreviation wt% is used for weight%, and always refers to weight% TBAB. The term phase equilibria always refers to hydrate phase equilibria.

Table 4.2: Collected CO_2/ TBAB phase equilibria data.

Paper	TBAB Concentration /weight%
Mohammadi et al. (2011)	5, 10, 16.7, 25, 35, 50
Ye and Zhang (2012)	5, 10, 19, 32, 55
Long et al. (2016)	1.76, 14
Verrett et al. (2015)	5, 10, 40
Deschamps and Dalmazzone (2009)	40
Arjmandi et al. (2007)	10, 42.7
Duc et al. (2007)	5, 10, 40, 65
Lin et al. (2008)	4.43, 7.02, 9.01

Some of the collected data gave TBAB concentration in mol%. This data was converted to wt%. The simple conversion from bar to MPa was also done for a few data sets.

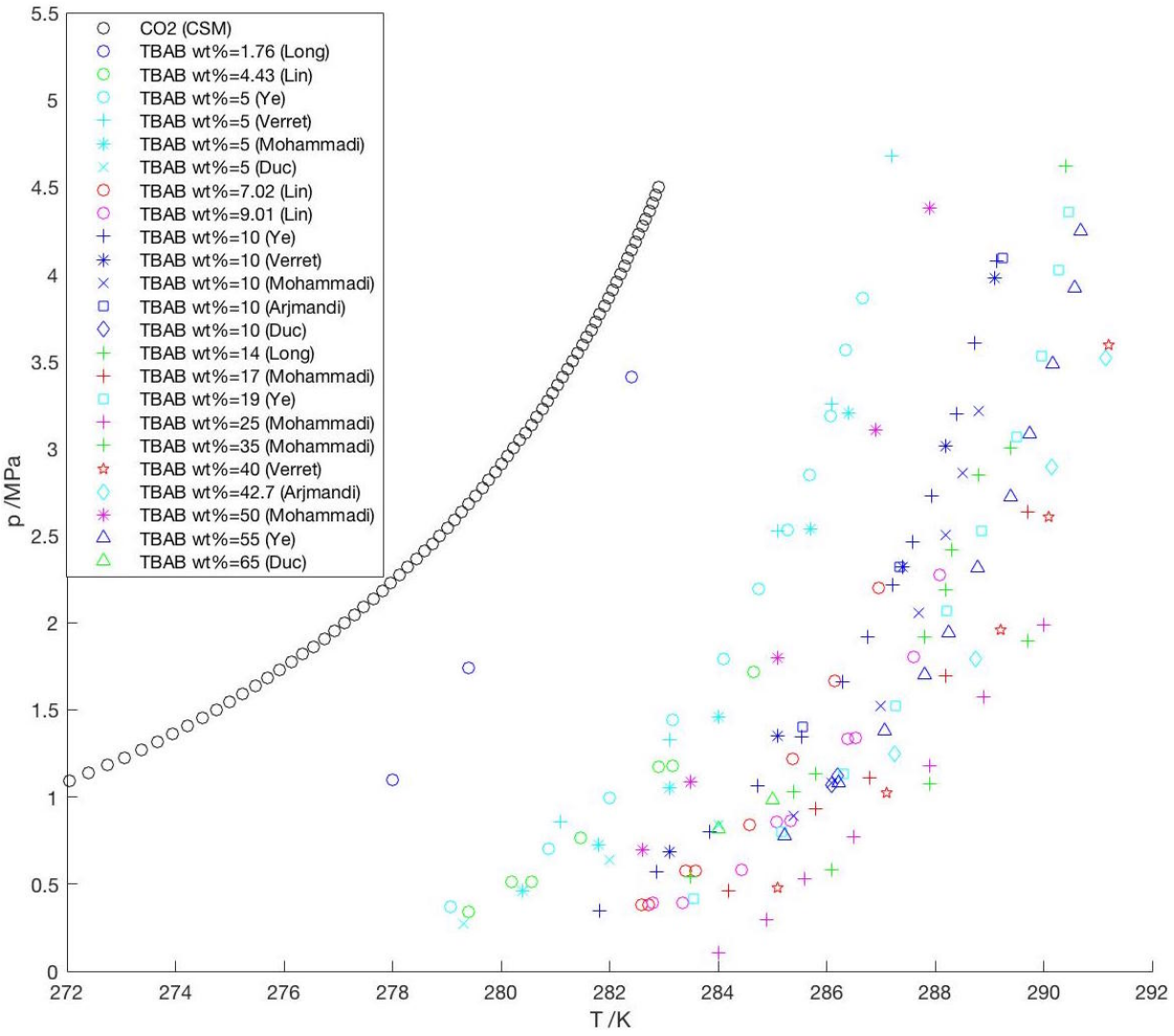

Figure 4.8: Collected CO_2/ TBAB phase equilibria data. Data for a given concentration is plotted in the same colour. CO_2 (CSM) refers to CSM data points, and not the modelledCO_2 curve.

Data from the different papers were plotted separately. Each plot includes the CO_2 equilibria curve (eq. 4.1), empirical data points and an exponential fit of experimental data points. R^2 was calculated for all exponential fits by using the function “rsqaure”. An exponential fit was chosen as the CO_2 phase equilibria model is an exponential function, and the shape of the CO_2/ TBAB phase equilibria curve is believed to be similar. The initial hypothesis was that CO_2/ TBAB phase equilibria curves are horizontal shifts of the CO_2 phase equilibria curve. All plots are displayed, with a short discussion following. The plots are presented in the order of table 4.8.

Mohammadi et al. (2011)

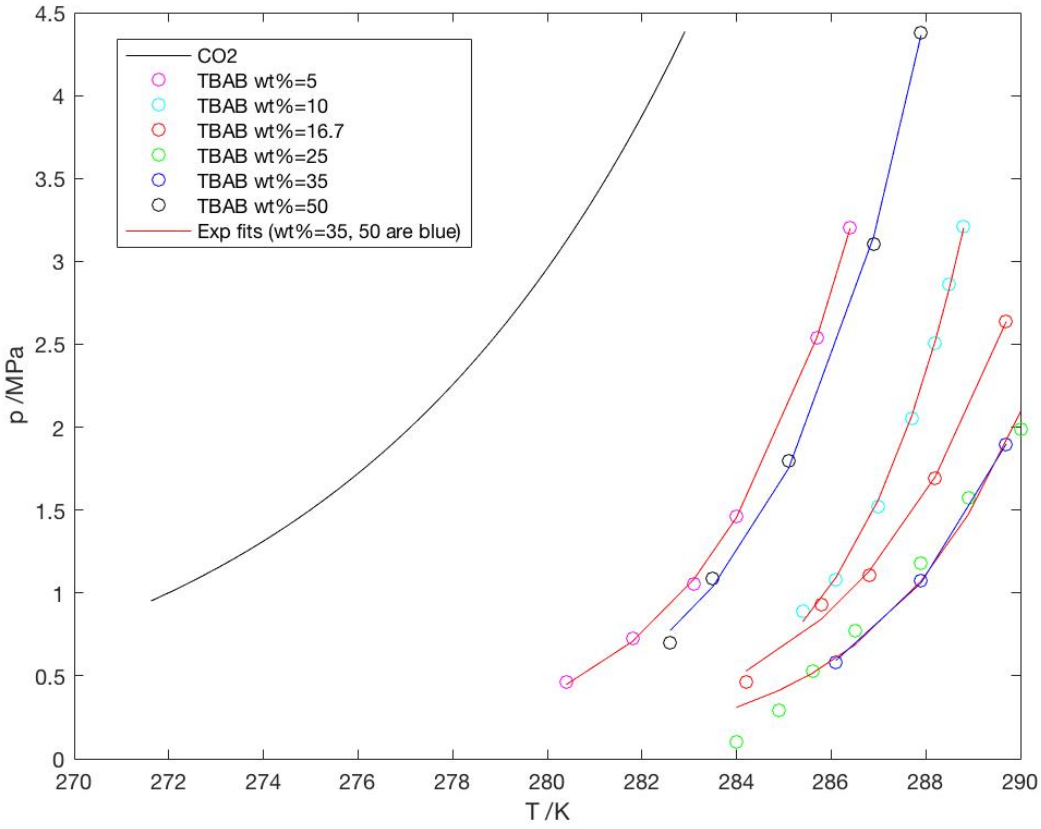

Figure 4.9: CO_2/ TBAB hydrate phase equilibria. Data from (Mohammadi et al., 2011).

R^2 values are > 0.99, except for R^2 for 25 wt% where R^2=0.967. This means that the exponential fits are good fits. This is as expected considering the horizontal shift hypothesis. Note that the shift is believed to be to the right, opposite of the inhibitor phase equilibria curves, which are shifted to the left. The shift is expected to be of increasing length until a limit has been reached, the limit being decided by the concentration corresponding to maximum cavity occupation. Modelling will test this hypothesis.

Although all exponential fits are good fits, it does not mean that the horizontal shift hypothesis is confirmed. The shapes of the CO_2/ TBAB phase equilibria curves are different to CO_2 phase equilibria curve. The hypothesis would be confirmed if the curves had the same shape, but with varying shift to the right (the greater the concentration, the greater the shift). Note that concentrations higher than 40 wt%, are not expected to follow this trend, as the hydration num-

ber has been exceeded. Hydration number is related to maximum cavity occupation. Excess TBAB is believed to inhibit and not promote hydrate phase equilibria.

Considering fig. 4.9 the 5 wt% TBAB curve and the 10 wt% TBAB curve have a similar shape (based on visual observation). The 50 wt% curve also has a similar shape to 5 wt% and 10 wt%, but it is not within the range of the model. In addition to this a similar shape is observed for 16.7 wt% and 25/35 wt% curves. The curves corresponding to wt% 25/35 are nearly the exact same, this is not in agreement with the hypothesis that the greater the TBAB concentration (until the limit of 40 wt%), the greater the horizontal shift (to the right) of the phase equilibria curve. As wt% 35 is close to the upper limit of the concentration range, a possible explanation for the result is that the effect of adding too much TBAB has taken place. It is hard to define the exact upper concentration limit, as the maximum cavity occupation based on the hydration number of TBAB is a theoretical value, and may not be the case in this experimental setting. In addition to this, the assumption that only type A is present is a simplification.

The exponential fits in blue are interesting: 35 wt% due to what already has been discussed and 50 wt% as it is past the concentration that corresponds to the theoretical maximum cavity occupation (the upper concentration limit). The equilibria curve for 50 wt% is moved to the left, agreeing with the hypothesis.

Running the script CO2_TBAB_3_fits.m in appendix B gives all exponential fit equations and associated R^2 values. As all data in table 4.2 was collected and plotted before starting the modelling of the CO_2/ TBAB hydrate phase equilibria, the equations of the exponential fits are not part of the discussion at this point. Exponential fits are merely plotted to check if the data follows an exponential trend (as was hypothesized) and to get an idea of if the shapes are similar. The script for plotting the data by Mohammadi et al. (2011), CO2_TBAB_Mohammadi, is provided in appendix B as an example. The scripts for plotting the other collected data are of the same form, and not included. All experimental data is tabulated in appendix A.

Ye and Zhang (2012)

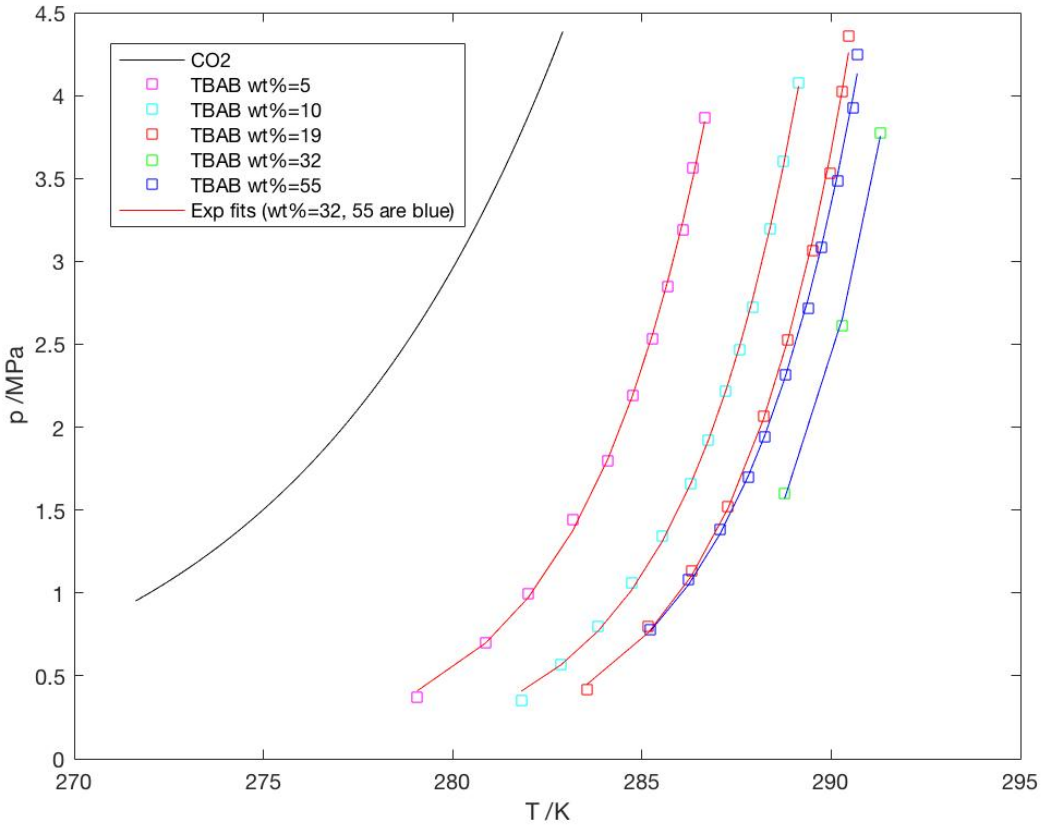

Figure 4.10: CO_2/ TBAB hydrate phase equilibria. Data from Ye and Zhang (2012).

Data from Ye and Zhang (2012) can be fitted well to exponential functions. Note that the data for 32 wt% may be over-fitted as there are only three available data points. For all concentrations R^2 > 0.99. The shapes of the different curves are similar, suggesting that modelling would be fairly simple. Note that the shape of the CO_2/ TBAB curves appears to be different from the CO_2 curve. This questions the hypothesis that the CO_2/ TBAB curve is a horizontal shift of the CO_2 curve. When it comes to 32 wt% it is hard to draw a conclusion about its shape.

The curves corresponding to 19 wt% and 55 wt% are very similar, so they were plotted in different colours to be able to distinguish them. 55 wt% is expected to have felt the effect of adding too much TBAB. As with the data from Mohammadi et al. (2011) (see fig. 4.9) the data from Ye and Zhang (2012) gives evidence for the fact that too much TBAB has a negative effect.

The shift to the left for 55 wt% is however significantly less than the shift to the left for 50 wt% by Mohammadi et al. (2011). The fact that there are so few available data points for the second largest concentration (32 wt%) makes it hard to evaluate how much the curve for 55 wt% is shifted. The effect of exceeding the upper limit of the concentration range is interesting to study, but as the aim of this thesis is to develop a model for TBAB as a hydrate promoter, it will not be the main focus.

Long et al. (2016)

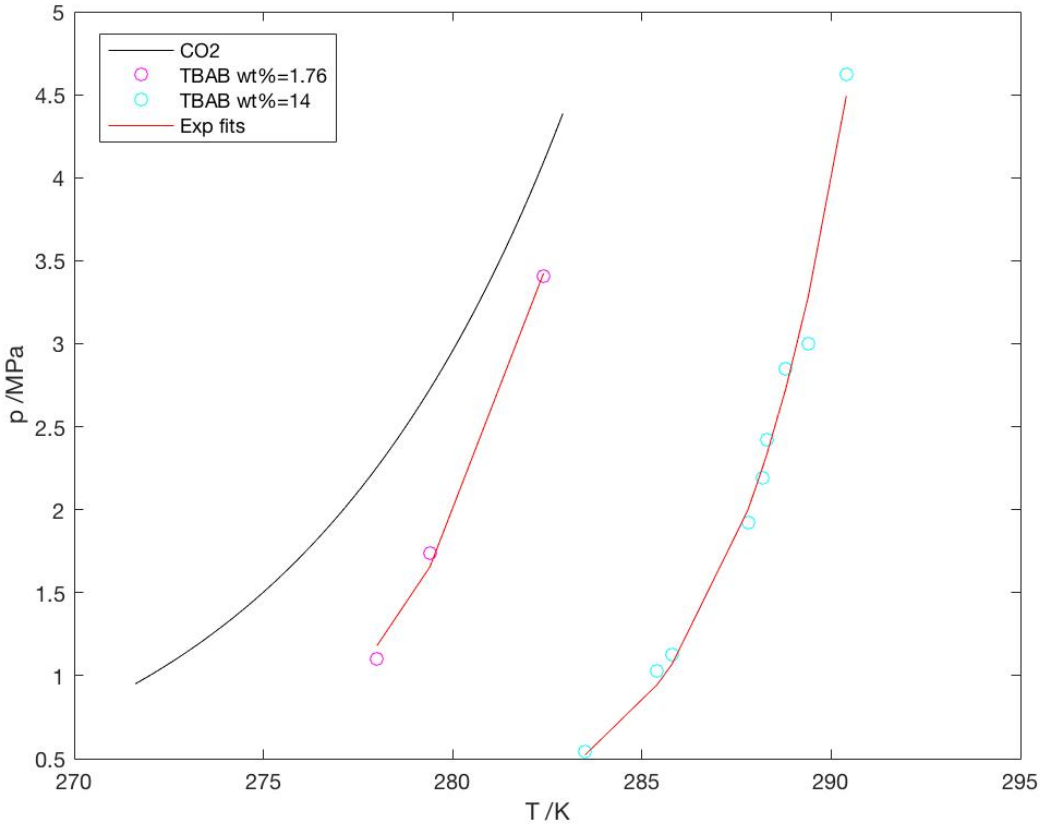

Figure 4.11: CO_2/ TBAB hydrate phase equilibria. Data from Long et al. (2016).

Data from Long et al. (2016) may suffer from overfitting, as there are only three available experimental data points for one of the concentrations. As there is only one concentration that should be considered for discussion, there is not a lot to discuss, as there is no basis for comparison.

Verrett et al. (2015)

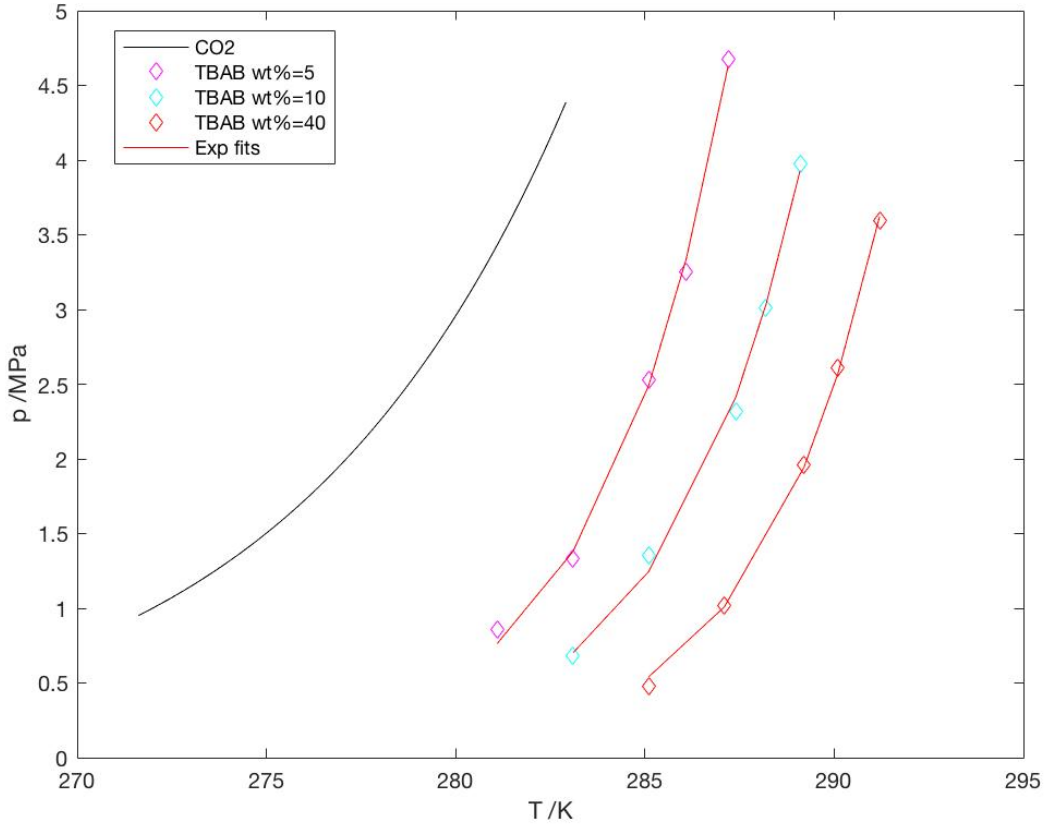

Figure 4.12: CO_2/ TBAB hydrate phase equilibria. Data from Verrett et al. (2015).

All the exponential fits have an R^2 value > 0.99. The shape of the fits are similar based on visual observation. The data also suggests that a simple horizontal shift from CO_2 phase equilibria is not sufficient to model CO_2/ TBAB phase equilibria. The shape of the different CO_2/ TBAB phase equilibria curves appear to be similar, suggesting that modelling should still be carried out. For Verrett et al. (2015) data 40 wt% seems to be on the boundary i.e. at maximum cavity occupation, leading to maximum promotion effect. Increasing the wt% is expected to result in a curve shifted to the left. Uncertainties are presented by Verrett et al. (2015): u(T)=0.1 K and u(P)=0.009 MPa, but as mentioned they will not be a large part of the discussion, as only the results of the experiments have been considered.

Deschamps and Dalmazzone (2009)

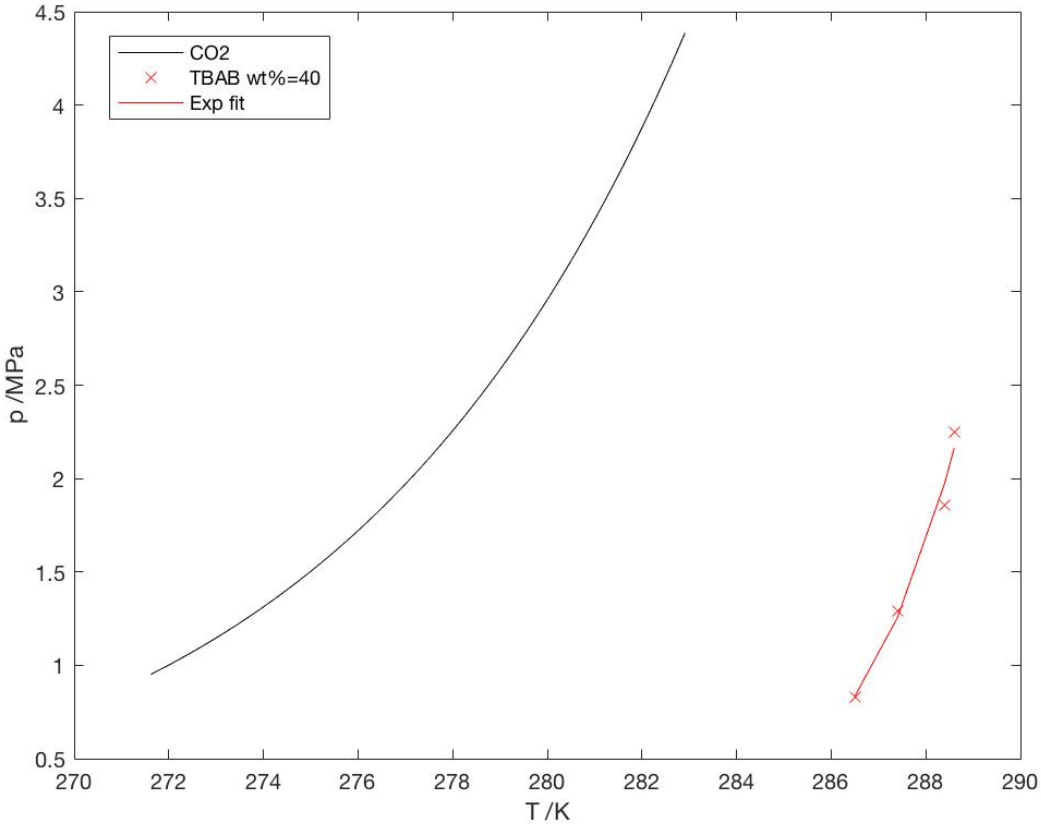

Figure 4.13: CO_2/ TBAB hydrate phase equilibria. Data from Deschamps and Dalmazzone (2009).

The exponential fit is a good fit, but ideally there should be more data points. When it comes to shape, there is nothing to compare with (except for CO_2) as only data for one concentration is presented by Deschamps and Dalmazzone (2009). The curve will be compared to data from other experiments later, but from visual observation, comparing it to the other plots in this section, it appears to be at (or before) maximum cavity occupation. This provides evidence for the hypothesis about the promotion range.

Arjmandi et al. (2007)

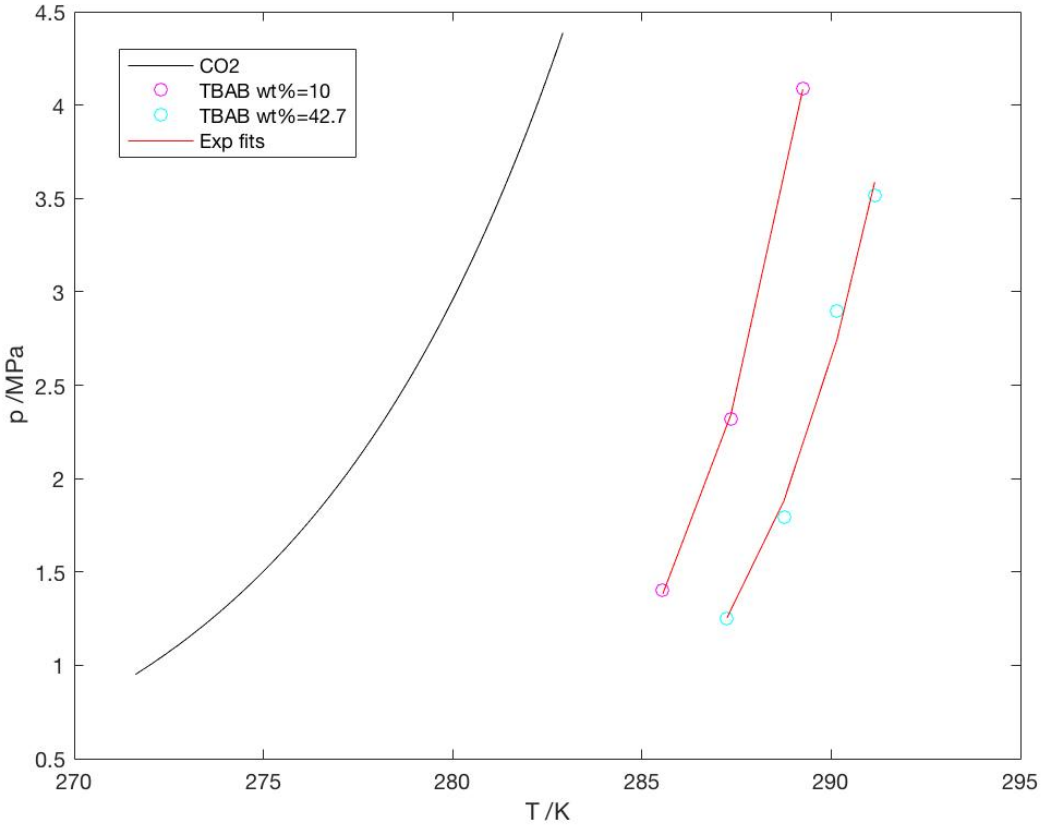

Figure 4.14: CO_2/ TBAB hydrate phase equilibria. Data from Arjmandi et al. (2007).

There are few available data points meaning that overfitting may be an issue. Plotting the data from Arjmandi et al. (2007) with data from other papers would allow for evaluation of this. TBAB wt% 42.7 does not seem to have experienced the effect of exceeding maximum cavity occupation, this shows that the exact upper limit is hard to quantify. However it is hard to draw a conclusion on whether 42.7 wt% causes a very high promotion effect when there is no available data for the concentrations between 10 wt% and 42.7 wt%.

Duc et al. (2007)

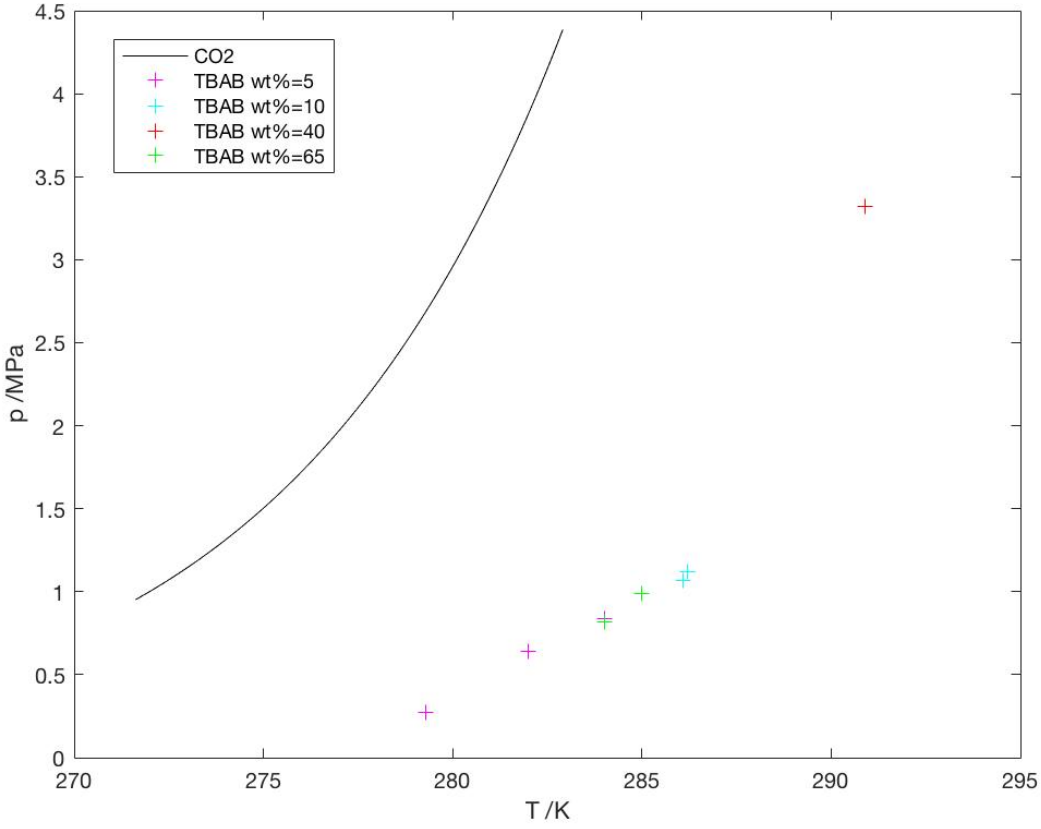

Figure 4.15: CO_2/ TBAB hydrate phase equilibria. Data from Duc et al. (2007).

As there are so few available data points, data from Duc et al. (2007) will not be considered for modelling. There is little value in studying exponential fits. The plot is however included, as the presented data may be used to test the final model.

Lin et al. (2008)

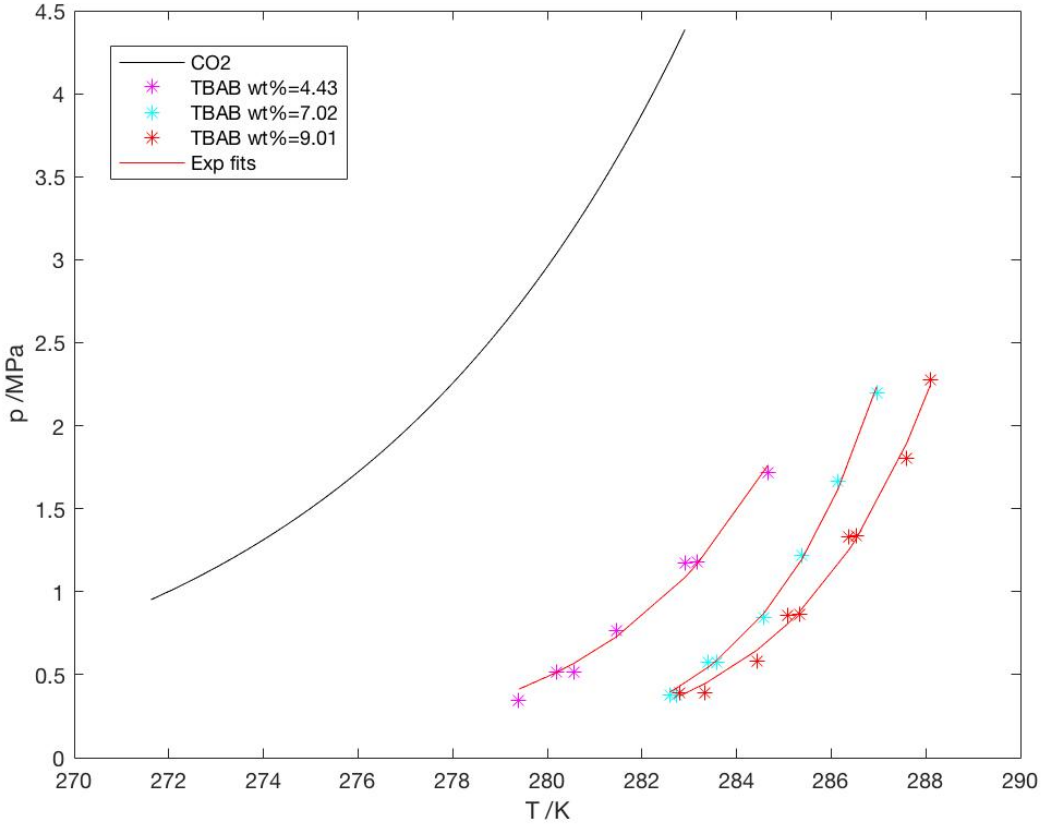

Figure 4.16: CO_2/ TBAB hydrate phase equilibria. Data from Lin et al. (2008).

Exponential fitting is very successful, and it does not suffer from overfitting (the number of data points is satisfactory). The shapes of the exponential curves are somewhat similar, but the curves 4.43 wt% and wt 9.01 % appear to be the most similar. The concentration range is narrow and low-value. As most of the collected data has a wider concentration range, the development of the final model will be based on a wider concentration range. This means that the accuracy of the model with low concentration inputs, may suffer.

Once the presented data had been collected and plotted, further data processing could begin. As much data as possible was collected as the more available data, the better the starting point for modelling. Note that many of the considered papers are recent, showing that it is an area of interest today. In addition to this there are small chances that opposing results have been found since publishing. The next step was to gather data from a given TBAB concentration. The data for a given concentration was then plotted together with an exponential fit by Matlab for the gathered data. This was carried out for 5, 10 and 40 TBAB weight%. The exponential fit functions are displayed in section 4.4: Modelling (4.3, 4.4 and 4.5), and they are to be used for modelling (the exponential fit functions for 5, 10 and 40 wt% phase equilibria are what the modelled curves should overlap). The choice to model these curves was based on: amount of available data (several sources) and the accuracy of the fit. The fact that the shapes of the fits were somewhat similar is ideal. The collection of data points and the exponential fits for the collection of data points for all three concentrations are seen in figure 4.17. The range being wt% 5 and wt% 40 meant that the hypothesized promotion range was seen as covered (pure CO_2 was also to be used for modelling).

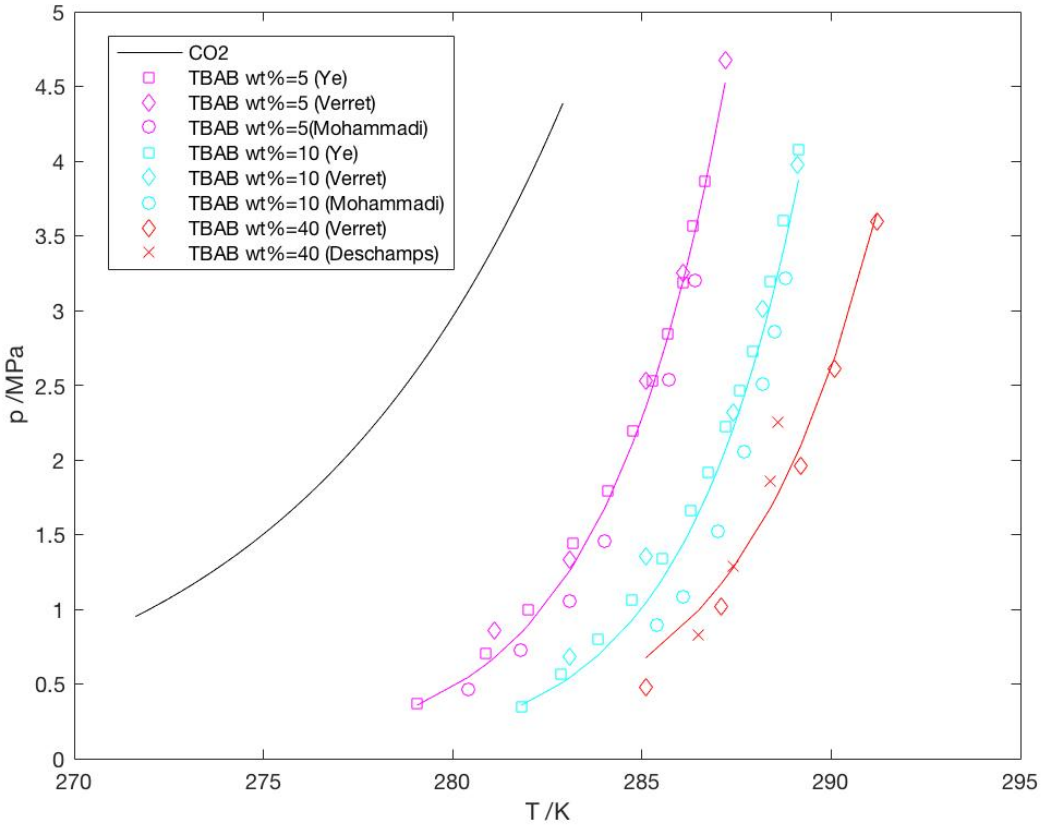

Figure 4.17: CO_2/ TBAB hydrate phase equilibria. . Solid lines are exponential fits. Data from: Mohammadi et al. (2011), Ye and Zhang (2012), Verrett et al. (2015) and Deschamps and Dalmazzone (2009).

The exponential fits are satisfactory based on visual observation and R^2 values (see table 4.3). When it comes to the data for 10 wt% TBAB phase equilibria it is clear that the data from Mohammadi et al. (2011) is on the opposite side of the exponential fit compared to the other data points. Nevertheless, the R^2 of the collection of data for 10 wt% phase equilibria is satisfactory. The R^2 of the collection of data for 40 wt% phase equilibria is slightly lower than that for the collection of data of 10 wt% phase equilibria. More experimental data for 40 wt% phase equilibria is desired. In terms of the shape of the curves 5 wt% phase equilibria and 10 % phase equilibria appear to be more similar. Whereas 40 wt% phase equilibria appears to be similar to CO_2 phase equilibria. 5 wt% phase equilibria has the best fit and 40 wt% phase equilibria has the worst. The curves in figure 4.17 is what the model should produce for 5 wt%, 10 wt% and 40 wt% phase equilibria.

Table 4.3: R^2 of 5, 10 and 40 wt% data.

Weight% TBAB	Data source	R^2 of exponential fit
5	Ye and Zhang (2012)	0.9988
5	Verrett et al. (2015)	0.9975
5	Mohammadi et al. (2011)	0.9998
5	Ye and Zhang (2012), Verrett et al. (2015), Mohammadi et al. (2011)	0.9856
10	Ye and Zhang (2012)	0.9992
10	Verrett et al. (2015)	0.9966
10	Mohammadi et al. (2011)	0.9986
10	Ye and Zhang (2012), Verrett et al. (2015), Mohammadi et al. (2011)	0.9582
40	Verrett et al. (2015)	0.9989
40	Deschamps and Dalmazzone (2009)	0.9811
40	Verrett et al. (2015), Deschamps and Dalmazzone (2009)	0.9510

4.4 Modelling

The modelling procedure will be presented with accompanying discussion. Two approaches were carried out, as the first approach did not result in a satisfactory model. Approach 1 resulted in an implicit model (Model 1) whereas approach 2 resulted in an explicit model (Model 2).

Approach 1

The hypothesis that the CO_2/ TBAB phase equilibria curve is a horizontal shift of the pure CO_2 phase equilibria curve, means that the curves could be expressed as eq. 4.2:

$$p(T) = a^{b(T-c)} + d \tag{4.2}$$

where a, b and d are constants, and c is a function of TBAB concentration. Constant a determines vertical stretching/ compression, constant b determines horizontal stretching/compression, parameter c shifts the graph horizontally and constant d shifts the graph vertically. Note that a positive c shifts the curve to the right. The hypothesis is that d=0. If d$\neq$ 0 for CO_2 or CO_2/ TBAB phase equilibria, the curves are not horizontal shifts of each other. Note that c is termed parameter and not constant as horizontal shifts would involve c not being a constant value. The modelling in this section is based on considering the effect of the different constants/ parameters and trial and error. Considering the validity of the selected CO_2 phase equilibria model (eq. 4.2) and the horizontal shift hypothesis, the value of a and b for the CO_2/ TBAB phase equilibria curves should the same as in the CO_2 phase equilibria model (eq. 4.1). The plotting of the collected data has suggested that this is not the case, as the shape of the CO_2 phase equilibria curve and the CO_2/ TBAB phase equilibria curves appears to be different.

Modelling is based on the CO_2 phase equilibria equation (eq. 4.1) and the exponential fits listed below. Eq. 4.3 is for 5 wt% phase equilibria, eq. 4.4 is for 10 wt% phase equilibria and eq. 4.5 is for 40 wt% phase equilibria. The Matlab outputs are also provided.

$$p(T) = (5.811 \times 10^{-39})e^{0.3118T} \tag{4.3}$$

$$p(T) = (5.689 \times 10^{-41})e^{0.3252T} \tag{4.4}$$

$$p(T) = (3.682 \times 10^{-35})e^{0.2767T} \tag{4.5}$$

```
exp_fit_w5 =
     General model Exp1:
     exp_fit_w5(x) = a*exp(b*x)
     Coefficients (with 95% confidence bounds):
       a =   5.811e-39  (-3.344e-38, 4.507e-38)
       b =      0.3118  (0.2882, 0.3354)

exp_fit_w10 =
     General model Exp1:
     exp_fit_w10(x) = a*exp(b*x)
     Coefficients (with 95% confidence bounds):
       a =   5.689e-41  (-5.851e-40, 6.989e-40)
       b =      0.3252  (0.286, 0.3643)

exp_fit_w40 =
     General model Exp1:
     exp_fit_w40(x) = a*exp(b*x)
     Coefficients (with 95% confidence bounds):
       a =   3.682e-35  (-6.226e-34, 6.962e-34)
       b =      0.2767  (0.2149, 0.3385)
```

Six modelling attempts with approach 1 were done. The modelling attempts will be presented and discussed. Constant values are displayed in headings (subscripts indicate where values are from), and c values are displayed in plots. A Matlab script was made for each attempt. See appendix B for example scripts: APPROACH_1_ATTEMPT_2, APPROACH_1_ATTEMPT_6. The scripts for all the attempts are of the same form.

Attempt #1: a=a_{CO_2}, b=b_{CO_2}

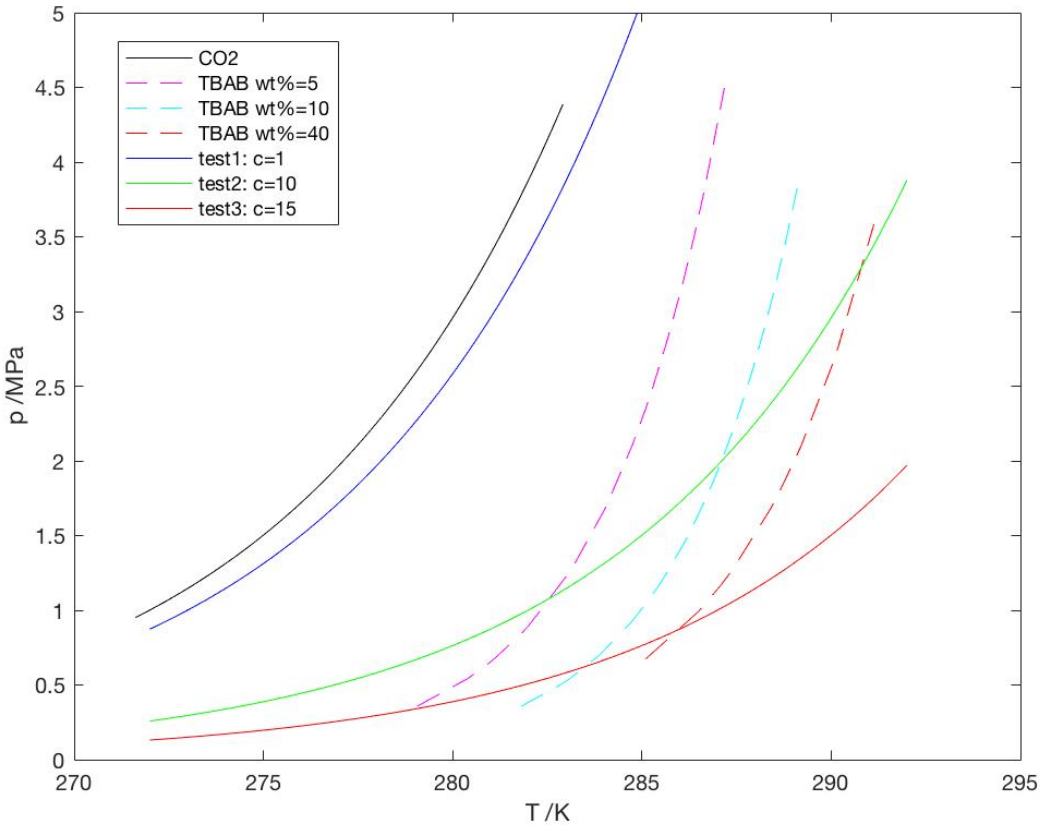

Figure 4.18: CO_2/ TBAB hydrate phase equilibria modelling attempt 1.

Attempt #1 proves that a horizontal shift of CO_2 phase equilibria model (eq. 4.1) is not satisfactory. When the test curves are shifted far enough to the right, they overlap the phase equilibria exponential fits for several concentrations. The slope of the test curves is not steep enough.

The remaining attempts try to model CO_2 and CO_2/ TBAB phase equilibria with eq. 4.2 with different a and b values. The rest of the approach 1 modelling is to the test whether a horizontal shift of different curve can model both CO_2 and CO_2/ TBAB phase equilibria. Considering the high reliability of the CO_2 phase equilibria model (eq. 4.1), this is not likely. Nevertheless, the initial hypothesis that a horizontal shift is sufficient, is further tested.

Attempt #2: a=$a_{5wt\%}$, b=$b_{5wt\%}$

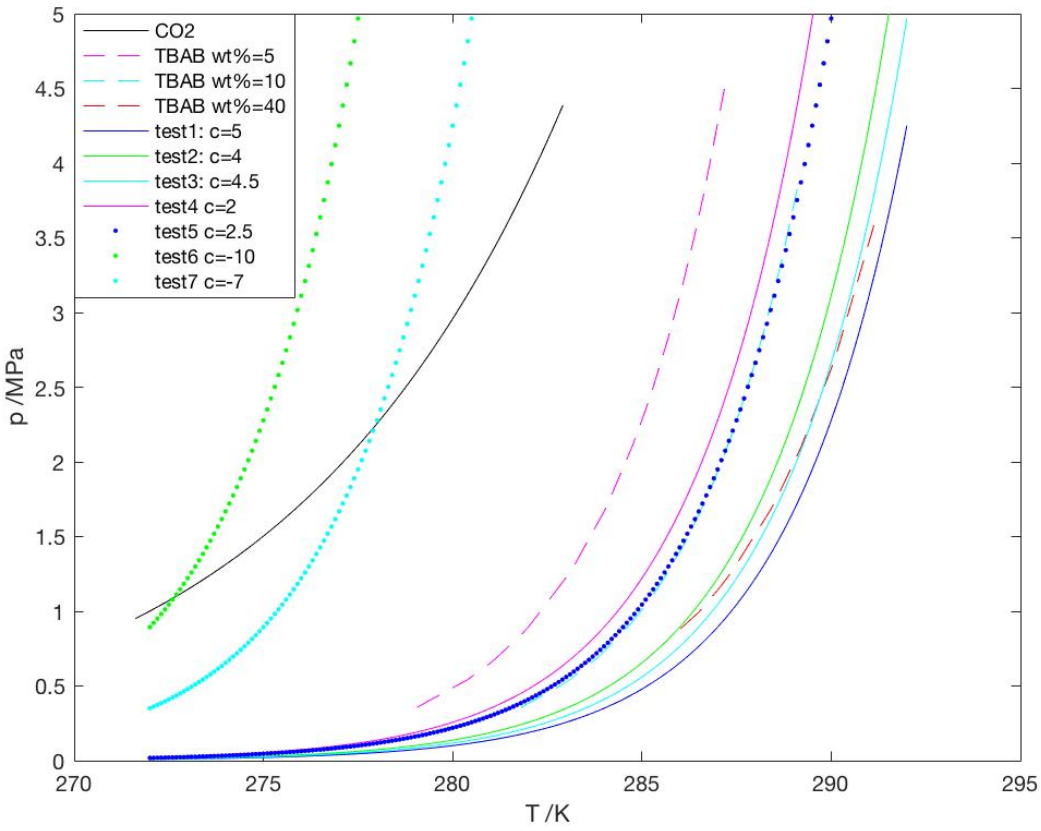

Figure 4.19: CO_2/ TBAB hydrate phase equilibria modelling attempt 2.

Test 1-3 was trial and error to model 40 wt% phase equilibria, test 4, 5 was trial and error to model 10 wt% phase equilibria and test 6, 7 was trial and error to model CO_2 phase equilibria. a and b of the equation for 5 wt% phase equilibria were used, as the 5 wt% phase equilibria exponential fit was the best fit (R^2 closest to 1) compared to the 10 and 40 wt% phase equilibria exponential fits. The attempt is as expected a bad model for pure CO_2 phase equilibria. 10 wt% (c=4.5) and 40 wt% (c=2.5) phase equilibria could be modelled most successfully. The shape of the modelled curve is most similar to that of 10 wt% phase equilibria and the modelled curve is satisfactory for the entire range, this is not the case for 40 wt% phase equilibria.

Attempt #3: a/ b equally weighted average of a_{CO_2} and $a_{5wt\%}$/ b_{CO_2} and $b_{5wt\%}$, c=0

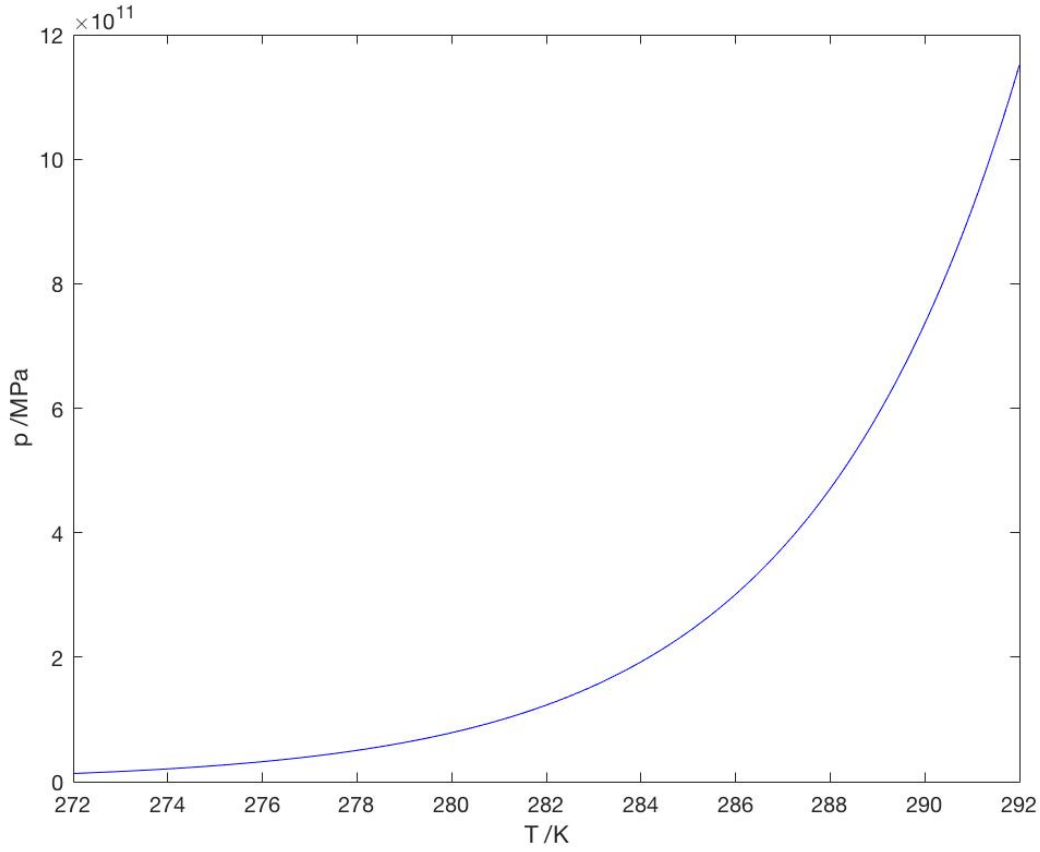

Figure 4.20: CO_2/ TBAB hydrate phase equilibria modelling attempt 3.

The modelled curve (a, b and c as in title) explodes the pressure range. Note that the y-limit in the script had to be changed to be able to see the curve. Including a c would not solve the problem of the extremely steep gradient. When equations 4.3, 4.4 and 4.5 were plotted together with the modelled curve, they appeared to be straight lines along the x-axis. Equations 4.3, 4.4 and 4.5 were therefor not included in the plot.

Attempt #4:a=$a_{40wt\%}$, b=$b_{40wt\%}$

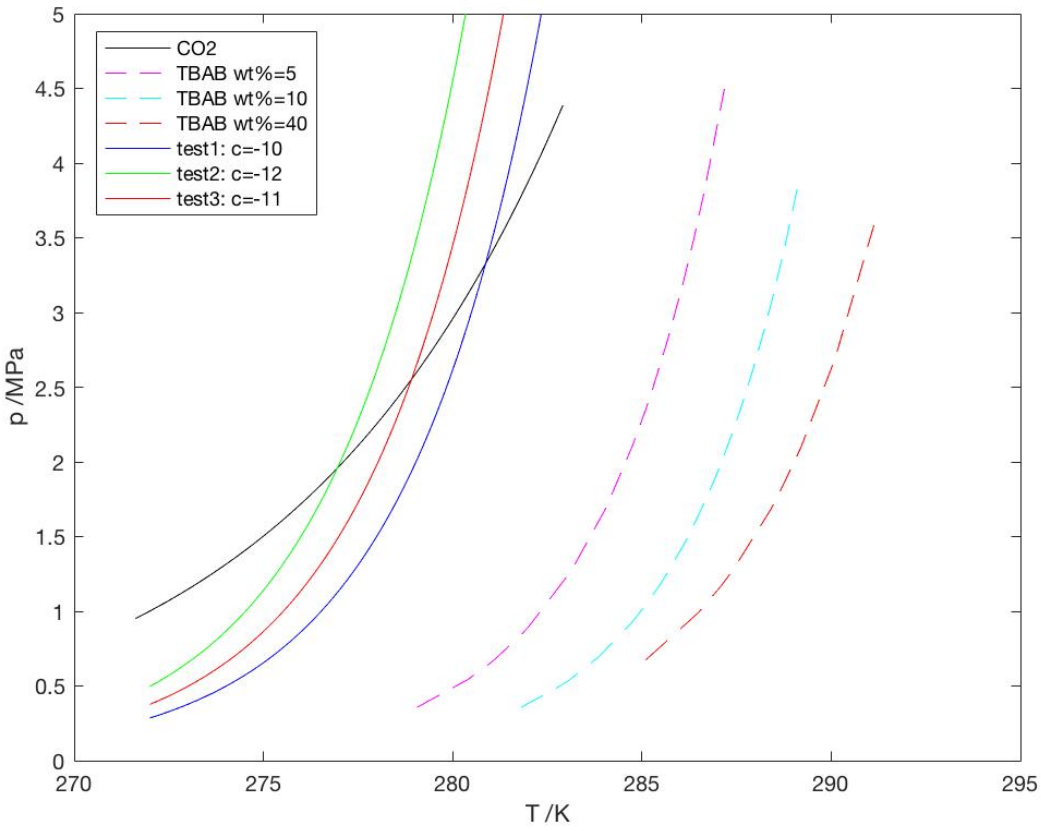

Figure 4.21: CO_2/ TBAB hydrate phase equilibria modelling attempt 4.

This attempt was to see if the the 40 wt% phase equilibria exponential fit could be used to model CO_2 phase equilibria (as the 40 wt% phase equilibria exponential fit appears to have the most similar shape to the CO_2 phase equilibria curve). c values were chosen based on distance to the CO_2 phase equilibria curve. The modelling was not successful, the curve was still too steep. Based on this there was no reason to attempt to model 5 wt% phase equilibria and 10 wt% phase equilibria.

Attempt #5:a=$a_{40wt\%}$, b=0.27, (d=0)

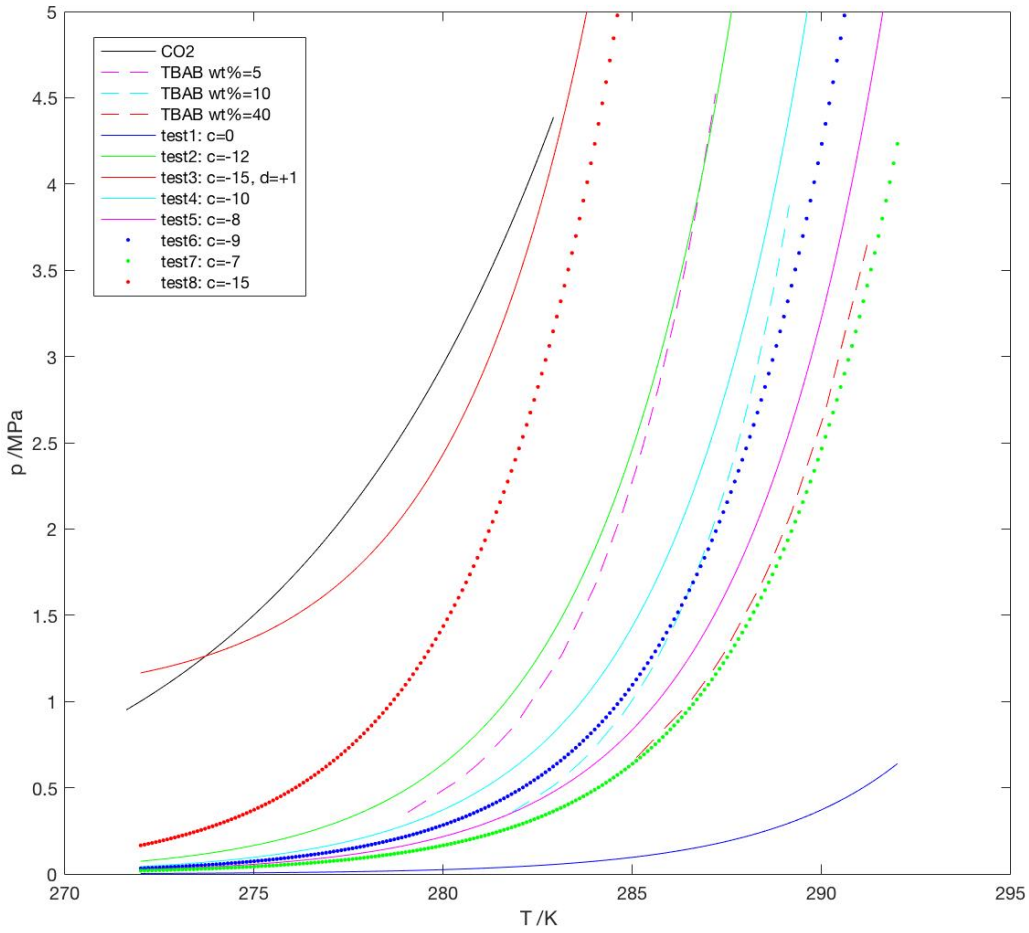

Figure 4.22: CO_2/ TBAB hydrate phase equilibria modelling attempt 5.

The aim of this attempt was to make the shape of the curves somewhere in between the shape of the CO_2 phase equilibria curve and the phase equilibria curves for 5 wt%, 10 wt% and 40 wt%. The b-value was found by trial and error, trying to make the curve less steep. b values between b of the CO_2 phase equilibria curve and b of 40 wt% phase equilibria exponential fit were tested. The first value that was tested was b=0.2. This resulted in no curve being shown on the plot (the y-limit was set to 5 MPa). The value of b was increased until a curve was observed, and then it was kept at this value. This happened at b=0.27. Once b was chosen, different c values were tested (initially c=0). The most successful modelling was: test 2 for 5 wt% phase equilibria, test 3

for CO_2 phase equilibria, test 6 for 10 wt% phase equilibria and test 7 for 40 wt% phase equilibria. See fig. 4.22 for details. Note that for test 3 a d was added. This was done after it was observed that the graph with no d, would be better fit if the curve was shifted vertically. The initial graph (d=0) is displayed as test 8. Although adding a d produces a better result, it is not ideal as the result is an implicit model. Including a d in the CO_2 phase equilibria model means that CO_2/ TBAB phase equilibria can not be seen as a horizontal shift of the CO_2 phase equilibria curve. In addition to an expression for ΔT, the following would need to be included when defining the model:

$$p(T) = \begin{cases} ae^{b(T-(-15))} + 1 & \text{if } x = 0 \\ ae^{b(T-(-15+\Delta T))} & \text{if } 0 < x \leq \Delta T \end{cases} \tag{4.6}$$

where x is weight% TBAB in the water phase and ΔT is the promotion temperature. The first equation is for pure CO_2 phase equilibria (c=-15, d=1, as shown in in fig. 4.22), and the second equations is for CO_2/ TBAB phase equilibria.

The result was a better fit for CO_2 than attempt 2, 3, 4, but far from satisfactory.

Attempt #6:a=$a_{40wt\%}$, b=0.271, (d=1)

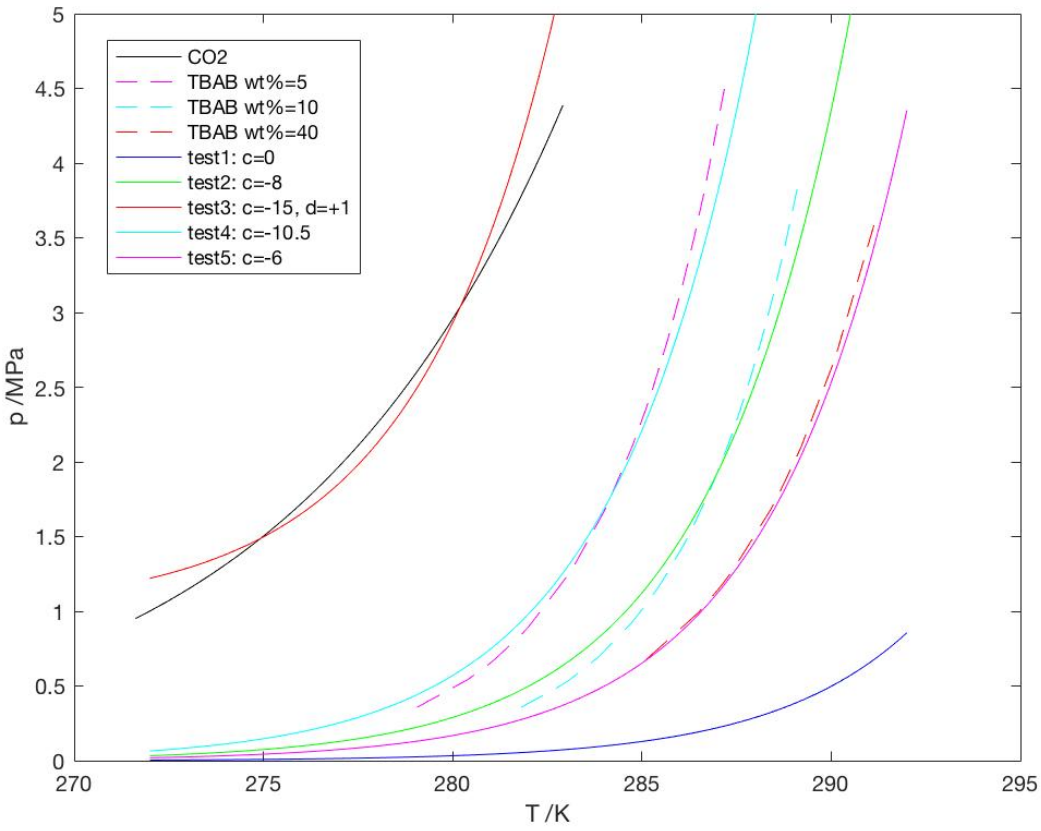

Figure 4.23: CO_2/ TBAB hydrate phase equilibria modelling attempt 6.

The aim was to further improve attempt #5. Trial and error led to the conclusion that a should not be changed, whereas b should be changed slightly to b=0.271. This led to a steeper slope, and thereby an increased accuracy for pure CO_2 phase equilibria. The accuracy of the CO_2 phase equilibria curve is however still not acceptable. Increasing the steepness of the slope even more, would sacrifice the accuracy of the CO_2/ TBAB phase equilibria curves. The accuracy of the CO_2/ TBAB phase equilibria curves are comparable to that of attempt 5 by visual observation. This can be checked by comparing R^2 values. The most successful modelling was: test 3 for CO_2 phase equilibria, test 4 for 5 wt% phase equilibria, test 2 for 10 wt% phase equilibria and test 5 for 40 wt% phase equilibria. Note that for this attempt d=1 is added to the equation for pure CO_2 making the model implicit. This model would also have the form of eq. 4.6.

Attempt 6 was the last attempt and the most successful attempt, so further modelling (finding an expression for ΔT) was carried out. As attempt 6 includes a d in the expression for pure CO_2 it was concluded that CO_2/ TBAB phase equilibria could not be modelled well by a horizontal shift from pure CO_2 phase equilibria. This led to the hypothesis being changed to CO_2/ TBAB phase equilibria being a more complex shift of CO_2 phase equilibria. From the modelling attempts it appears that CO_2/ TBAB phase equilibria curves for different concentrations may be modelled as horizontal shifts of each other.

For the further modelling procedure see APPROACH_1_ATTEMPT_6 script, appendix B. To find an expression for ΔT a correlation between ΔT and wt% TBAB had to be determined. Note that ΔT is not c in eq. 4.2 but the difference from the c in the equation for CO_2 phase equilibria (c=-15), as shown in eq. 4.6. For 10 wt% ΔT=7 (-15+7=-8), for 5 wt% ΔT=4.5 (-15+4.5=-10.5) and for 40 wt% ΔT=9 (-15+9=-6). A matrix was made in Matlab; the first column was wt% (5 10 40), and the second column was ΔT (4.5 7 9). The built-in function polyfit was then used to find the correlation between them. A polynomial fit was used as it modelled the data well. R^2 was calculated by the function rsqaure (see appendix B for script) giving R^2=1. The well-known inhibitor formulas (eq. 3.1, 3.2 and 3.3) are polynomial functions. Overfitting may be an issue, so ideally more data-points (wt%, ΔT) should be used. The polynomial fit is seen in eq. 4.7.

$$\Delta T(x) = -0.0124x^2 + 0.6857x + 1.3819 \tag{4.7}$$

Following this a function to calculate ΔT was made it Matlab. The function was named deltaT_m1, as it calculates ΔT for Model 1. deltaT_m1 takes in a concentration (x) and writes out ΔT. A function was made so that the model could easily be used and checked for any given concentration. The Matlab function is displayed.

```
function deltaT = deltaT_m1( x ) %x is weight%

% polynomial coefficients by built in polynomial fit function in matlab.
poly_coeff=[-0.0124    0.6857    1.3810];

deltaT=poly_coeff(1)*x^(2)+poly_coeff(2)*x+poly_coeff(3);

end
```

deltaT_m1 was first used to calculate the ΔT of 5 wt%, 10 wt% and 40 wt%, so that the function could be checked. The function was checked by plotting eq. 4.8 together with test 2, test 4 and test 5 (see fig. 4.24). The curves overlap meaning that function deltaT_m1 is correct.

$$
\begin{aligned}
p(T) &= \begin{cases} ae^{b(T-(-15))}+1 & \text{if } x=0 \\ ae^{b(T-(-15+\Delta T))} & \text{if } 0<x\leq \Delta T \end{cases} \\
a &= 3.683\times 10^{-35} \\
b &= 0.271 \\
\Delta T(x) &= -0.0124x^2+0.6857x+1.3819
\end{aligned}
\tag{4.8}
$$

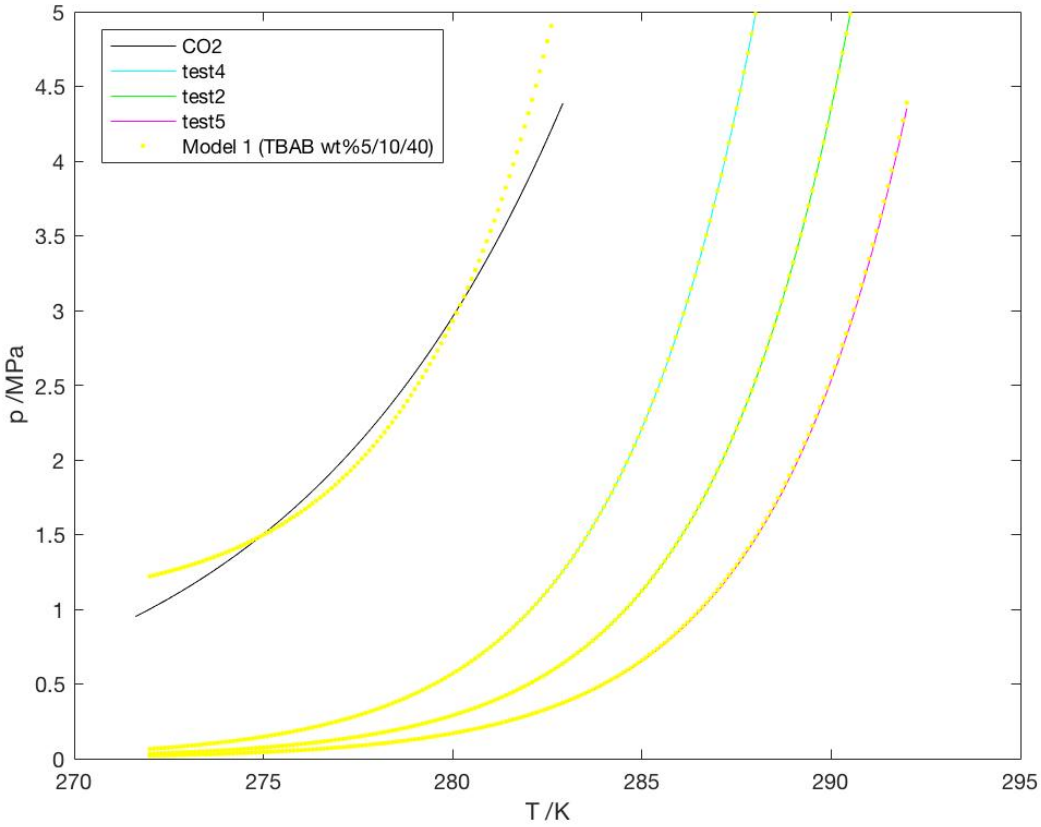

Figure 4.24: Testing CO_2/ TBAB deltaT_m1 equation (Model 1).

In order to be able to evaluate the model, its accuracy for other concentrations than those used to find the ΔT and weight% TBAB correlation, must be checked. ΔT was calculated for the concentrations in table 4.4 using the function deltaT_m1. Following this pressure was calculated for the temperature range to be considered (T_{model}=272-292K) by Model 1 (eq. 4.8) and plotted together with experimental data points. The results of the plotting in summarized in table 4.4. Graphical results for a collection of the concentrations are seen in fig. 4.25. For plots of all concentrations see appendix C.

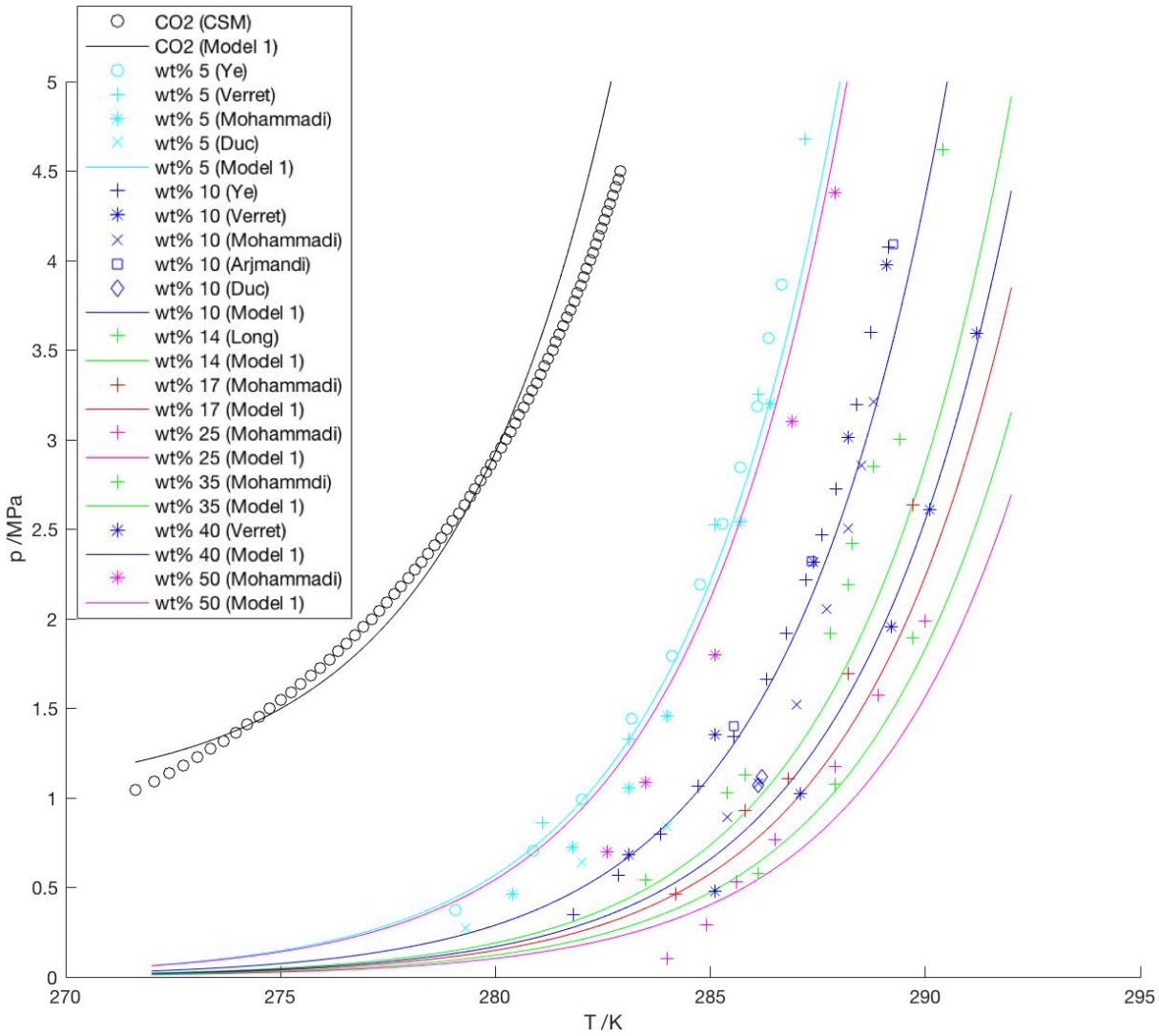

Figure 4.25: Testing Model 1. CO_2 (CSM) refers to CSM data points. wt% refers to wt% TBAB. Note that 10 wt% and 40 wt% (Verret) have the same colour and symbol. 40 wt% is the furthest to the right. The same is the case for 14 wt% (Long) and 35 wt% (Mohammadi), 35 wt% (Mohammadi) is the furthest to the right.

Table 4.4: Evaluation of Model 1.

Weight%	Evaluation of model
0 (CO_2)	Not satisfactory. Wrong shape, but the best fit of the carried out attempts.
1.76	Too far to the right. This may suggest that the model is a bad fit for low concentrations. Low concentrations are close to pure CO_2 where a vertical shift has been included.
4.43	Slightly to the left. The shape fits the data well.
5	Ok. Apart from data from Duc et al. (2007). Note that Duc et al. (2007) presents very few data points, making it challenging to evaluate the phase equilibria trend of the data points.
7.02	Too far to the left. Shape ok.
9.01	Too far to the left. Shape ok.
10	Ok.
14	Slightly to the right.
17	Slightly to the right.
19	Too far to the right. The data points suggest a steeper curve than the model curve.
25	Ok. Many of the data points are on the left side of the curve, suggesting the model could be improved.
35	Ok. More data points are desired.
40	Ok.
43	Does not affect the validity of the model as the concentration is not within its range (this also goes for the remaining concentrations). Slightly to the left. May be because maximum cavity occupation has been reached.
50	Slightly to the left.
55	Very much to the left.
65	To the left of CO_2. Very steep gradient.

The solid lines in fig. 4.25 from left to right are for 5 wt% , 50 wt%, 10 wt%, 14 wt%, 40 wt%, 17 wt%, 35 wt% and 25 wt%. The hypothesis that the maximum promotion is at maximum cavity occupation (40 wt% TBAB) is falsified. The fact that many of the plots considering data points from a single paper did not present this (40 wt% seemed to cause maximum promotion effect) is because the other concentrations plotted (<25 wt%) caused less promotion than 40 wt%. Examples of such plots are the plots showing the data from Verrett et al. (2015) and Arjmandi et al. (2007). It could be speculated that the model is incorrect and not the hypothesis, but as the model and the experimental data show the same trend, it is concluded that the hypothesis that maximum promotion is at maximum cavity occupation is incorrect. Model 1 and experimental data show that: the promotion effect increases with weight% TBAB until 25 wt%, 35 wt% TBAB shifts the curve a little to the left, 40 wt% TBAB shifts the curve a little more to the left and at TBAB wt% 50 the curve is little to the right of TBAB wt% 5 (it has been shifted far to the left).

The fact that 50 wt% has very undesirable results agrees with what has been previously discussed in relation to cavity filling and promotion effect. When it comes to the fact that thw 35 wt% and 40 wt% curvesare still far too the right, this is believed to because maximum cavity occupation has not been reached, so there is still a promotion effect (even though it is not at maximum). As a result of these observations, the hypothesis regarding maximum promotion effect is changed to maximum promotion occuring at 25 wt% TBAB.

The model is accurate for other concentrations than 5 wt%, 10 wt% and 40 wt% meaning that overfitting of $\Delta T(x)$ is not a significant issue. Defining $\Delta T(x)$ based on more concentrations may however improve the accuracy of the model. The accuracy of the CO_2 model of Model 1 is, on the other hand, not sufficient. The motivation for using the implicit model is low; eq. 4.1 might as well be used to model pure CO_2, and relying on two equation for predicting CO_2/ TBAB phase equilibria is tedious. Further work was related to creating an explicit model. This work is referred to as “Approach 2”.

The work related to creating Model 1 has resulted in that the original hypothesis has been altered twice. The altered hypothesis is that the shape of the CO_2 phase equilibria curve and CO_2/TBAB phase equilibria curve is different (a horizontal shift of the CO_2 phase equilibria curve is not sufficient to model for CO_2/ TBAB phase equilibria), and that the maximum promotion effect is at a concentration lower than that corresponding to maximum cavity occupation.

Note that the shape of the CO_2/ TBAB phase equilibria curves for different concentrations (within the range of the model) is still believed to be the same (in the sense that the CO_2/ TBAB phase equilibria curve for one concentration can be modelled as a horizintal shift of the CO_2/ TBAB phase equilibria curve for another concentration). Approach 2 will test the altered hypothesis.

Approach 2

The aim of approach 2 was to make an explicit model. Previous modelling has shown that the shape of the CO_2 phase equilibria curve and the CO_2/ TBAB phase equilibria curves is different. The fact that a simple horizontal shift is not sufficient to model the shift between CO_2 phase equilibria and CO_2/ TBAB phase equilibria, means that ΔT is not constant for a given concentration. Most of the Approach 1 modelling is based on this assumption, limiting the accuracy of the results. Adding a d to the CO_2 expression (attempt 5, 6) means that ΔT from CO_2 is not constant for a given concentration. The result when a d had been added was not satisfactory.

To explicitly express that ΔT is not constant for a given concentration, a ΔT expression that is a function of concentration and temperature had to be found. Note that the well-recognized inhibitor formulas express ΔT as a function of concentration only. The starting point was to find an expression for ΔT for a given concentration (x), $\Delta T_x = f(T)$. Note that $\Delta p_{x=f(p)}$ could also be used for modelling, resulting in a model $\Delta p(p,x)$. The first option is chosen as it is the convention for phase equilibria models.

After $\Delta T_x = f(T)$ had been found for all concentrations to be considered, the resulting expressions were used to find an expression for $\Delta T_x = f(x, T)$. This method was carried out for two attempts, which will be presented in this chapter. The script Model 2, which presents approach 2, attempt 2, is provided as an example script (see appendix B). Note that the procedure is very similar for the two attempts. For clarity when reading this chapter, it is recommended that the list of equations is consulted.

Attempt #1

Attempt 1 was based on the exponential fits of the experimental data for 5 wt%, 10 wt% and 40 wt% (eq. 4.3, 4.4, 4.5) and the CO_2 model (eq. 4.1).A description of the modelling procedure follows.

1. **Finding $T_x(p)$, ΔT_x.**

   Before being able to find an expression for ΔT_x, T(p) expressions for CO_2 and the TBAB concentrations to be considered had to be found. T(p) was found from the available p(T) expressions for CO_2 (eq. 4.1) and TBAB wt% 5 , 10 and 40 (4.3, 4.4, 4.5). The rearranged functions will have the form of eq. 4.9.

$$T(p) = a\ln(p \times b) \tag{4.9}$$

   The rearranging of the p(T) expressions was not performed in Matlab, but the new a and b values were stored as variables in the Matlab script. To avoid confusion the a and b values of the logarithmic function will be referred to as a_{log} and b_{log}. The values of a_{log} and b_{log} are displayed in table 4.5.

Table 4.5: Coefficients of logarithmic functions, $T_x(p)$.

Weight% TBAB	a_{log}	b_{log}
0 (CO_2)	7.3855	9.8522×10^{15}
5	3.2072	1.7211×10^{38}
10	3.0750	1.7578×10^{40}
40	3.6140	2.7160×10^{34}

T(p) was then calculated for the pressure range of the CO_2 model (see fig. 4.5) for all cases (CO_2 and the three TBAB concentrations). It is important that the same pressure range is taken in for all concentrations, including pure CO_2, as ΔT was calculated by eq. 4.10:

$$\Delta T_x = T_x - T_{CO_2} \tag{4.10}$$

where T_x is the temperature vector for a given concentration (wt%) and T_{CO_2} is the temperature vector for CO_2. The temperature vectors are calculated by the defined $T_x(p)$ and $T_{CO_2}(p)$ expressions, where a given element in all vectors corresponds to the temperature value at the same pressure. ΔT_x is the shift from the CO_2/ TBAB curve, for the given TBAB concentration, to the CO_2 curve in a phase equilibria plot (p vs T).

2. **Finding $\Delta T_x(T)$**

   To find a correlation between ΔT for a given concentration (ΔT_x) and T, ΔT_x is plotted against the corresponding T_x. T_x had been calculated in the previous step. This was done for 5 wt%, 10 wt% and 40 wt% (see fig 4.26).

   The relationships appeared to be linear, so a linear fit was tested. The Matlab function polyfit was applied, this time 1st degree was specified. See table 4.6 for results. R^2=1 for all concentrations, so a linear fit is a perfect fit. The linear fits were plotted, together with the ΔT_x data points (see fig.4.26). The figure shows that the lower the temperature for a given concentration, the larger the ΔT.

Table 4.6: Coefficients of linear fits, $\Delta T_x(T)$.

Weight% TBAB	a_{lin}	b_{lin}
5	-1.3028	378.2464
10	-1.4018	412.4147
40	-1.0436	313.5932

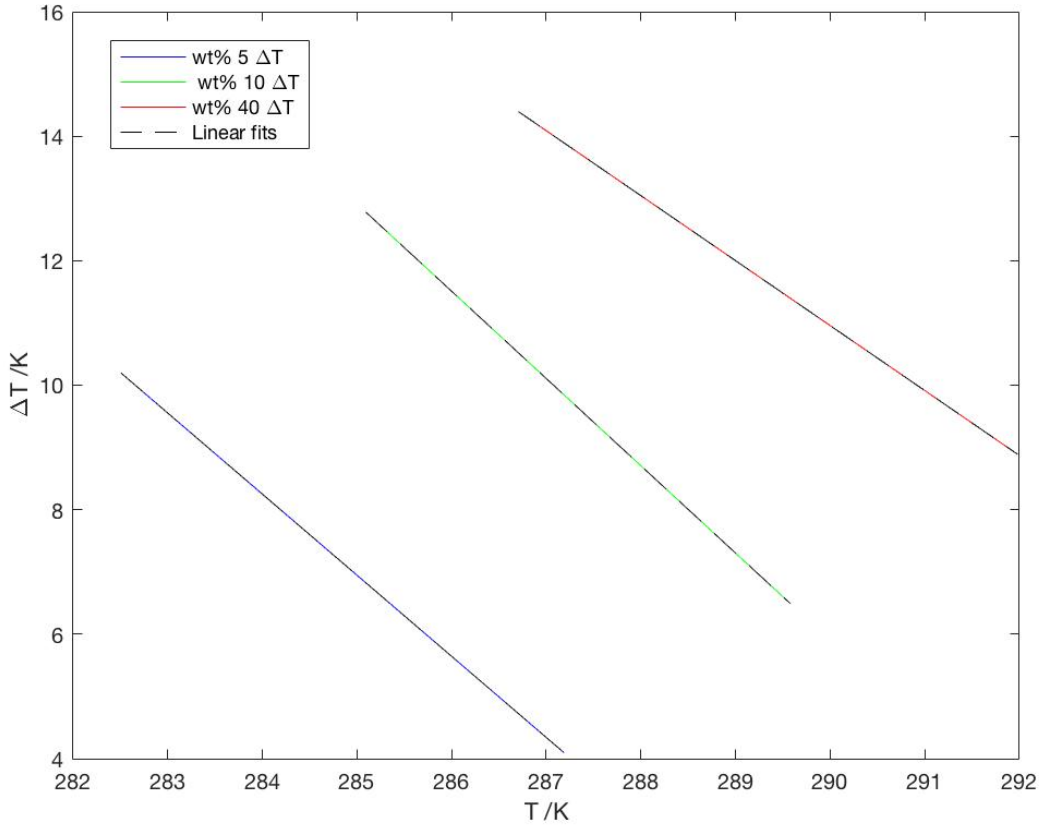

Figure 4.26: ΔT vs. T for TBAB weight% 5, 10 and 40 and linear fits.

As ΔT_x is plotted against T_x, the $\Delta T_x(T)$ expression from the linear fit is the shift from the CO_2/ TBAB phase equilibria curve to the CO_2 phase equilibria curve. In the final expression ($\Delta T(x, T)$), ΔT should be expressed as the shift from the CO_2 phase equilibria curve.

3. **Finding ΔT(x, T)**

The next and final step was to find a correlation between $\Delta T(T)$ and concentration (x). As all the $\Delta T_x(T)$ expressions are linear, a possible solution is to express $\Delta T(x, T)$ as eq. 4.11:

$$\Delta T(x, T) = aT + b(x) \tag{4.11}$$

where a is a constant and b(x) expresses a shift as a function of concentration.

This would require a common a value for the $\Delta T_x(T)$ functions. If a, the gradient, is constant, b(x) can be seen as a shift a long the curve (the shift is a shift of the curve itself). As a is not equal for the curves plotted in fig. 4.26, a common a value must be found by trial and error. Finding such an a, that was able to match all three curves accurately, was not successful. Attempt 1 was left at this.

Attempt #2

The modelling procedure is the same as for attempt 1. As with attempt 1 the CO_2 model (eq. 4.1) is used for CO_2 phase equilibria, and TBAB concentrations to be considered are 5 wt%, 10 wt% and 40 wt%.

In attempt 2 the a in eq. 4.11 did not have to be found by trial and error. This is because CO_2/ TBAB phase equilibria (expressed as p(T)) was expressed by Model 1 (4.8) and not by exponential fits of experimental data (4.3, 4.4, 4.5). This meant that the a of the rearranged $T_x(p)$ expressions had the same value (see table 4.7).

1. **Finding $T_x(p)$, ΔT_x.**

   Model 1 (eq. 4.8) was used to express p(T) for 5, 10 and 40 weight% TBAB. Note that $\Delta T(x)$ had to be calculated for the three concentrations. Following this the $p_x(T)$ expressions were rearranged to $T_x(p)$ expressions. The coefficients of the $T_x(p)$ expressions, and $T_{CO_2}(p)$, are displayed in table 4.7.

Table 4.7: Coefficients of logarithmic functions, $T_x(p)$.

Weight% TBAB	a_{log}	b_{log}
0 CO_2	7.3855	9.8522×10^{15}
5	3.6900	1.5781×10^{33}
10	3.6900	3.1072×10^{33}
40	3.6900	5.3426×10^{33}

As the functions to be rearranged (eq. 4.2) have the same a, except for the CO_2 function, the rearranged functions also have the same a (a_{log}). Note that the b_{log} is not the same. All b_{log} values are the same order of magnitude.

2. **Finding $\Delta T_x(T)$**

Once ΔT_x had been calculated for the three concentrations (see attempt 1 for method), ΔT_x was plotted against the corresponding T_x for 5, 10 and 40 wt% (see fig. 4.27).Note that T_x was calculated by eq. 4.9 with a_{log} and b_{log} from table 4.7.

This time the slopes of the three curves are the same. Linear fits were found for the plotted data. R^2=1 for all the linear fits. The linear coefficients (a_{lin}, b_{lin}) are displayed in table 4.8.

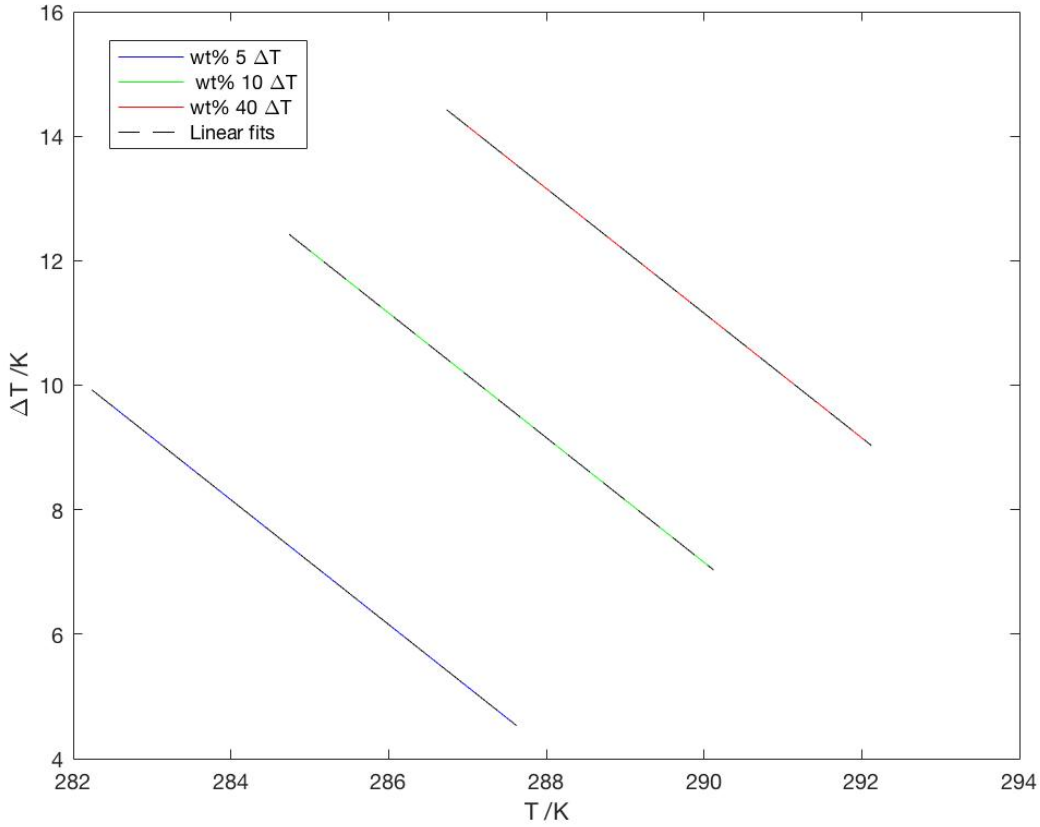

Figure 4.27: ΔT vs. T for TBAB weight% 5, 10 and 40 and linear fits.

Table 4.8: Coefficients of linear fits, $\Delta T_x(T)$.

Weight% TBAB	a_{lin}	b_{lin}
5	-1.0015	292.5777
10	-1.0015	297.5814
40	-1.0015	301.5844

3. **Finding ΔT(x, T)**

   Considering eq. 4.11 a is constant and already known (a_{lin} in table 4.8), where as b(x) had to be modelled. To find b(x), b was plotted against concentration (x). A polynomial curve of second order was fitted to the data, providing b(x) (see. eq 4.12). The polynomial fit was a perfect fit (R^2=1).

$$b(x) = -0.0248x^2 + 1.3724x + 286.33 \tag{4.12}$$

   A definition of a and b(x), meant that modelling was complete. So that ΔT(x, T) expresses the shift from pure CO_2 phase equilibria to CO_2/ TBAB phase equilibria, a and b(x) are defined with the opposite sign (positive instead of negative) in the final model. A ΔT(x, T) expression with a negative a and b(x) expresses the shift from CO_2/ TBAB phase equilibria to CO_2 phase equilibria. The shift from CO_2 phase equilibria to CO_2/ TBAB phase equilibria is the same as that from CO_2/ TBAB phase equilibria to CO_2 phase equilibria, but in the opposite direction.

   This means that the developed model, Model 2, is defined as:

$$\begin{aligned} \Delta T(x,T) &= aT + b(x) \\ a &= 1.0015 \\ b(x) &= 0.0248x^2 - 1.3724x - 286.33 \end{aligned} \tag{4.13}$$

   where ΔT is the promotion temperature from CO_2 phase equilibria and x is the TBAB concentration in the water phase expressed as weight%.

A function for Model 2, deltaT_m2, was made in Matlab:

```
function deltaT = deltaT_m2( x, T ) % x is weight%

a=1.0015;
b_poly_coeff=[0.0248   -1.3724    -286.33];

deltaT= (a*T)+(b_poly_coeff(1)*x^(2)+b_poly_coeff(2)*x+b_poly_coeff(3));

end
```

Making a function makes it more convenient to use and check the model. CO_2/ TBAB phase equilibria was calculated for a range of concentrations. The input temperature was a temperature vector with range 273.15 K to 292 K (the increments were 0.1 K). Once ΔT had been calculated for the concentrations to be considered, ΔT was added to the CO_2 model (eq. 4.1).The results are plotted in figure 4.28.

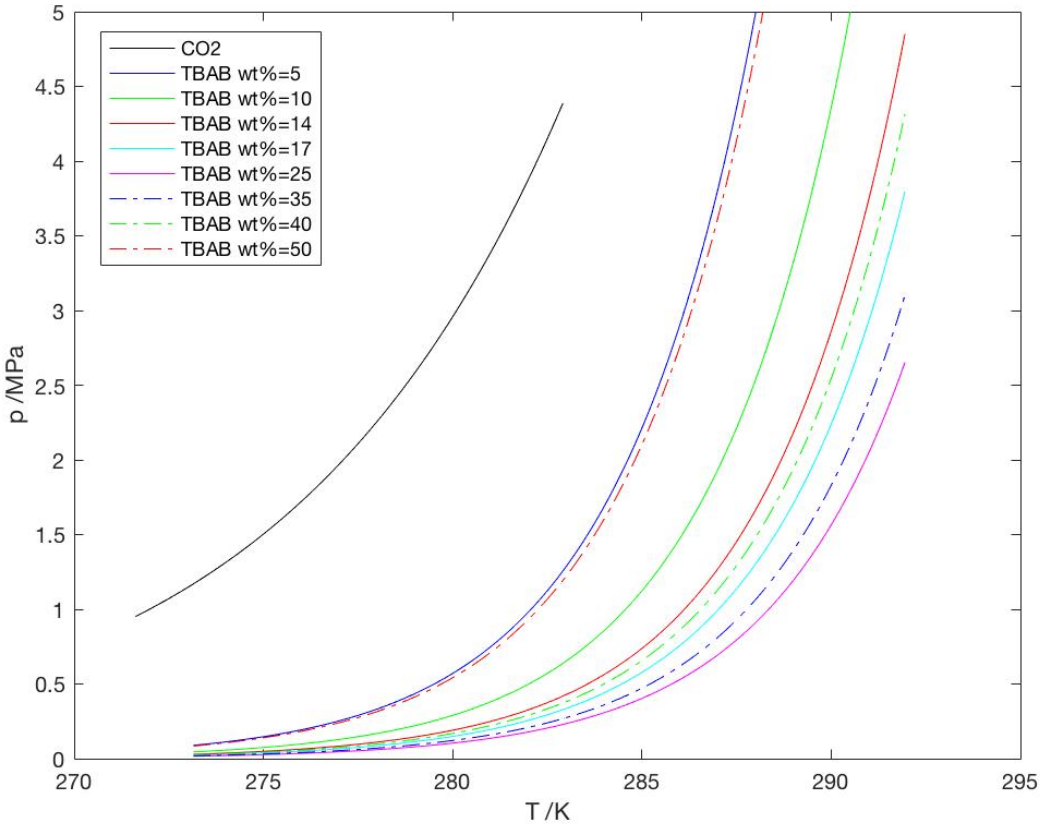

Figure 4.28: Model 2 CO_2/ TBAB phase equilibria.

The concentrations in fig. 4.28 (Model 2) are the same as those in fig. 4.25 (Model 1) , meaning that the curves should overlap. The modelling procedure outlined in approach 2, attempt 2 resulting in Model 2, should produce the same results as Model 1 (apart from for for CO_2). Model 1 and Model 2 for the concentrations 5, 10, 14, 17, 25, 35, 40 and 50 were plotted together to check this. See fig. 4.29.

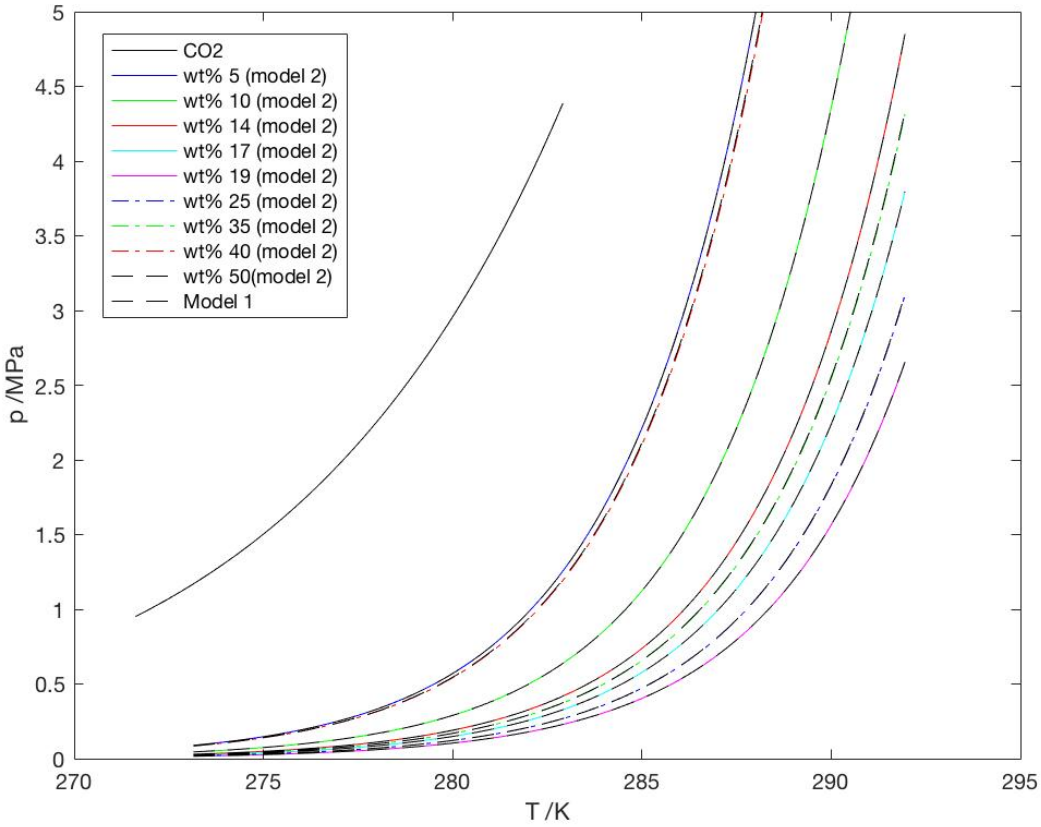

Figure 4.29: CO_2/ TBAB phase equilibria by Model 1 and Model 2.

From fig. 4.29 it is clear that Model 1 for a given concentration overlaps Model 2 for a given concentration. This gives a visual representation of that modelling is successful. Model 2 is an explicit model producing the same result as the implicit model Model 1 for CO_2/ TBAB phase equilibria. As the models produce the same results, the revised hypothesis remains; the CO_2 and CO_2/ TBAB phase equilibria curves are not the same shape, and maximum promotion effect occurs at 25 wt% TBAB. Note that the shape of the various CO_2/ TBAB phase equilibria curves is the same, they are horizontal shifts of eachother. Fig. 4.29 also shows that the promotion effect (ΔT) for a given concentration decreases with increasing temperature and pressure.

For concentrations exceeding the concentration of maximum promotion effect, a dash-dot line has been used, to emphasize the effect (see fig. 4.28) . Model 2 is not checked against experimental data as Model 1 is. See fig. 4.25 as well as table 4.4 (CO_2 is not to be considered). Not all the concentration in table 4.4 have been plotted for Model 2. The model(s) is the most

successful for 5, 10, 25, 35 and 40 wt% TBAB phase equilibria. 40 wt% was initially set as the upper limit of the phase equilibria model due to the belief that maximum cavity occupation led to maximum promotion effect. Although this hypothesis has been falsified, the upper limit is kept, so that the effect of adding more TBAB, than that corresponding to maximum promotion effect, can be studied by applying Model 2. Exceeding 40 wt% makes the model less accurate, which is believed to be because maximum cavity occupation has been reached.

Model 2 is preferred over Model 1 as it is explicit. It does not involve a bad fit for CO_2 phase equilibria and only consists of one equation. However, the accuracy of Model 2 is still seen as an area of improvement. Model 2 models the Model 1 equation for CO_2/ TBAB phase equilibria (the CO_2/ TBAB phase equilibria result is the same). Model 1 (Approach 1, Attempt 6) consists of both a CO_2 phase equilibria equation and a CO_2/ TBAB phase equilibria equation. Approach 1, Attempt 6 is the best overall fit for both CO_2 and CO_2/ TBAB phase equilibria. As the modelling procedure resulting in Model 2 (Approach 2, Attempt 2) only depends on a model for CO_2/ TBAB phase equilibria, it is believed that its accuracy could be increased by being based on a better model for this. An example of such a model is from Approach 1, Attempt 2. Model 1 is not the best fit for CO_2/ TBAB phase equilibria alone. In summary the accuracy of an explicit CO_2/ TBAB model is expected to increase if a more accurate implicit CO_2/ TBAB phase equilibria model is used for modelling. Another way of increasing accuracy is – as already mentioned - to consider more TBAB concentrations when modelling. Model 2 is the final model. The listed ways of improving the model is seen as future work.

Chapter 5

Conclusion

The potential advantages of hydrate based technologies encourage the development of hydrate promoter models. There are few known hydrate promoter models today, as opposed to the well known hydrate inhibitor models. Hydrate promoters cause milder hydrate phase equilibria condition, increasing the hydrate area. A hydrate promoter works as a catalyst for hydrate formation, and thereby separation of guest gas molecules form a solution. The discussed hydrate based technologies are: hydrate based desalination, hydrate based gas capture (CO_2 capture) and hydrate based gas transport and storage. The chapters about hydrate based technologies present a discussion of the parameters affecting efficiency and common hydrate promoters. Advantages of hydrate based technologies include reduced costs and improved safety. The fact that the operating conditions for hydrate formation are mild (promoters making them even milder) and that hydrates have a high level of stability, provide explanation for this. Successful development of hydrate promoter models is believed to benefit the discussed technologies. With this in mind, the main objective and aim of this master thesis was to develop a model for phase equilibria of CO_2 hydrates in aqueous solutions of tetrabutylammonium bromide (TBAB). Making a model for TBAB is desirable as TBAB is known to reduce hydrate forming pressure and increase hydrate forming temperature. The amount of available experimental data for CO_2/ TBAB hydrate phase equilibria made a modelling attempt possible. Two modelling approaches were carried out, as the first approach led to the development of an implicit model. The aim was to develop an explicit model. The first modelling approach tested the initial hypothesis that CO_2/ TBAB phase equilibria is a horizontal shift of CO_2 phase equilibria, the shift being to the right.

This would mean that ΔT was constant for a given TBAB concentration. The hypothesis was falsified, and it was concluded that the shifts of the CO_2/ TBAB phase equilibria curves from the pure CO_2 phase equilibria curve had to be more complex. The most successful attempt from approach 1, termed Model 1, resulted in an implicit model that was a poor fit for pure CO_2. Note that Model 1 did not model CO_2/ TBAB phase equilibria as a horizontal shift of CO_2 phase equilibria as a vertical shift was included for CO_2. Approach 1 modelling also falsified the hypothesis that maximum promotion effect occurs at the concentration corresponding to maximum cavity occupation. Considering this, the aim of approach 2 was to develop an explicit model that tested the revised hypothesis regarding shape (more complex shift between CO_2 and CO_2/ TBAB phase equilibria) and concentration (maximum promotion at 25 weight% TBAB). Note that modelling approach 1 did suggest that CO_2/ TBAB phase equilibria curves for different concentrations are horizontal shifts of eachother, which encouraged further modelling attempts.

Approach 2 did not consider the general exponential equation, as approach 1 did. It was more mathematical as it involved obtaining two correlations; a correlation between ΔT and T for a given concentration, and a correlation between parameter b and concentration (x) for eq. 4.11. In addition to this, it was not based on trial and error. Modelling approach 1 only required one correlation (ΔT(x)). Modelling approach 2 was successful when it modelled the CO_2/ TBAB phase equilibria curves of Model 1. This resulted in Model 2, the final model. The explicit model, Model 2, expresses ΔT(T,x). Approach 1 attempted to express CO_2/ TBAB phase equilibria as ΔT(x), without satisfactory results. Defining ΔT(T, x) produces a more complex expression for ΔT, but the result is more accurate, and the model is therefor preferred. With the development of Model 2, the aim of the master thesis had been reached; an explicit phase equilibria model of CO_2 hydrates in aqueous solutions of tetrabutylammonium bromide (TBAB) had been developed. Model 2 is in agreement with the altered hypothesis, it models a more complex shift than a horizontal shift between CO_2 and CO_2/ TBAB phase equilibria, and it shows that the promotion effect increases with TBAB concentration until 25 weight%. In addition to this, the model shows that the promotion effect for a given concentration is the largest for low temperature and low pressure (ΔT decreases with increasing T and p), and that CO_2/ TBAB phase equilibria curves for any concentrations (within the range of the model) are horizontal shifts of CO_2/ TBAB phase equilibria curves for other concentrations. The most accurate modelling results are for TBAB

weight% 5, 10, 25, 35 and 40, covering the range of the model.

The uncertainty of the developed model is challenging to quantify and not part of the discussion. Checking the model with already existing models such as those presented by Joshi et al. (2012) and Garcia and Clarke (2014) would aid evaluation of the accuracy of the model. Note that Model 2 is a lot more simple and easy to use than the few known existing models, which is seen as an advantage. When it comes to the uncertainty of the experimental data used for modelling, the uncertainties from the different experiments are likely to cancel each other out.

The fact that the hydrate promoter model is for industry use, which is a different environment than a lab environment, should be taken into account when considering use. The phase equilibria conditions for a given hydrate are constant, but the required energy to achieve these conditions varies. Many lab experiments use a stirred tank reactor, where the agglomeration of the hydrate crystals become an obstacle for hydrate formation. This means that obtaining phase equilibria conditions in the real world (for hydrate based technologies) may require less energy than obtaining the same conditions in the lab, which is advantages.

Model 2 meets the objective of the thesis (the result is an explicit model), but ways to create a more accurate CO_2/ TBAB phase equilibria model have been identified. The identified ways are; basing modelling on data from more concentrations (three concentration were used in this thesis) and carrying out approach 2, attempt 2 with a more accurate implicit model.

The developed model has only been based on CO_2/ TBAB phase equilibria data, meaning that it in theory only can be used to predict CO_2/ TBAB phase equilibria. The well known inhibitor models are general and can be used for any hydrate guest. Data collection and modelling for other TBAB hydrates, is required to draw a conclusion regarding whether Model 2 can be used for such hydrates. However, it is hypothesized that Model 2 would be a good prediction for all TBAB hydrates, considering what has been found for hydrate inhibitors. Encouraged future work is to test this for TBAB, as well as to develop models for other hydrate promoters, based on both experimental data and theory (EOS). Such models, allow for development of software to be used in hydrate based technologies. Model 2 may be seen as a step towards software development, and thereby a step towards commercialization of hydrate based technologies. With the increased focus on efficiency in the oil and gas industry in recent times, the importance of the development of hydrate promoter models should not be underestimated.

Appendix A

Tables

Table A.1: CO_2 CSM phase equilibria.

T /K	p /MPa	T /K	p /MPa	T /K	p /MPa	T /K	p /MPa
252.816	5.00E-01	284.754	20.576	286.399	40.652	287.678	60.727
273.567	1.303	284.83	21.379	286.456	41.455	287.723	61.53
277.527	2.1061	284.904	22.182	286.512	42.258	287.768	62.333
280.009	2.9091	284.978	22.985	286.568	43.061	287.812	63.136
281.717	3.7121	285.051	23.788	286.624	43.864	287.857	63.939
282.924	4.5152	285.122	24.591	286.679	44.667	287.9	64.742
283.04	5.3182	285.193	25.394	286.733	45.47	287.944	65.545
283.15	6.1212	285.263	26.197	286.787	46.273	287.987	66.348
283.257	6.9242	285.332	27	286.84	47.076	288.029	67.152
283.361	7.7273	285.401	27.803	286.893	47.879	288.072	67.955
283.462	8.5303	285.468	28.606	286.946	48.682	288.113	68.758
283.561	9.3333	285.535	29.409	286.998	49.485	288.155	69.561
283.657	10.136	285.601	30.212	287.049	50.288	288.196	70.364
283.751	10.939	285.666	31.015	287.1	51.091	288.237	71.167
283.843	11.742	285.731	31.818	287.151	51.894	288.277	71.97
283.933	12.545	285.795	32.621	287.201	52.697	288.317	72.773
284.021	13.348	285.858	33.424	287.251	53.5	288.357	73.576
284.108	14.152	285.921	34.227	287.3	54.303	288.396	74.379
284.194	14.955	285.982	35.03	287.348	55.106	288.435	75.182
284.278	15.758	286.044	35.833	287.397	55.909	288.474	75.985
284.36	16.561	286.104	36.636	287.445	56.712	288.512	76.788
284.441	17.364	286.164	37.439	287.492	57.515	288.55	77.591
284.521	18.167	286.224	38.242	287.539	58.318	288.587	78.394
284.6	18.97	286.283	39.045	287.586	59.121	288.625	79.197
284.678	19.773	286.341	39.848	287.632	59.924	288.661	80

Table A.2: CO_2 CSM phase equilibria.

T /K	p /MPa	T /K	p /MPa	T /K	p /MPa	T /K	p /MPa
252.816	5.00E-01	275.475	1.6364	279.654	2.7727	282.054	3.9091
254.912	5.45E-01	275.701	1.6818	279.775	2.8182	282.128	3.9545
256.868	5.91E-01	275.921	1.7273	279.893	2.8636	282.2	4
258.703	6.36E-01	276.134	1.7727	280.009	2.9091	282.271	4.0455
260.433	6.82E-01	276.341	1.8182	280.123	2.9545	282.341	4.0909
262.07	7.27E-01	276.542	1.8636	280.234	3	282.409	4.1364
263.625	7.73E-01	276.738	1.9091	280.343	3.0455	282.476	4.1818
265.105	8.18E-01	276.928	1.9545	280.45	3.0909	282.542	4.2273
266.519	8.64E-01	277.114	2	280.555	3.1364	282.607	4.2727
267.873	9.09E-01	277.294	2.0455	280.657	3.1818	282.67	4.3182
269.172	9.55E-01	277.47	2.0909	280.758	3.2273	282.732	4.3636
270.42	1	277.641	2.1364	280.857	3.2727	282.793	4.4091
271.622	1.0455	277.808	2.1818	280.953	3.3182	282.852	4.4545
272.055	1.0909	277.971	2.2273	281.048	3.3636	282.911	4.5
272.404	1.1364	278.13	2.2727	281.141	3.4091	282.929	4.5455
272.738	1.1818	278.285	2.3182	281.232	3.4545	282.935	4.5909
273.059	1.2273	278.436	2.3636	281.322	3.5	282.942	4.6364
273.368	1.2727	278.584	2.4091	281.409	3.5455	282.949	4.6818
273.665	1.3182	278.729	2.4545	281.495	3.5909	282.955	4.7273
273.951	1.3636	278.87	2.5	281.58	3.6364	282.962	4.7727
274.227	1.4091	279.008	2.5455	281.663	3.6818	282.968	4.8182
274.494	1.4545	279.143	2.5909	281.744	3.7273	282.975	4.8636
274.751	1.5	279.275	2.6364	281.824	3.7727	282.981	4.9091
275	1.5455	279.404	2.6818	281.902	3.8182	282.988	4.9545
275.241	1.5909	279.53	2.7273	281.979	3.8636	282.994	5

Table A.3: Deaton and Frost (1946) CO_2 phase equilibria (Sloan and Koh, 2008).

T /K	p /MPa
273.7	1.324
273.7	1.324
274.3	1.393
274.3	1.42
274.3	1.42
275.4	1.613
276.5	1.848
277.6	2.075
277.6	2.082
277.6	2.103
278.7	2.427
278.7	2.413
279.8	2.758
279.8	2.786
280.9	3.213
281.5	3.53
281.9	3.709
282.6	4.13
282.9	4.323

Table A.4: Larson (1955) CO_2 phase equilibria (Sloan and Koh, 2008)

T /K	p /MPa
271.8	1.048
271.9	1.048
272.2	1.089
272.5	1.11
273.1	1.2
273.4	1.234
273.5	1.241
273.9	1.317
274.1	1.351
274.4	1.386
275	1.51
275.1	1.496
275.7	1.634
276	1.682
276.2	1.717
276.5	1.806
276.9	1.889
277.2	1.951
277.8	2.137
278	2.165
278.6	2.344
278.8	2.448
279.1	2.53
279.2	2.544
279.8	2.73
280.1	2.861
280.2	2.923
280.5	3.02
280.8	3.158
281.1	3.282
281.5	3.475
281.9	3.634
282	3.689
282.3	3.868
283.1	4.468
283.2	4.502

Table A.5: Vlahakis et al (1955) CO_2 phase equilibria (Sloan and Koh, 2008).

T /K	p /MPa	T /K	p /MPa
271.6	1.04	277.7	2.093
271.7	1.045	277.7	2.127
271.7	1.043	278.1	2.23
272	1.088	278.6	2.372
272.1	1.096	278.7	2.4
272.3	1.117	278.8	2.411
272.7	1.163	279.2	2.541
273.1	1.218	279.7	2.737
273.1	1.222	280.1	2.879
273.6	1.3	280.4	2.989
273.9	1.342	280.7	3.134
274.2	1.387	281.2	3.327
274.7	1.462	281.4	3.471
274.7	1.472	281.8	3.626
275.3	1.569	281.8	3.68
275.7	1.651	282.2	3.833
276.1	1.742	282.3	3.947
276.6	1.844	282.6	4.082
276.7	1.849	282.7	4.165
277	1.927	282.9	4.311
277.2	1.983	283.2	4.508
277.2	1.984	283.2	4.509

Table A.6: Fan and Guo (1999) CO_2 phase equilibria (Sloan and Koh, 2008).

T /K	p /MPa
273.6	1.31
274.2	1.39
275.2	1.57
276.4	1.81
278.5	2.25
279.2	2.52
280.3	3.04

Table A.7: CO_2/ 5 wt% TBAB (Mohammadi et al., 2011).

T /K	p /MPa
280.4	0.462
281.8	0.725
283.1	1.054
284	1.459
285.7	2.54
286.4	3.201

Table A.8: CO_2/ 10 wt% TBAB (Mohammadi et al., 2011).

T /K	p /MPa
285.4	0.891
286.1	1.081
287	1.523
287.7	2.055
288.2	2.504
288.5	2.858
288.8	3.212

Table A.9: CO_2/ 16.7 wt% TBAB (Mohammadi et al., 2011).

T /K	p /MPa
284.2	0.464
285.8	0.931
286.8	1.107
288.2	1.692
289.7	2.637

Table A.10: CO_2/ 25 wt% TBAB (Mohammadi et al., 2011).

T /K	p /MPa
284	0.104
284.9	0.293
285.6	0.53
286.5	0.769
287.9	1.178
288.9	1.575
290	1.989

Table A.11: CO_2/ 35 wt% TBAB (Mohammadi et al., 2011).

T /K	P /MPa
286.1	0.581
287.9	1.074
289.7	1.895

Table A.12: CO_2/ 50 wt% TBAB (Mohammadi et al., 2011).

T /K	p /MPa
282.6	0.698
283.5	1.086
285.1	1.8
286.9	3.104
287.9	4.38

Table A.13: CO_2/ 5 wt% TBAB (Ye and Zhang, 2012).

T /K	p /MPa
286.66	3.865
286.35	3.567
286.08	3.187
285.69	2.845
285.29	2.531
284.75	2.191
284.1	1.795
283.17	1.442
282	0.993
280.87	0.702
279.06	0.372

Table A.14: CO_2/ 10 wt% TBAB (Ye and Zhang, 2012).

T /K	p /MPa
289.14	4.075
288.73	3.602
288.4	3.197
287.93	2.726
287.59	2.466
287.22	2.219
286.76	1.919
286.3	1.662
285.54	1.343
284.72	1.063
283.85	0.801
282.87	0.569
281.81	0.349

Table A.15: CO_2/ 19 wt% TBAB (Ye and Zhang, 2012).

T /K	p /MPa
290.46	4.357
290.28	4.021
289.97	3.53
289.5	3.066
288.86	2.525
288.21	2.069
287.28	1.523
286.31	1.135
285.17	0.799
283.55	0.416

Table A.16: CO_2/ 32 wt% TBAB (Ye and Zhang, 2012).

T /K	p /MPa
291.3	3.775
290.3	2.614
288.77	1.599

Table A.17: CO_2/ 55 wt% TBAB (Ye and Zhang, 2012).

T /K	p /MPa
290.69	4.249
290.57	3.922
290.17	3.486
289.75	3.084
289.4	2.719
288.78	2.315
288.24	1.941
287.8	1.698
287.06	1.38
286.22	1.079
285.23	0.778

Table A.18: CO_2/ 1.76 wt% TBAB (Long et al., 2016).

T /K	p /MPa
278.00	1.100
279.40	1.740
282.40	3.410

Table A.19: CO_2/ 14 wt% TBAB (Long et al., 2016).

T /K	p /MPa
283.5	0.540
285.4	1.030
285.8	1.130
287.8	1.920
288.2	2.190
288.3	2.420
288.8	2.850
289.4	3.000
290.4	4.620

Table A.20: CO_2/ 5 wt% TBAB (Verrett et al., 2015).

T /K	p /MPa
281.1	0.859
283.1	1.329
285.1	2.526
286.1	3.254
287.2	4.678

Table A.21: CO_2/ 10 wt% TBAB (Verrett et al., 2015).

T /K	p /MPa
283.1	0.683
285.1	1.352
287.4	2.317
288.2	3.011
289.1	3.975

Table A.22: CO_2/ 40 wt% TBAB (Verrett et al., 2015).

T /K	p /MPa
285.1	0.477
287.1	1.021
289.2	1.957
290.1	2.609
291.2	3.594

Table A.23: CO_2/ 40 wt% TBAB (Deschamps and Dalmazzone, 2009).

T /K	p /MPa
286.5	0.83
287.4	1.29
288.4	1.86
288.6	2.25

Table A.24: CO_2/ 10 wt% TBAB (Arjmandi et al., 2007).

T /K	p /MPa
285.55	1.400
287.35	2.320
289.25	4.090

Table A.25: CO_2/ 42.7 wt% TBAB (Arjmandi et al., 2007).

T /K	p /MPa
287.25	1.248
288.75	1.793
290.15	2.896
291.15	3.517

Table A.26: CO_2/ 5 wt% TBAB (Duc et al., 2007).

T /K	p /MPa
279.3	0.273
282	0.64
284	0.84

Table A.27: CO_2/ 10 wt% TBAB (Duc et al., 2007).

T /K	p /MPa
286.1	1.07
286.2	1.12

Table A.28: CO_2/ 40 wt% TBAB (Duc et al., 2007).

T /K	p /MPa
290.9	3.32

Table A.29: CO_2/ 65 wt% TBAB (Duc et al., 2007).

T /K	p /MPa
284	0.815
285	0.986

Table A.30: CO_2/ 4.43 wt% TBAB (Lin et al., 2008).

T /K	p /MPa
279.4	0.344
280.19	0.515
280.56	0.513
281.46	0.763
282.91	1.172
283.16	1.179
284.66	1.715

Table A.31: CO_2/ 7.02 wt% TBAB (Lin et al., 2008).

T /K	p /MPa
282.59	0.379
282.72	0.379
283.4	0.578
283.58	0.575
284.58	0.842
285.38	1.216
286.14	1.667
286.96	2.199

Table A.32: CO_2/ 9.01 wt% TBAB (Lin et al., 2008).

T /K	p /MPa
282.79	0.391
283.34	0.393
284.43	0.583
285.07	0.859
285.33	0.866
286.38	1.333
286.53	1.339
287.6	1.803
288.09	2.274

Appendix B

Matlab Scripts

CO2_phase_eq_full_range.m

```
clear all
close all
clc

m = csvread('CO2_phase_eq_full_range.csv');

% Extracting temperature and pressure data

T=m(:,1);

p=m(:,2);

% CSM CO2 phase equilibrium plot

figure(1)
plot(T,p,'k'); hold on
title('CO2 phase equilibrium by CSM')
xlabel('T /K')
ylabel('p /MPa')
```

CO2_phase_eq_with_disc.m

```
clear all
close all
```

```
clc

m = csvread('CO2_phase_eq.csv');
% pressure range up to 5MPa

% Extracting temperature and pressure data

T=m(:,1);

p=m(:,2);

% CSM CO2 phase equilibrium plot

figure(1)
plot(T,p,'k'); hold on
title('CO2 phase equilibrium by CSM')
xlabel('T /K')
ylabel('p /MPa')
```

CO2_phase_eq_with_fits.m

```
clear all
close all
clc

m = csvread('CO2_phase_eq.csv'); %get CO2 phase eq data

% Extracting temperature and pressure data

T1=m(:,1); % T1 is the temperature of the full range

p1=m(:,2);

% Limiting the range

[idx]=find(T1>=271.622 & T1<=282.911);

```

```
17 T=T1(idx);
18
19 p=p1(idx);
20
21 % CSM CO2 phase equilibrium plot
22
23 figure(1)
24 plot(T,p,'k'); hold on
25 % title('CO2 phase equilibrium ')
26 xlabel('T /K')
27 ylabel('p /MPa')
28
29 % Built in function for polynomial fit coefficients
30
31 poly_coeff=polyfit(T,p,2) % polynomial of 2nd order
32
33 % Built in function for evaluation of polynomial fit
34
35 poly_fit_p=polyval(poly_coeff,T);
36
37 [r2_poly rmse_poly] = rsquare(p,poly_fit_p)
38
39 % Adding polynomial fit to plot
40
41 plot(T,poly_fit_p,'--','Color', 'b'); hold on
42
43 legend('CO2 phase equilibrium by CSM','Polynomial fit')
44
45 % Table displaying polynomial fit error
46
47 poly_table = table(T,p,poly_fit_p,p-poly_fit_p,'VariableNames',{'T','p','
       PolyFit','PolyFitError'})
48
49 % Exponential fit:
50
51 % Built in function that creates exponential fit of data. Ouput: general
```

```
52 % model and coefficients (with 95% confidence bounds)
53
54 exp_fit=fit(T,p,'exp1')
55 figure(2)
56 plot(exp_fit,T,p)
57
58 % Extracting coefficient values
59
60 exp_coeff=coeffvalues(exp_fit);
61
62 % Evaluating exponential function
63
64 exp_fit_p=exp_coeff(1)*exp(exp_coeff(2)*T);
65
66 [r2_exp rmse_exp] = rsquare(p,exp_fit_p)
67
68 % Plotting exponential fit
69
70 figure (3)
71 plot(T,p,'k'); hold on
72 title('CO2 phase equilibrium ')
73 xlabel('T /K')
74 ylabel('P /MPa')
75 plot(T,exp_fit_p,'--','Color', 'r'); hold on
76
77 legend('CO2 phase equilibrium by CSM','Exponential fit')
78
79 % Table displaying exponential fit error
80
81 exp_table = table(T,p,exp_fit_p,p-exp_fit_p,'VariableNames',{'T','p','ExpFit',
       'ExpFitError'})
82
83
84 figure(4)
85 plot(T,p,'k'); hold on
86 % title('CO2 phase equilibrium ')
```

```
xlabel('T /K')
ylabel('p /MPa')
plot(T,poly_fit_p,'--','Color', 'b'); hold on
plot(T,exp_fit_p,'--','Color', 'r'); hold on
legend('CO2 phase equilibrium by CSM','Polynomial fit','Exponential fit')
```

CO2_sloan.m

```
clear all
close all
clc

% Opening data sets as matrices. CSM CO2 phase eq data, empricial CO2 phase eq
    data
% tabulated in Sloan(2008)


m = csvread('CO2_phase_eq.csv');


m_Deaton=csvread('CO2_phase_eq_Deaton.csv'); %Deaton and Frost
m_Larson=csvread('CO2_phase_eq_Larson.csv');
m_Vlahakis=csvread('CO2_phase_eq_Vlahakis.csv');
m_Fan=csvread('CO2_phase_eq_Fan.csv');

% Extracting temperature and pressure data:

T1=m(:,1);
p1=m(:,2);

% Limiting the range of the CO2 data (no discontinuities)

[idx]=find(T1>=271.622 & T1<=282.911);
T=T1(idx);
p=p1(idx);

T_Deaton=m_Deaton(:,1);
```

```
p_Deaton=m_Deaton(:,2);

T_Larson=m_Larson(:,1);
p_Larson=m_Larson(:,2);

T_Vlahakis=m_Vlahakis(:,1);
p_Vlahakis=m_Vlahakis(:,2);

T_Fan=m_Fan(:,1);
p_Fan=m_Fan(:,2);


figure(1)
plot(T,p,'k'); hold on % CSM CO2 phase equilibria
title('CO2 phase equilibria')
xlabel('T /K')
ylabel('P /MPa')

% Adding empirical data to plot

scatter(T_Deaton, p_Deaton,'m', 's'); hold on
scatter(T_Larson,p_Larson,'c','s');  hold on
scatter(T_Vlahakis,p_Vlahakis,'r','s'); hold on
scatter(T_Fan,p_Fan,'b','s');  hold off

legend('CSM','Deaton and Frost (1946)', ...
    'Larson (1955)', 'Vlahakis et al (1972)', 'Fan and Guo (1999)')
```

rsquare.m

```
function [r2 rmse] = rsquare(y,f,varargin)
% Compute coefficient of determination of data fit model and RMSE
%
% [r2 rmse] = rsquare(y,f)
% [r2 rmse] = rsquare(y,f,c)
%
% RSQUARE computes the coefficient of determination (R-square) value from
```

```
% actual data Y and model data F. The code uses a general version of
% R-square, based on comparing the variability of the estimation errors
% with the variability of the original values. RSQUARE also outputs the
% root mean squared error (RMSE) for the user's convenience.
%
% Note: RSQUARE ignores comparisons involving NaN values.
%
% INPUTS
%   Y       : Actual data
%   F       : Model fit
%
% OPTION
%   C       : Constant term in model
%             R-square may be a questionable measure of fit when no
%             constant term is included in the model.
%   [DEFAULT] TRUE : Use traditional R-square computation
%            FALSE : Uses alternate R-square computation for model
%                    without constant term [R2 = 1 - NORM(Y-F)/NORM(Y)]
%
% OUTPUT
%   R2      : Coefficient of determination
%   RMSE    : Root mean squared error
%
% EXAMPLE
%   x = 0:0.1:10;
%   y = 2.*x + 1 + randn(size(x));
%   p = polyfit(x,y,1);
%   f = polyval(p,x);
%   [r2 rmse] = rsquare(y,f);
%   figure; plot(x,y,'b-');
%   hold on; plot(x,f,'r-');
%   title(strcat(['R2 = ' num2str(r2) '; RMSE = ' num2str(rmse)]))
%
% Jered R Wells
% 11/17/11
% jered [dot] wells [at] duke [dot] edu
```

```
%
% v1.2 (02/14/2012)
%
% Thanks to John D'Errico for useful comments and insight which has helped
% to improve this code. His code POLYFITN was consulted in the inclusion of
% the C-option (REF. File ID: #34765).

if isempty(varargin); c = true;
elseif length(varargin)>1; error 'Too many input arguments';
elseif ~islogical(varargin{1}); error 'C must be logical (TRUE||FALSE)'
else c = varargin{1};
end

% Compare inputs
if ~all(size(y)==size(f)); error 'Y and F must be the same size'; end

% Check for NaN
tmp = ~or(isnan(y),isnan(f));
y = y(tmp);
f = f(tmp);

if c; r2 = max(0,1 - sum((y(:)-f(:)).^2)/sum((y(:)-mean(y(:))).^2));
else r2 = 1 - sum((y(:)-f(:)).^2)/sum((y(:)).^2);
    if r2<0
    % http://web.maths.unsw.edu.au/~adelle/Garvan/Assays/GoodnessOfFit.html
        warning('Consider adding a constant term to your model') %#ok<WNTAG>
        r2 = 0;
    end
end

rmse = sqrt(mean((y(:) - f(:)).^2));
```

CO2_TBAB_Mohammadi.m

```
clear all
close all
clc
```

```
4
5  % Opening data sets as matrices. CO2 phase eq data, CO2/TBAB eq data with
6  % TBAB wt% = 5, 10, 16.7, 25, 35 and 50 by Mohammadi et al (2011).
7  % Matlab does not allow for points in matrix names.
8  % Weight frac is rounded of if necessary.
9  % w=wt%
10
11
12 m = csvread('CO2_phase_eq.csv');
13 m_w5_M=csvread('TBAB_w5_Mohammadi.csv');
14 m_w10_M=csvread('TBAB_w10_Mohammadi.csv');
15 m_w17_M=csvread('TBAB_w16.7_Mohammadi.csv');
16 m_w25_M=csvread('TBAB_w25_Mohammadi.csv');
17 m_w35_M=csvread('TBAB_w35_Mohammadi.csv');
18 m_w50_M=csvread('TBAB_w50_Mohammadi.csv');
19
20 % Extracting temperature and pressure data:
21
22 T1=m(:,1);
23 p1=m(:,2);
24
25 % Limiting the range of the CO2 data (no discontinuities)
26
27 [idx]=find(T1>=271.622 & T1<=282.911);
28 T=T1(idx);
29 p=p1(idx);
30
31 T_w5_M=m_w5_M(:,1);
32 p_w5_M=m_w5_M(:,2);
33
34 T_w10_M=m_w10_M(:,1);
35 p_w10_M=m_w10_M(:,2);
36
37 T_w17_M=m_w17_M(:,1);
38 p_w17_M=m_w17_M(:,2);
39
```

```
40 T_w25_M=m_w25_M(:,1);
41 p_w25_M=m_w25_M(:,2);
42
43 T_w35_M=m_w35_M(:,1);
44 p_w35_M=m_w35_M(:,2);
45
46 T_w50_M=m_w50_M(:,1);
47 p_w50_M=m_w50_M(:,2);
48
49 % For modelling purposes the exponential fit of the limited range CSM CO2
50 % data (without discontinuities) will be considered as the CO2 equilibrium
51 % curve.
52
53 % Exponential fit:
54
55 % Built in function that creates exponential fit to data. Ouput: general
56 % model and coefficients (with 95% confidence bounds)
57
58 exp_fit=fit(T,p,'exp1')
59
60 % Extracting coefficient values
61
62 exp_coeff=coeffvalues(exp_fit);
63
64 %Evaluating exponential function
65
66 exp_fit_p=exp_coeff(1)*exp(exp_coeff(2)*T);
67
68 [r2 rmse] = rsquare(p,exp_fit_p)
69
70 % Plotting CO2 equilibrium curve (exponential fit) and experimental data
71
72 figure(1)
73 plot(T,exp_fit_p,'k'); hold on
74 % title('CO2/ TBAB phase equilibria (Mohammadi et al)')
75 xlabel('T /K')
```

```
ylabel('p /MPa')

% Scatter plots for experimental data

scatter(T_w5_M,p_w5_M,'m'); hold on
scatter(T_w10_M,p_w10_M,'c');  hold on
scatter(T_w17_M,p_w17_M,'r'); hold on
scatter(T_w25_M,p_w25_M,'g');  hold on
scatter(T_w35_M,p_w35_M,'b'); hold on
scatter(T_w50_M,p_w50_M,'k'); hold off

legend('CO2','TBAB wt%=5', ...
    'TBAB wt%=10', 'TBAB wt%=16.7', 'TBAB wt%=25', 'TBAB wt%=35', ...
    'TBAB w=50')

figure(2)

plot(T,exp_fit_p,'k'); hold on
% title('CO2/ TBAB phase equilibria (Mohammadi et al) ')
xlabel('T /K')
ylabel('p /MPa')

% Scatter plots for experimental data

scatter(T_w5_M,p_w5_M,'m'); hold on
scatter(T_w10_M,p_w10_M,'c');  hold on
scatter(T_w17_M,p_w17_M,'r'); hold on
scatter(T_w25_M,p_w25_M,'g');  hold on
scatter(T_w35_M,p_w35_M,'b'); hold on
scatter(T_w50_M,p_w50_M,'k'); hold on

% Creating and plotting exponential fits

exp_fit_w5_M=fit(T_w5_M,p_w5_M,'exp1') % writing out details of fit
exp_coeff_w5_M=coeffvalues(exp_fit_w5_M);
exp_fit_p_w5_M=exp_coeff_w5_M(1)*exp(exp_coeff_w5_M(2)*T_w5_M);
```

```
112 plot(T_w5_M,exp_fit_p_w5_M, 'Color', 'r'); hold on
113
114 [r2_w5_M rmse_w5_M] = rsquare(p_w5_M,exp_fit_p_w5_M)
115
116 exp_fit_w10_M=fit(T_w10_M,p_w10_M,'exp1')
117 exp_coeff_w10_M=coeffvalues(exp_fit_w10_M);
118 exp_fit_p_w10_M=exp_coeff_w10_M(1)*exp(exp_coeff_w10_M(2)*T_w10_M);
119 plot(T_w10_M,exp_fit_p_w10_M, 'Color', 'r'); hold on
120
121 [r2_w10_M rmse_w10_M] = rsquare(p_w10_M,exp_fit_p_w10_M)
122
123 exp_fit_w17_M=fit(T_w17_M,p_w17_M,'exp1')
124 exp_coeff_w17_M=coeffvalues(exp_fit_w17_M);
125 exp_fit_p_w17_M=exp_coeff_w17_M(1)*exp(exp_coeff_w17_M(2)*T_w17_M);
126 plot(T_w17_M,exp_fit_p_w17_M, 'Color', 'r'); hold on
127
128 [r2_w17_M rmse_w17_M] = rsquare(p_w17_M,exp_fit_p_w17_M)
129
130 exp_fit_w25_M=fit(T_w25_M,p_w25_M,'exp1')
131 exp_coeff_w25_M=coeffvalues(exp_fit_w25_M);
132 exp_fit_p_w25_M=exp_coeff_w25_M(1)*exp(exp_coeff_w25_M(2)*T_w25_M);
133 plot(T_w25_M,exp_fit_p_w25_M, 'Color', 'r'); hold on
134
135 [r2_w25_M rmse_w25_M] = rsquare(p_w25_M,exp_fit_p_w25_M)
136
137 exp_fit_w35_M=fit(T_w35_M,p_w35_M,'exp1')
138 exp_coeff_w35_M=coeffvalues(exp_fit_w35_M);
139 exp_fit_p_w35_M=exp_coeff_w35_M(1)*exp(exp_coeff_w35_M(2)*T_w35_M);
140 plot(T_w35_M,exp_fit_p_w35_M, 'Color', 'b'); hold on
141
142 [r2_w35_M rmse_w35_M] = rsquare(p_w35_M,exp_fit_p_w35_M)
143
144 exp_fit_w50_M=fit(T_w50_M,p_w50_M,'exp1')
145 exp_coeff_w50_M=coeffvalues(exp_fit_w50_M);
146 exp_fit_p_w50_M=exp_coeff_w50_M(1)*exp(exp_coeff_w50_M(2)*T_w50_M);
147 plot(T_w50_M,exp_fit_p_w50_M, 'Color', 'b'); hold off
```

```
148
149 [r2_w50_M rmse_w50_M] = rsquare(p_w50_M,exp_fit_p_w50_M)
150
151 legend('CO2','TBAB wt%=5', ...
152     'TBAB wt%=10', 'TBAB wt%=16.7', 'TBAB wt%=25', 'TBAB wt%=35', ...
153     'TBAB wt%=50', 'Exp fits (wt%=35, 50 are blue)')
```

CO2_TBAB_3_fits.m

```
1  clear all
2  close all
3  clc
4
5  m = csvread('CO2_phase_eq.csv');
6  m_w5_Y=csvread('TBAB_w5_Ye.csv');
7  m_w5_V=csvread('TBAB_w5_Verret.csv');
8  m_w5_M=csvread('TBAB_w5_Mohammadi.csv');
9  m_w10_Y=csvread('TBAB_w10_Ye.csv');
10 m_w10_V=csvread('TBAB_w10_Verret.csv');
11 m_w10_M=csvread('TBAB_w10_Mohammadi.csv');
12 m_w40_V=csvread('TBAB_w40_Verret.csv');
13 m_w40_D=csvread('TBAB_w40_Deschamps.csv');
14
15 % Extracting temperature and pressure data:
16
17 T1=m(:,1);
18 p1=m(:,2);
19
20 % Limiting the range of the CO2 data (no discontinuities
21
22 [idx]=find(T1>=271.622 & T1<=282.911);
23 T=T1(idx);
24 p=p1(idx);
25
26 T_w5_Y=m_w5_Y(:,1);
27 p_w5_Y=m_w5_Y(:,2);
28
```

```
29 T_w5_V=m_w5_V(:,1);
30 p_w5_V=m_w5_V(:,2);
31
32 T_w5_M=m_w5_M(:,1);
33 p_w5_M=m_w5_M(:,2);
34
35 T_w10_Y=m_w10_Y(:,1);
36 p_w10_Y=m_w10_Y(:,2);
37
38 T_w10_V=m_w10_V(:,1);
39 p_w10_V=m_w10_V(:,2);
40
41 T_w10_M=m_w10_M(:,1);
42 p_w10_M=m_w10_M(:,2);
43
44
45 T_w40_V=m_w40_V(:,1);
46 p_w40_V=m_w40_V(:,2);
47
48 T_w40_D=m_w40_D(:,1);
49 p_w40_D=m_w40_D(:,2);
50
51 % For modelling purposes the exponential fit of the limited range CSM CO2
52 % data (without discontinuities) will be considered as the CO2 equilibrium
53 % curve.
54
55 % Exponential fit:
56
57 % Built in function that creates exponential fit to data. Ouput: general
58 % model and coefficients (with 95% confidence bounds)
59
60 exp_fit=fit(T,p,'exp1')
61
62 % Extracting coefficient values
63
64 exp_coeff=coeffvalues(exp_fit);
```

```
65
66  %Evaluating exponential function
67
68  exp_fit_p=exp_coeff(1)*exp(exp_coeff(2)*T);
69
70  [r2 rmse] = rsquare(p,exp_fit_p);
71
72  % Plotting CO2 equilibrium curve (exponential fit) and experimental data
73
74  figure(1)
75  plot(T,exp_fit_p,'k'); hold on
76  % title('CO2/ TBAB phase equilibria')
77  xlabel('T /K')
78  ylabel('p /MPa')
79
80
81  % plotting experimental data data
82
83  %wt% 5
84  scatter(T_w5_Y,p_w5_Y,'m','s'); hold on
85  scatter(T_w5_V,p_w5_V,'m','d');  hold on
86  scatter(T_w5_M,p_w5_M,'m'); hold on
87
88  %wt% 10
89  scatter(T_w10_Y,p_w10_Y,'c','s'); hold on
90  scatter(T_w10_V,p_w10_V,'c','d');  hold on
91  scatter(T_w10_M,p_w10_M,'c'); hold on
92
93  %wt% 40
94
95  scatter(T_w40_V,p_w40_V,'r','d'); hold on
96  scatter(T_w40_D,p_w40_D,'r','x');  hold on
97
98
99  % Defining variables needed for exponential fit of collected data.
100 % In order to produce exponential fit from,
```

```
% data set it must be sorted. The matlab function sortrows(A) sorts the
% rows of a matrix in ascending order based on the elements in the first
% columns.

m_w5_unsorted=[m_w5_Y;m_w5_V;m_w5_M]; % making one matrix with all 5wt% data
m_w5=sortrows(m_w5_unsorted); % sorting matrix for fitting purposes.
T_w5=m_w5(:,1);
p_w5=m_w5(:,2);

m_w10_unsorted=[m_w10_Y;m_w10_V;m_w10_M]; % making one matrix with all 10wt%
    data
m_w10=sortrows(m_w10_unsorted); % sorting matrix for fitting purposes
T_w10=m_w10(:,1);
p_w10=m_w10(:,2);

m_w40_unsorted=[m_w40_V;m_w40_D];% making one matrix with all 40wt% data
m_w40=sortrows(m_w40_unsorted); % sorting matrix for fitting purposes
T_w40=m_w40(:,1);
p_w40=m_w40(:,2);

exp_fit_w5=fit(T_w5,p_w5,'exp1') % writing out details of fit
exp_coeff_w5=coeffvalues(exp_fit_w5);
exp_fit_p_w5=exp_coeff_w5(1)*exp(exp_coeff_w5(2)*T_w5);
plot(T_w5,exp_fit_p_w5, 'Color', 'm'); hold on

exp_fit_w10=fit(T_w10,p_w10,'exp1') % writing out details of fit
exp_coeff_w10=coeffvalues(exp_fit_w10);
exp_fit_p_w10=exp_coeff_w10(1)*exp(exp_coeff_w10(2)*T_w10);
plot(T_w10,exp_fit_p_w10, 'Color', 'c'); hold on

exp_fit_w40=fit(T_w40,p_w40,'exp1') % writing out details of fit
exp_coeff_w40=coeffvalues(exp_fit_w40);
exp_fit_p_w40=exp_coeff_w40(1)*exp(exp_coeff_w40(2)*T_w40);
plot(T_w40,exp_fit_p_w40, 'Color', 'r'); hold off

legend('CO2','TBAB wt%=5 (Ye)', 'TBAB wt%=5 (Verret)', ...
```

```
    'TBAB wt%=5(Mohammadi)', 'TBAB wt%=10 (Ye)', 'TBAB wt%=10 (Verret)', ...
    'TBAB wt%=10 (Mohammadi)', 'TBAB wt%=40 (Verret)',...
    'TBAB wt%=40 (Deschamps)')



[r2_w5 rmse_w5] = rsquare(p_w5,exp_fit_p_w5)
[r2_w10 rmse_w10] = rsquare(p_w10,exp_fit_p_w10)
[r2_w40 rmse_w40] = rsquare(p_w40,exp_fit_p_w40)
```

APPROACH1_1_ATTEMPT_2.m

```
clear all
close all
clc

% APPROACH 1, ATTEMPT 2


% reading all files to be considered (wt% 5, 10, 40)

m = csvread('CO2_phase_eq.csv');
m_w5_Y=csvread('TBAB_w5_Ye.csv');
m_w5_V=csvread('TBAB_w5_Verret.csv');
m_w5_M=csvread('TBAB_w5_Mohammadi.csv');
m_w10_Y=csvread('TBAB_w10_Ye.csv');
m_w10_V=csvread('TBAB_w10_Verret.csv');
m_w10_M=csvread('TBAB_w10_Mohammadi.csv');
m_w40_V=csvread('TBAB_w40_Verret.csv');
m_w40_D=csvread('TBAB_w40_Deschamps.csv');

% Extracting temperature and pressure data:

T1=m(:,1);
p1=m(:,2);

% Limiting the range of the CO2 data (no discontinuities)
```

```
26
27 [idx]=find(T1>=271.622 & T1<=282.911);
28 T=T1(idx);
29 p=p1(idx);
30
31 T_w5_Y=m_w5_Y(:,1);
32 p_w5_Y=m_w5_Y(:,2);
33
34 T_w5_V=m_w5_V(:,1);
35 p_w5_V=m_w5_V(:,2);
36
37 T_w5_M=m_w5_M(:,1);
38 p_w5_M=m_w5_M(:,2);
39
40 T_w10_Y=m_w10_Y(:,1);
41 p_w10_Y=m_w10_Y(:,2);
42
43 T_w10_V=m_w10_V(:,1);
44 p_w10_V=m_w10_V(:,2);
45
46 T_w10_M=m_w10_M(:,1);
47 p_w10_M=m_w10_M(:,2);
48
49
50 T_w40_V=m_w40_V(:,1);
51 p_w40_V=m_w40_V(:,2);
52
53 T_w40_D=m_w40_D(:,1);
54 p_w40_D=m_w40_D(:,2);
55
56 % For modelling purposes the exponential fit of the limited range CSM CO2
57 % data (without discontinuities) will be considered as the CO2 equilibrium
58 % curve.
59
60 % Exponential fit:
61
```

```
% Built in function that creates exponential fit to data. Ouput: general
% model and coefficients (with 95% confidence bounds)

exp_fit=fit(T,p,'exp1');

% Extracting coefficient values

exp_coeff=coeffvalues(exp_fit);

%Evaluating exponential function

exp_fit_p=exp_coeff(1)*exp(exp_coeff(2)*T);

[r2 rmse] = rsquare(p,exp_fit_p);

figure(1)
plot(T,exp_fit_p,'k'); hold on
% title('CO2/ TBAB phase equilibria modelling 2')
xlabel('T /K')
ylabel('p /MPa')
ylim([0 5]) % limit is set to pressure range

% defining variables needed for exponential fit of collected data.
% In order to produce exponential fit from,
% data set it must be sorted. The matlab function sortrows(A) sorts the
% rows of a matrix in ascending order based on the elements in the first
% columns.

m_w5_unsorted=[m_w5_Y;m_w5_V;m_w5_M]; % making one matrix with all 5wt%
%data
m_w5=sortrows(m_w5_unsorted); % sorting matrix for fitting purposes
T_w5=m_w5(:,1);
p_w5=m_w5(:,2);

m_w10_unsorted=[m_w10_Y;m_w10_V;m_w10_M]; % making one matrix with all
%10wt% data
```

```
m_w10=sortrows(m_w10_unsorted); % sorting matrix for fitting purposes
T_w10=m_w10(:,1);
p_w10=m_w10(:,2);

T_model=(272:0.1:292)'; %needs to be defined before to properly evaluate
%how well model works for w40

m_w40_unsorted=[m_w40_V;m_w40_D];% making one matrix with all 40wt% data
m_w40=sortrows(m_w40_unsorted); % sorting matrix for fitting purposes
T_w40=m_w40(:,1);
p_w40=m_w40(:,2);

exp_fit_w5=fit(T_w5,p_w5,'exp1');
exp_coeff_w5=coeffvalues(exp_fit_w5);
exp_fit_p_w5=exp_coeff_w5(1)*exp(exp_coeff_w5(2)*T_w5);
plot(T_w5,exp_fit_p_w5, '--', 'Color', 'm'); hold on

exp_fit_w10=fit(T_w10,p_w10,'exp1');
exp_coeff_w10=coeffvalues(exp_fit_w10);
exp_fit_p_w10=exp_coeff_w10(1)*exp(exp_coeff_w10(2)*T_w10);
plot(T_w10,exp_fit_p_w10, '--','Color', 'c'); hold on

exp_fit_w40=fit(T_w40,p_w40,'exp1');
exp_coeff_w40=coeffvalues(exp_fit_w40);
exp_fit_p_w40=exp_coeff_w40(1)*exp(exp_coeff_w40(2)*T_w40);
plot(T_w40,exp_fit_p_w40, '--','Color', 'r'); hold on


% [r2_w5 rmse_w5] = rsquare(p_w5,exp_fit_p_w5);
% [r2_w10 rmse_w10] = rsquare(p_w10,exp_fit_p_w10);
% [r2_w40 rmse_w40] = rsquare(p_w40,exp_fit_p_w40);

% Modelling:

% Type of function: f(x)=a*exp*(b*(x-c)). Where c is  a function of the
%concentration.
```

```
134
135 % ATTEMPT 2
136
137 % a and b are defined as a and b of exp_fit_w5 as this was the best fit (r2
138 % closest to 1
139
140 % defining variables needed for model:
141
142 T_model=(272:0.1:292)'; % this gives a vector of 201*1 which is considered
143 % sufficeintly accurate
144
145 a=exp_coeff_w5(1);
146 b=exp_coeff_w5(2);
147
148 % c=5;
149 test_1=a*exp(b*(T_model-5));
150 plot(T_model, test_1, 'b');% eval: can see that it is shifted too far right
151
152 % c=4;
153 test_2=a*exp(b*(T_model-4));
154 plot(T_model, test_2, 'g');  % eval: too far left
155
156 % c=4.5;
157 test_3=a*exp(b*(T_model-4.5));
158 plot(T_model, test_3, 'c');  % eval: satisfactory for wt% 40
159
160 % attempting to model wt10
161
162 % expfit for w5 does not need to be shifted as much to the right
163
164 % c=2;
165 test_4=a*exp(b*(T_model-2));
166 plot(T_model, test_4, 'm'); % eval: too far left
167
168 % c=2.5;
169 test_5=a*exp(b*(T_model-2.5));
```

```
plot(T_model, test_5, '.','Color', 'b'); % eval: satisfactory. even better.


% attempting to model wt0. expected to be harder as the shape is different.
% needs to be shifted to the left

% c=-10; visual estimation (number of units shifted)
test_6=a*exp(b*(T_model+10));
plot(T_model, test_6, '.','Color', 'g'); % eval: too far left and wrong
%shape


 % c=-7;
test_7=a*exp(b*(T_model+7));
plot(T_model, test_7, '.','Color', 'c'); hold on % wrong shape but can not
%get a lot better with this model


legend('CO2','TBAB wt%=5', 'TBAB wt%=10', ....
    'TBAB wt%=40', 'test1: c=5', 'test2: c=4', 'test3: c=4.5',...
    'test4 c=2', 'test5 c=2.5', 'test6 c=-10', 'test7 c=-7')
```

APPROACH1_1_ATTEMPT_6.m

```
clear all
close all
clc

% APPROACH 1, ATTEMPT 6

% reading all files to be considered (wt% 5, 10, 40)

m = csvread('CO2_phase_eq.csv');
m_w5_Y=csvread('TBAB_w5_Ye.csv');
m_w5_V=csvread('TBAB_w5_Verret.csv');
m_w5_M=csvread('TBAB_w5_Mohammadi.csv');
m_w10_Y=csvread('TBAB_w10_Ye.csv');
```

```
m_w10_V=csvread('TBAB_w10_Verret.csv');
m_w10_M=csvread('TBAB_w10_Mohammadi.csv');
m_w40_V=csvread('TBAB_w40_Verret.csv');
m_w40_D=csvread('TBAB_w40_Deschamps.csv');

% Extracting temperature and pressure data:

T1=m(:,1);
p1=m(:,2);

% Limiting the range of the CO2 data (no discontinuities)

[idx]=find(T1>=271.622 & T1<=282.911);
T=T1(idx);
p=p1(idx);

T_w5_Y=m_w5_Y(:,1);
p_w5_Y=m_w5_Y(:,2);

T_w5_V=m_w5_V(:,1);
p_w5_V=m_w5_V(:,2);

T_w5_M=m_w5_M(:,1);
p_w5_M=m_w5_M(:,2);

T_w10_Y=m_w10_Y(:,1);
p_w10_Y=m_w10_Y(:,2);

T_w10_V=m_w10_V(:,1);
p_w10_V=m_w10_V(:,2);

T_w10_M=m_w10_M(:,1);
p_w10_M=m_w10_M(:,2);


T_w40_V=m_w40_V(:,1);
```

```
50 p_w40_V=m_w40_V(:,2);
51
52 T_w40_D=m_w40_D(:,1);
53 p_w40_D=m_w40_D(:,2);
54
55 % For modelling purposes the exponential fit of the limited range CSM CO2
56 % data (without discontinuities) will be considered as the CO2 equilibrium
57 % curve.
58
59 % Exponential fit:
60
61 % Built in function that creates exponential fit to data. Ouput: general
62 % model and coefficients (with 95% confidence bounds)
63
64 exp_fit=fit(T,p,'exp1');
65
66 % Extracting coefficient values
67
68 exp_coeff=coeffvalues(exp_fit);
69
70 %Evaluating exponential function
71
72 exp_fit_p=exp_coeff(1)*exp(exp_coeff(2)*T);
73
74 [r2 rmse] = rsquare(p,exp_fit_p);
75
76 figure(1)
77 plot(T,exp_fit_p,'k'); hold on
78 % title('CO2/ TBAB phase equilibria modelling 7')
79 xlabel('T /K')
80 ylabel('p /MPa')
81 ylim([0 5])
82
83 % defining variables needed for exponential fit of collected data.
84 % In order to produce exponential fit from,
85 % data set it must be sorted. The matlab function sortrows(A) sorts the
```

```
% rows of a matrix in ascending order based on the elements in the first
% columns.

m_w5_unsorted=[m_w5_Y;m_w5_V;m_w5_M]; % making one matrix with all 5wt% data
m_w5=sortrows(m_w5_unsorted); % sorting matrix for fitting purposes
T_w5=m_w5(:,1);
p_w5=m_w5(:,2);

m_w10_unsorted=[m_w10_Y;m_w10_V;m_w10_M]; % making one matrix with all 10wt%
    data
m_w10=sortrows(m_w10_unsorted); % sorting matrix for fitting purposes
T_w10=m_w10(:,1);
p_w10=m_w10(:,2);

T_model=(272:0.1:292)'; %needs to be defined before to properly evaluate how
    well model works for w40

m_w40_unsorted=[m_w40_V;m_w40_D];% making one matrix with all 40wt% data
m_w40=sortrows(m_w40_unsorted); % sorting matrix for fitting purposes
T_w40=m_w40(:,1);
p_w40=m_w40(:,2);

exp_fit_w5=fit(T_w5,p_w5,'exp1');
exp_coeff_w5=coeffvalues(exp_fit_w5);
exp_fit_p_w5=exp_coeff_w5(1)*exp(exp_coeff_w5(2)*T_w5);
plot(T_w5,exp_fit_p_w5, '--', 'Color', 'm'); hold on

exp_fit_w10=fit(T_w10,p_w10,'exp1');
exp_coeff_w10=coeffvalues(exp_fit_w10);
exp_fit_p_w10=exp_coeff_w10(1)*exp(exp_coeff_w10(2)*T_w10);
plot(T_w10,exp_fit_p_w10, '--','Color', 'c'); hold on

exp_fit_w40=fit(T_w40,p_w40,'exp1');
exp_coeff_w40=coeffvalues(exp_fit_w40);
exp_fit_p_w40=exp_coeff_w40(1)*exp(exp_coeff_w40(2)*T_w40);
plot(T_w40,exp_fit_p_w40, '--','Color', 'r'); hold on
```

```
120
121 % % for entire range to be modeled --> not as good of a fit
122 % exp_fit_w40=fit(T_w40,p_w40,'exp1');
123 % exp_coeff_w40=coeffvalues(exp_fit_w40);
124 % exp_fit_p_w40=exp_coeff_w40(1)*exp(exp_coeff_w40(2)*T_model);
125 % plot(T_model,exp_fit_p_w40, '--','Color', 'r'); hold on
126
127 % commeted as values are not needed in this script
128
129 % [r2_w5 rmse_w5] = rsquare(p_w5,exp_fit_p_w5);
130 % [r2_w10 rmse_w10] = rsquare(p_w10,exp_fit_p_w10);
131 % [r2_w40 rmse_w40] = rsquare(p_w40,exp_fit_p_w40);
132
133 % Modelling:
134
135 % Type of function: f(x)=a*exp*(b*(x-c)). Where c is  a function of the
      concentration.
136
137 % ATTEMPT 6:
138
139 % Edit to attempt 5: b=0.271. model 6 tried to change a, but by keeping it
140 % to the a value of w40 it is closer to the a value of w5 and w10
141
142 T_model=(272:0.1:292)';% this gives a vector of 201*1 which is considered
143 % sufficeintly accurate
144 % note that there has been set a limit to the pressure range
145
146
147 a=exp_coeff_w40(1);
148 % b=exp_coeff(2); % together with exp_coeff_w40(1) creates a flat line along x
      -axis
149 % b=0.2; % random value in between w0 and w40 b. flat line
150 % b=0.25; % flat
151 b=0.271; % finally shown on graph
152
153
```

```
154 c=0; % only to get an idea of the shape
155 test_1=a*exp(b*(T_model+c));
156 plot(T_model, test_1, 'b'); hold on
157
158
159 c=-8;
160 test_2=a*exp(b*(T_model+8));
161 plot(T_model, test_2, 'g');  % eval: good modeling for w10. room for improving
        c
162
163 c=-15;
164 test_3=a*exp(b*(T_model+15))+1; % pretty good for w0. note that a d has been
       added!
165 plot(T_model, test_3, 'r');
166
167 c=-10.5;
168 test_4=a*exp(b*(T_model+10.5));
169 plot(T_model, test_4, 'c'); % eval: pretty good for w5 (10 and 11 is not
       sufficient). room for improving cs
170
171
172 c=-6;
173 test_5=a*exp(b*(T_model+6));
174 plot(T_model, test_5, 'm'); % eval: very good modelling for w40
175
176 legend('CO2','TBAB wt%=5', 'TBAB wt%=10', ....
177     'TBAB wt%=40', 'test1: c=0', 'test2: c=-8', 'test3: c=-15, d=+1', ...
178     'test4: c=-10.5', 'test5: c=-6')
179
180
181 % Evaluation of model:
182 % Making it less steep, would sacrifice accuracy of equilibrium curves wuth
183 % TBAB added.
184 % Attempt 6 is decided to be a good enough model to go further with.
185
186 % Making deltaT and x variables to be able to find a correlation
```

```
187 % DeltaT is the difference in c value for CO2 and the given TBAB
188 % concentration.
189
190
191 m_correlation=[5 10 40; 4.5 7 9]'
192
193 cons=m_correlation(:,1);
194 deltaT=m_correlation(:,2);
195
196
197 % the next step is to find a second degree polynomial fit
198 % option to plot correlation-
199
200 % figure(2)
201 % plot(x,deltaT,'k'); hold on
202 % title('')
203 % xlabel('')
204 % ylabel('')
205
206 % Built in function for polynomial fit coefficients
207
208 poly_coeff=polyfit(cons,deltaT,2) % polynomial of 2nd order
209
210 % Built in function for evaluation of polynomial fit
211
212 poly_fit_deltaT=polyval(poly_coeff, cons);
213
214 [r2_poly rmse_poly] = rsquare(deltaT,poly_fit_deltaT)
215
216 % Adding polynomial fit to plot
217
218 % plot(x,poly_fit_deltaT,'--','Color', 'b'); hold on
219 %
220 % legend('')
221
222 % Plotting CO2/ TBAB phase equilibria curves by using deltaT formula
```

```
223
224 %
225
226 % p=a*exp(b*(T-(-15+deltaT)))
227 %if w=0
228 % p=a*exp(b*(T-(-15))+1
229
230 %deltaT=poly_coeff(1)*cons^(2)+poly_coeff(2)*cons+poly_coeff(3)
231
232
233 % evaluation deltaT for the different concentrations with the made function
234 % deltaT_m1
235
236 deltaT_w5=deltaT_m1(5);
237 deltaT_w10=deltaT_m1(10);
238 deltaT_w40=deltaT_m1(40);
239
240 % defining variables to be plotted
241
242 p_w5_m7=a*exp(b*(T_model-(-15+deltaT_w5)));
243 p_w10_m7=a*exp(b*(T_model-(-15+deltaT_w10)));
244 p_w40_m7=a*exp(b*(T_model-(-15+deltaT_w40)));
245 p_w0_m7=a*exp(b*(T_model-(-15)))+1;
246
247 figure(3) % checking if modelled function is correct
248 plot(T,exp_fit_p,'k'); hold on
249
250 xlabel('T /K')
251 ylabel('p /MPa')
252 ylim([0 5])
253
254 plot(T_model, test_4, 'c'); hold on % test modelling for w5
255
256 plot(T_model, test_2, 'g'); hold on % test modelling for w10
257
258 plot(T_model, test_5, 'm'); hold on %  test modelling for w40
```

```
259
260 % testing model formula
261
262 plot(T_model, p_w5_m7, '.','Color', 'y');hold on
263
264 plot(T_model, p_w10_m7, '.','Color', 'y'); hold on
265
266 plot(T_model, p_w40_m7, '.','Color', 'y'); hold on
267
268 plot(T_model, p_w0_m7, '.','Color', 'y'); hold on
269
270
271 legend('CO2','test4', 'test2', ....
272     'test5', 'Model 1 (TBAB wt%5/10/40)')
```

model_2.m

```
1  clear all
2  close all
3  clc
4
5  % APPROACH 2, ATTEMPT 2
6
7  % The aim of approach 2, attempt 2 is to make an explicit model that is
8  % successful (approach 2, attempt 1 was not) by applying model 1.
9  % The different calculations in this script, are the same as those in the
10 % script for approach 2, attempt 1.
11
12
13 % Firstly an expression for deltaT as a function of T for a given
14 % concentration is determined. the concentration to be considered are wt %
15 % 5, 10 and 40.
16 % The equilibrium curve from model 1 will be used for these concentrations.
17 % The aim of model 2 is to improve model 1 in the sense that deltaT will be
18 % expressed explicitly.
19
20 % importing data needed
```

```
m = csvread('CO2_phase_eq.csv');

% Extracting temperature and pressure data:

T1=m(:,1);
p1=m(:,2);

% Limiting the range of the CO2 data (no discontinuities)

[idx]=find(T1>=271.622 & T1<=282.911);
T=T1(idx);
p=p1(idx);

% For modelling purposes the exponential fit of the limited range CSM CO2
% data (without discontinuities) will be considered as the CO2 equilibrium
% curve.

% Exponential fit:

% Built in function that creates exponential fit to data. Ouput: general
% model and coefficients (with 95% confidence bounds).

exp_fit=fit(T,p,'exp1')

% Extracting coefficient values:

exp_coeff=coeffvalues(exp_fit);

%Evaluating exponential function:

exp_fit_p=exp_coeff(1)*exp(exp_coeff(2)*T);

[r2 rmse] = rsquare(p,exp_fit_p);

% Plotting CO2 equilibrium curve (exponential fit) and experimental data:

```

```
figure(1)
plot(T,exp_fit_p,'k'); hold on
title('CO2/ TBAB phase equilibria exponential fits')
xlabel('T /K')
ylabel('p /MPa'); hold off

% Defining variables for other curves that need to be plotted:

T_model=(273.15:0.1:292)'; % The temperature range of the model starts
% at the triple point.


a=3.68164853199621e-35; %a=exp_coeff_w40(1);
b=0.271;

% The first step is to define T as a function of pressure instead of
% the other way around.
% this needs to be done for w0, w5, w10 and w40.

% Functions that need to be rearranged.
% p_w5=a*exp(b*(T-(15+deltaT(5)));
% p_w10=a*exp(b*(T-(15+deltaT(10)));
% p_w40=a*exp(b*(T-(15+deltaT(40)));
% and
% exp_fit_p=exp_coeff(1)*exp(exp_coeff(2)*T); % exp fit of CO2 CSM curve.
% Note that deltaT(x) was calculated before rearranging the eq.
% The rearranged functions will have the form.
% T=a*ln(b*P).

% Conversion was not done in Matlab.
% Defining variables of resulting logarithmic (natural) functions.
% A different naming system is used here to avoid confusion and overwriting
% previously defined variables

a0=7.38552;
b0=9852216748768474;
```

```
a5=3.69004;
b5=157808818229288259786113399809638 4;
a10=3.69004;
b10=3107175465839352269897335882907648;
a40=3.69004;
b40=534260896121719322672699944625766 4;

T0=a0*log(b0*p);
T5=a5*log(b5*p);
T10=a10*log(b10*p);
T40=a40*log(b40*p);

% p is taken in as the pressure range as all pressure ranges must be equal.
% p is the pressure range for the csm simulated data without
% discontinuities
% and the deltaT compared to w0 is the basis for this modelling.

%The next step is to calculate deltaT.
%deltaTx =Tx-T0. (This is the horizontal shift of p(T)). As a given element
%of Tx and T0 corresponds to the same pressure value.

deltaT5=T5-T0;
deltaT10=T10-T0;
deltaT40=T40-T0;

% The next step is to find correlation between deltaTx and T.
% deltaTx against Tx is plotted.

figure(2)
plot(T5,deltaT5,'b'); hold on
title('')
xlabel('T /K')
ylabel('\DeltaT /K')

plot(T10,deltaT10, 'g'); hold on

```

```
129 plot(T40,deltaT40, 'r'); hold on
130
131 % evaluation of figure 2: shapes are the same --> a linear fit is found.
132
133 %Built in function for polynomial fit coefficients
134
135 poly_coeff5=polyfit(T5, deltaT5, 1) % polynomial of 1st order
136
137 % Built in function for evaluation of polynomial fit
138
139 poly_fit_deltaT5=polyval(poly_coeff5,T5);
140
141 [r2_poly rmse_poly] = rsquare(deltaT5,poly_fit_deltaT5)
142
143 plot(T5,poly_fit_deltaT5, '--','Color', 'k'); hold on
144
145 poly_coeff10=polyfit(T10, deltaT10, 1)
146 poly_fit_deltaT10=polyval(poly_coeff10,T10);
147 [r2_poly rmse_poly] = rsquare(deltaT10,poly_fit_deltaT10)
148 plot(T10,poly_fit_deltaT10, '--','Color', 'k'); hold on
149
150 poly_coeff40=polyfit(T40, deltaT40, 1)
151 poly_fit_deltaT40=polyval(poly_coeff40,T40);
152 [r2_poly rmse_poly] = rsquare(deltaT40,poly_fit_deltaT40)
153 plot(T40,poly_fit_deltaT40, '--','Color', 'k'); hold on
154
155 legend ('wt% 5 \DeltaT', ' wt% 10 \DeltaT', 'wt% 40 \DeltaT', 'Linear fits')
156
157 % The next step is to obtain a correlation between deltaT(T) and cons.
158 % For now deltaT_x(T) has been defined.
159 % As all the deltaT(T) expressions are linear,
160 % a possible solution is to express deltaT(T,x) as eq x:
161 % deltaT(T,x)=a*T+b(x)
162
163 a_m2=1.0015; % a the same for all w5, w10 and w40, and is the
164 % a of the linear fits of deltaT_x(T).
```

```
165
166 % To find b, b was plotted against consentration (in excel), and a
167 % polynomial fit of second order was found. Perfect fit.
168 % Polynomial fit of b(cons):
169 % b_m2=(0.0248*(cons^2))+(-1.3724*cons)-286.33;
170
171
172 % Calculating b-values of model/ attempt:
173
174 b5_m2=(0.0248*(5^2))+(-1.3724*5)-286.33;
175 b10_m2=(0.0248*(10^2))+(-1.3724*10)-286.33;
176 b40_m2=(0.0249*(40^2))+(-1.3724*40)-286.33;
177
178 % the signs of a and b have been changed, so that the modelled shift is
179 % form CO2 phase equilibrium.
180
181 % Option to calculate r2 of deltaT(T, x)
182
183 % poly_coeff5_m2=[a_m2 b5_m2]
184 % poly_fit_deltaT5_m2=polyval(poly_coeff5_m2,T5);
185 % [r2_poly rmse_poly] = rsquare(deltaT5,poly_fit_deltaT5_m2)
186 %
187 % poly_coeff10_m2=[a_m2 poly_coeff10(2)]
188 % poly_fit_deltaT10_m2=polyval(poly_coeff10_m2,T10);
189 % [r2_poly rmse_poly] = rsquare(deltaT10,poly_fit_deltaT10_m2)
190 %
191 % poly_coeff40_m2=[a_m2 poly_coeff40(2)]
192 % poly_fit_deltaT40_m2=polyval(poly_coeff40_m2,T40);
193 % [r2_poly rmse_poly] = rsquare(deltaT40,poly_fit_deltaT40_m2)
194
195 % Plotting modelled function:
196 % (deltaT is the model)
197
198 figure(4)
199 plot(T,exp_fit_p,'k'); hold on
200 xlabel('T /K')
```

```
201 ylabel('p /MPa');
202 ylim([0 5]);
203
204
205 deltaT5_m2=a_m2*T_model+b5_m2;
206 p5_m2=exp_coeff(1)*exp(exp_coeff(2)*(T_model+deltaT5_m2));
207 plot(T_model,p5_m2,'c'); hold on
208
209 deltaT10_m2=a_m2*T_model+b10_m2;
210 p10_m2=exp_coeff(1)*exp(exp_coeff(2)*(T_model+deltaT10_m2));
211 plot(T_model,p10_m2,'m'); hold on
212
213 deltaT40_m2=a_m2*T_model+b40_m2;
214 p40_m2=exp_coeff(1)*exp(exp_coeff(2)*(T_model+deltaT40_m2));
215 plot(T_model,p40_m2,'y'); hold on
216
217 % Model 1 is plotted to check if model 2 produces the same result:
218
219 % Plot with 3 concentrations:
220
221 a_m1=3.681648531996213e-35;
222 b_m1=0.271;
223
224 % calculating deltaT for m1:
225
226 deltaT_w5=deltaT_m1(5); % Using model 1 function to calculate deltaT for m1
227 deltaT_w10=deltaT_m1(10);
228 deltaT_w40=deltaT_m1(40);
229
230 p_w5_m1=a_m1*exp(b_m1*(T_model-(-15+deltaT_w5)));
231 p_w10_m1=a_m1*exp(b_m1*(T_model-(-15+deltaT_w10)));
232 p_w40_m1=a_m1*exp(b_m1*(T_model-(-15+deltaT_w40)));
233
234
235 plot(T_model,  p_w5_m1,'--','Color', 'k');  hold on
236 plot(T_model, p_w10_m1,'--','Color', 'k'); hold on
```

```
237 plot(T_model, p_w40_m1,'--','Color', 'k'); hold on
238
239 legend ('CO2','wt% 5 (model 2)', 'wt% 10 (model 2)',...
240     'wt% 40 (model 2)', 'model 1')
241
242
243 % To make testing/ use easier a function was made.
244 % The function calculates the deltaT in model 2.
245 % The function is called deltaT_m2 and takes in a concentration and a
246 % temperature vector.
247
248 % Plotting more concentrations:
249
250 figure(3)
251 plot(T,exp_fit_p,'k'); hold on
252 xlabel('T /K')
253 ylabel('p /MPa');
254 ylim([0 5]);
255
256 deltaT_5_m2=deltaT_m2(5, T_model);
257 p_5_m2=exp_coeff(1)*exp(exp_coeff(2)*(T_model+deltaT_5_m2));
258 plot(T_model,  p_5_m2,'b');  hold on
259
260 deltaT_10_m2=deltaT_m2(10, T_model);
261 p_10_m2=exp_coeff(1)*exp(exp_coeff(2)*(T_model+deltaT_10_m2));
262 plot(T_model,  p_10_m2,'g');  hold on
263
264 deltaT_14_m2=deltaT_m2(14, T_model);
265 p_14_m2=exp_coeff(1)*exp(exp_coeff(2)*(T_model+deltaT_14_m2));
266 plot(T_model,  p_14_m2,'r');  hold on
267
268 deltaT_17_m2=deltaT_m2(17, T_model);
269 p_17_m2=exp_coeff(1)*exp(exp_coeff(2)*(T_model+deltaT_17_m2));
270 plot(T_model,  p_17_m2,'c');  hold on
271
272 deltaT_25_m2=deltaT_m2(25, T_model);
```

```
273 p_25_m2=exp_coeff(1)*exp(exp_coeff(2)*(T_model+deltaT_25_m2));
274 plot(T_model,  p_25_m2,'m');  hold on
275
276 deltaT_35_m2=deltaT_m2(35, T_model);
277 p_35_m2=exp_coeff(1)*exp(exp_coeff(2)*(T_model+deltaT_35_m2));
278 plot(T_model,  p_35_m2,'-.','Color','b');  hold on
279
280 deltaT_40_m2=deltaT_m2(40, T_model);
281 p_40_m2=exp_coeff(1)*exp(exp_coeff(2)*(T_model+deltaT_40_m2));
282 plot(T_model,  p_40_m2,'-.','Color','g');  hold on
283
284 deltaT_50_m2=deltaT_m2(50, T_model);
285 p_50_m2=exp_coeff(1)*exp(exp_coeff(2)*(T_model+deltaT_50_m2));
286 plot(T_model,  p_50_m2,'-.','Color','r');  hold on
287
288 % legend ('CO2', 'TBAB wt%=5', 'TBAB wt%=10', 'TBAB wt%=14', 'TBAB wt%=17',
      ...
289 %     'TBAB wt%=25', 'TBAB wt%=35', 'TBAB wt%=40', 'TBAB wt%=50')
290
291 % Checking model 2:
292
293 % Defining variables needed to plot model 1. Wt% 5, 10, 40 have already
294 % been defined.
295
296 % deltaT is deltaT for m1
297 deltaT_w14=deltaT_m1(14);
298 deltaT_w17=deltaT_m1(17);
299 deltaT_w25=deltaT_m1(25);
300 deltaT_w35=deltaT_m1(35);
301 deltaT_w50=deltaT_m1(50);
302
303 p_w5_m1=a_m1*exp(b_m1*(T_model-(-15+deltaT_w5)));
304 p_w10_m1=a_m1*exp(b_m1*(T_model-(-15+deltaT_w10)));
305 p_w14_m1=a_m1*exp(b_m1*(T_model-(-15+deltaT_w14)));
306 p_w17_m1=a_m1*exp(b_m1*(T_model-(-15+deltaT_w17)));
307 p_w25_m1=a_m1*exp(b_m1*(T_model-(-15+deltaT_w25)));
```

```
p_w35_m1=a_m1*exp(b_m1*(T_model-(-15+deltaT_w35)));
p_w40_m1=a_m1*exp(b_m1*(T_model-(-15+deltaT_w40)));
p_w50_m1=a_m1*exp(b_m1*(T_model-(-15+deltaT_w50)));

plot(T_model, p_w5_m1,'--','Color', 'k');  hold on
plot(T_model, p_w10_m1,'--','Color', 'k'); hold on
plot(T_model, p_w14_m1,'--','Color', 'k'); hold on
plot(T_model, p_w17_m1,'--','Color', 'k'); hold on
plot(T_model, p_w25_m1,'--','Color', 'k'); hold on
plot(T_model, p_w35_m1,'--','Color', 'k'); hold on
plot(T_model, p_w40_m1,'--','Color', 'k'); hold on
plot(T_model, p_w50_m1,'--','Color', 'k'); hold on

% The curves overlap, modelling is successful.

legend ('CO2','wt% 5 (model 2)', 'wt% 10 (model 2)', 'wt% 14 (model 2)',...
'wt% 17 (model 2)', 'wt% 19 (model 2)', 'wt% 25 (model 2)',...
    'wt% 35 (model 2)', 'wt% 40 (model 2)', 'wt% 50(model 2)', 'Model 1')
```

Appendix C

Plots

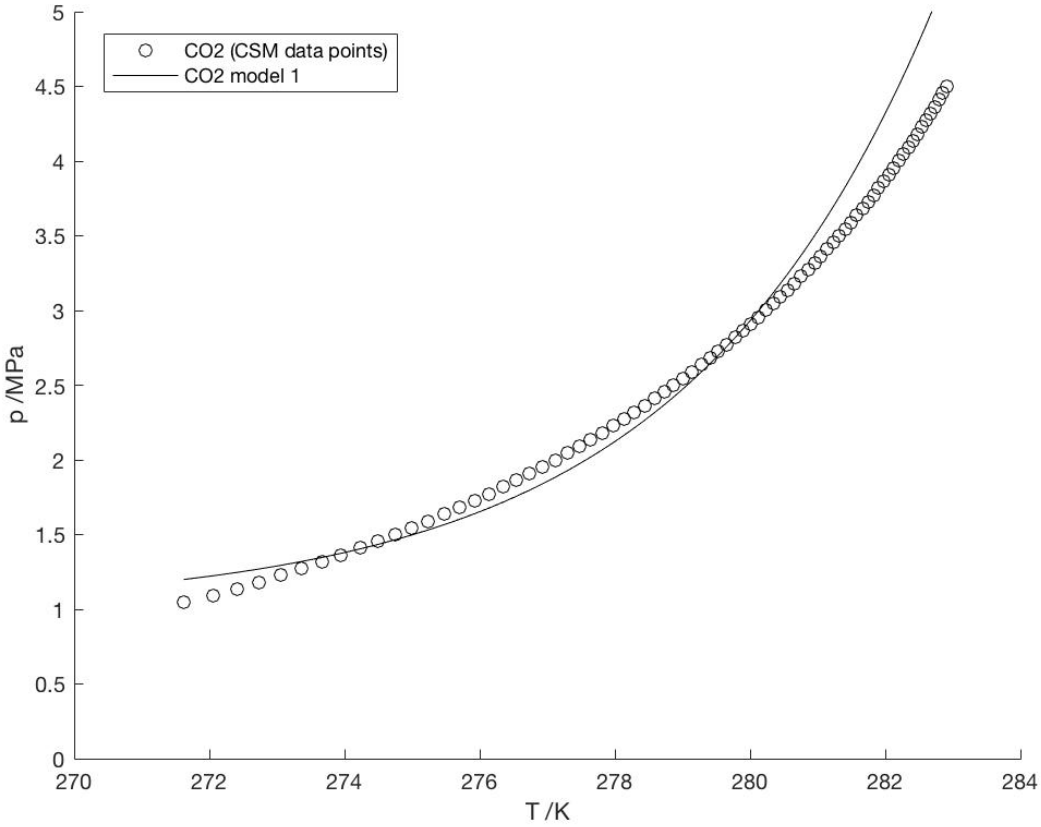

Figure C.1: CO_2/ TBAB phase equilibria. Note that Model 2 produces the same result as Model 1.

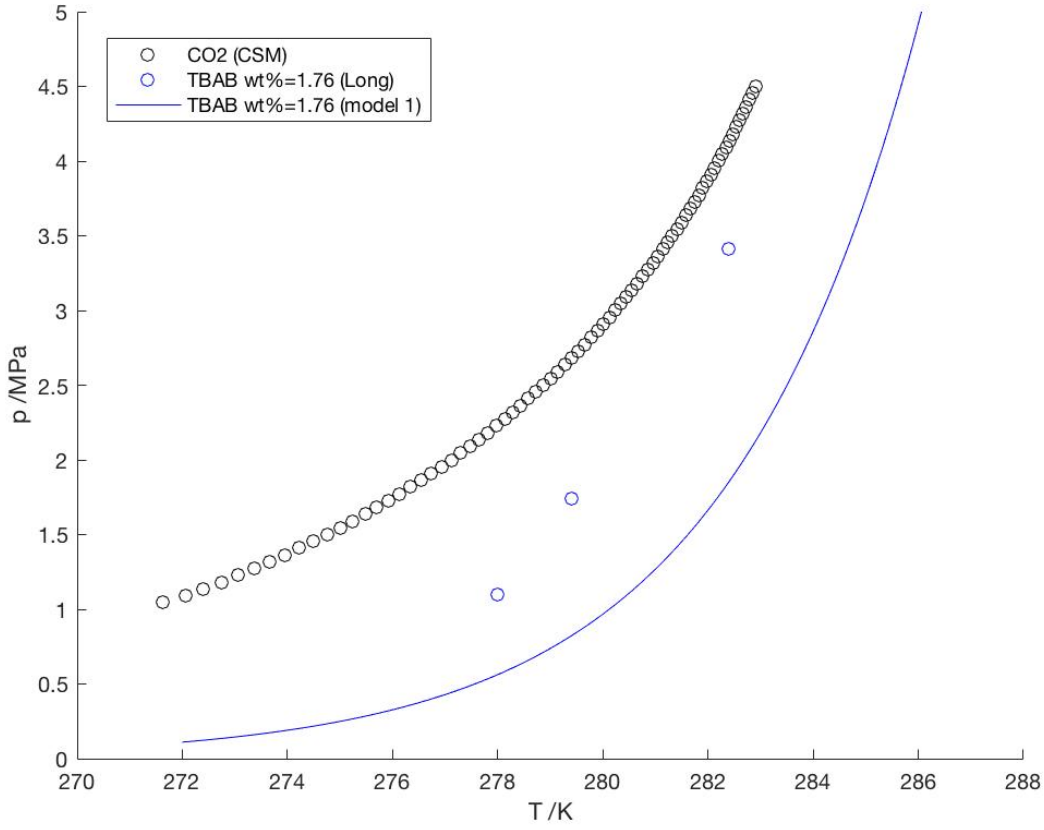

Figure C.2: CO_2/ TBAB phase equilibria. Note that Model 2 produces the same result as Model 1.

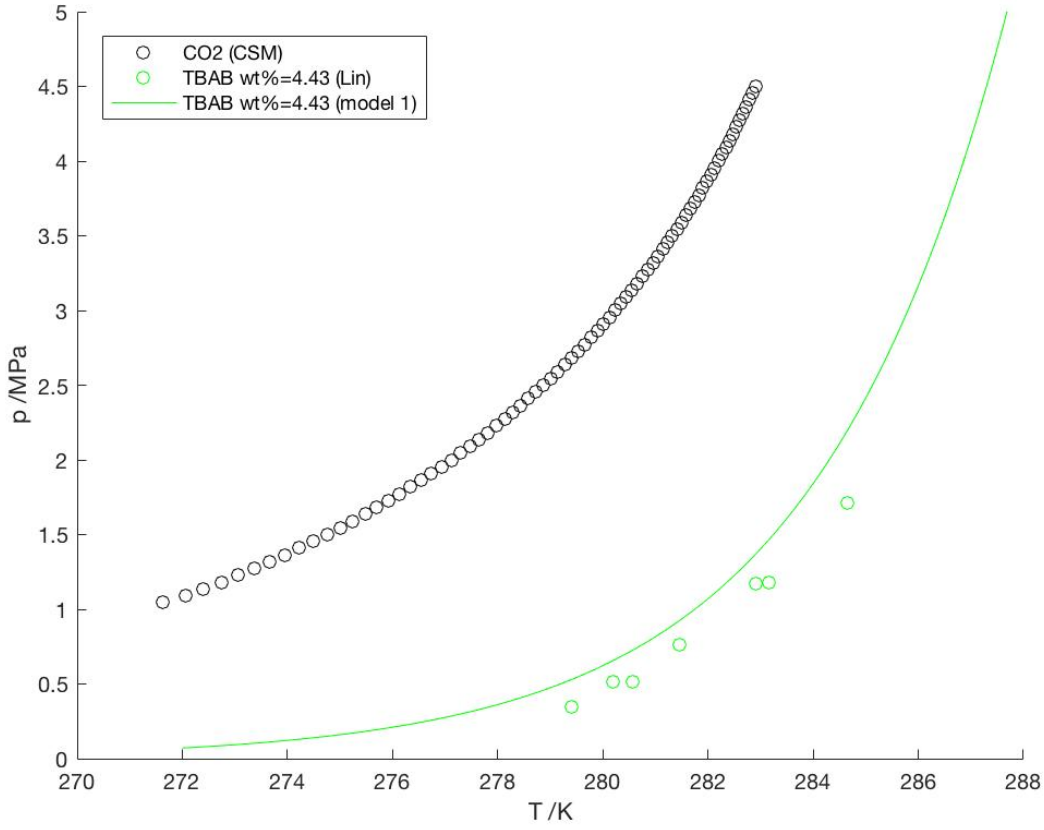

Figure C.3: CO_2/ TBAB phase equilibria. Note that Model 2 produces the same result as Model 1.

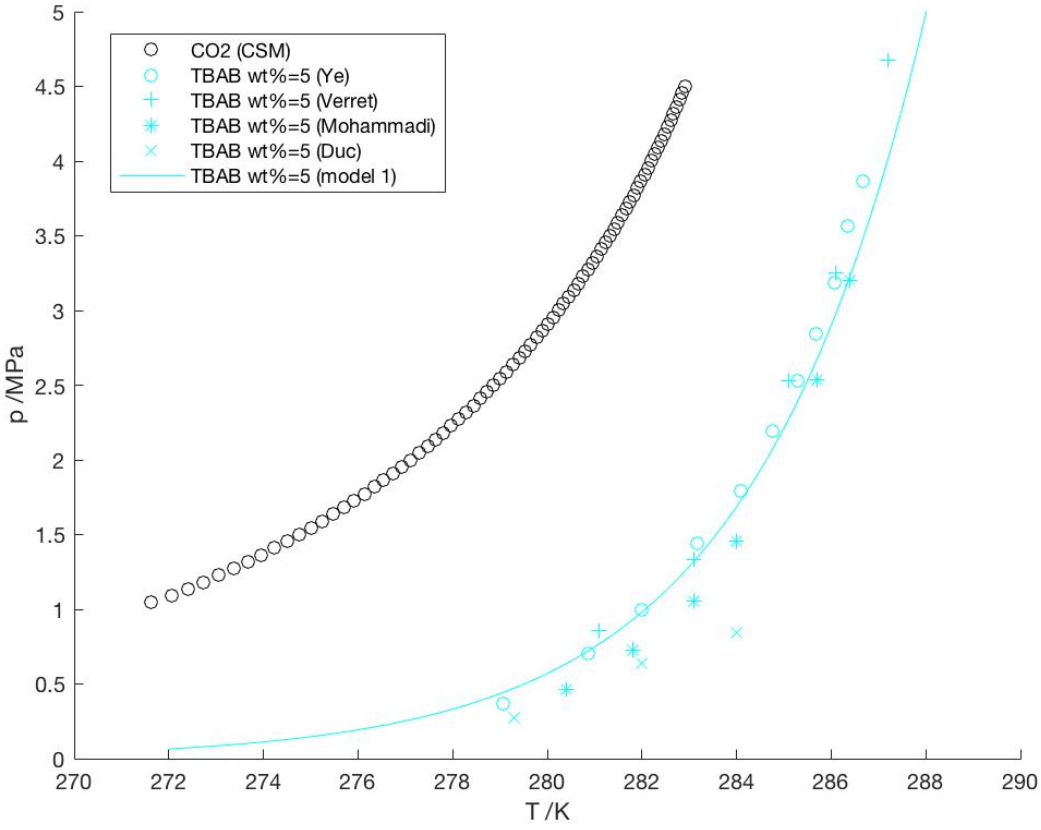

Figure C.4: CO_2/ TBAB phase equilibria. Note that Model 2 produces the same result as Model 1.

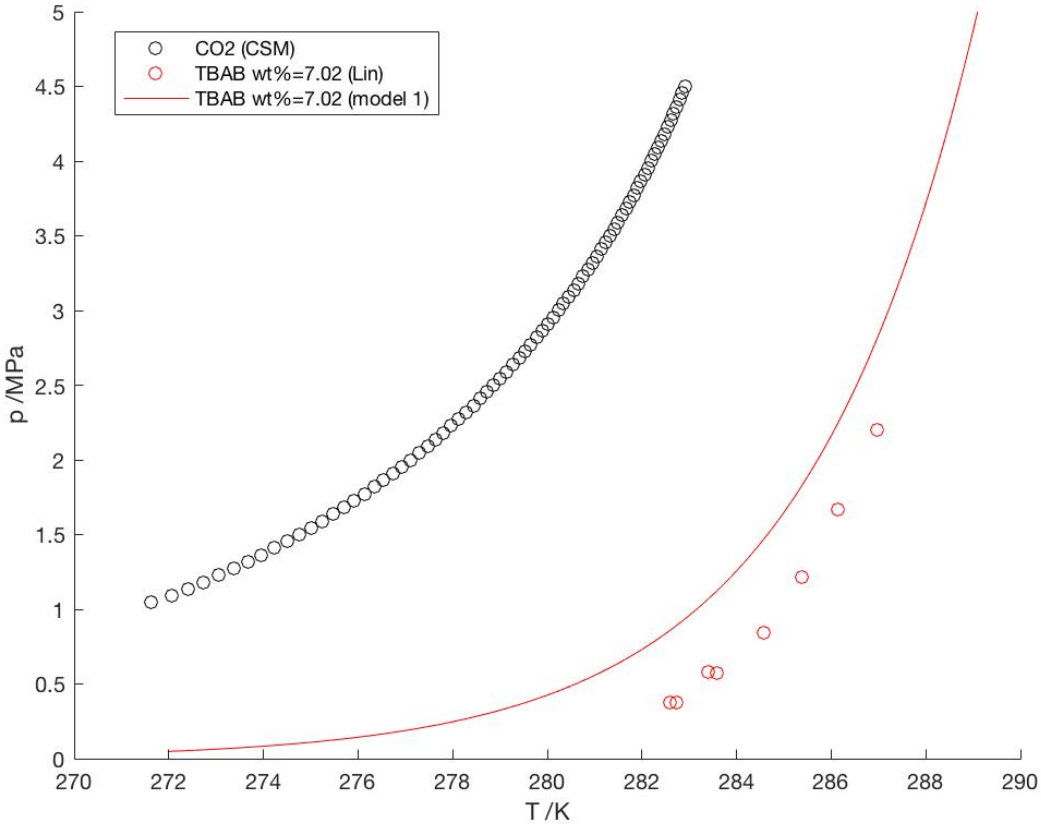

Figure C.5: CO_2/ TBAB phase equilibria. Note that Model 2 produces the same result as Model 1.

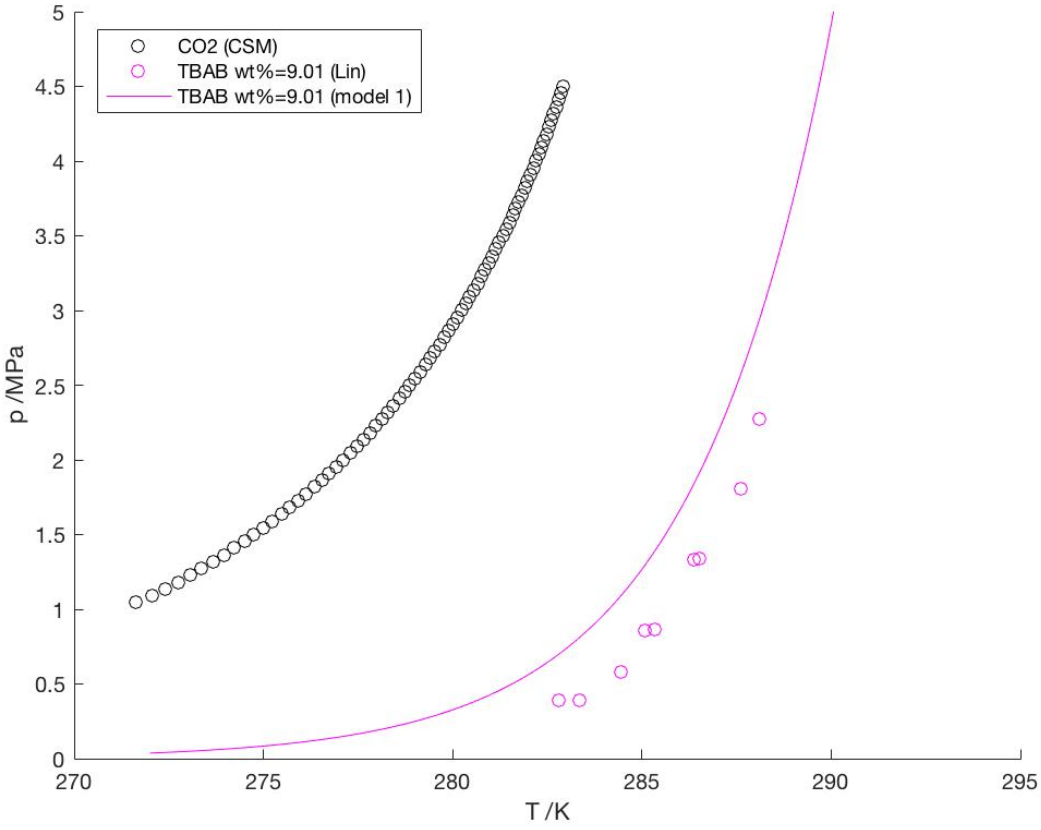

Figure C.6: CO_2/ TBAB phase equilibria. Note that Model 2 produces the same result as Model 1.

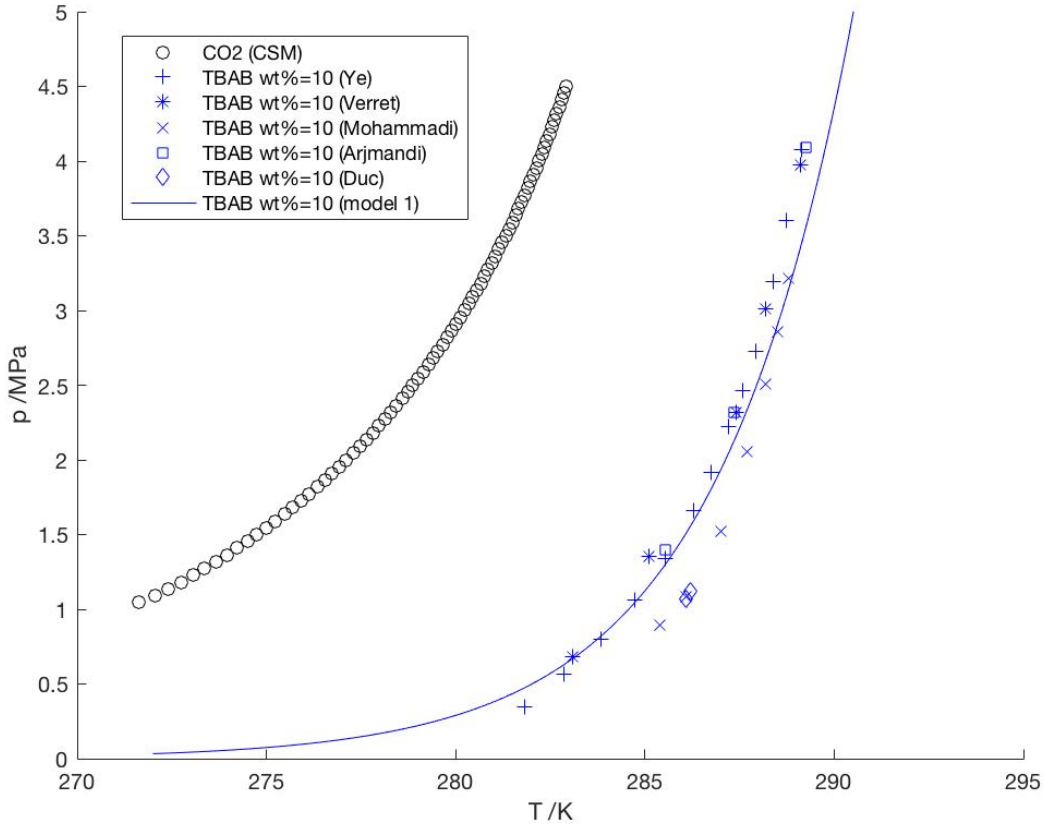

Figure C.7: CO_2/ TBAB phase equilibria. Note that Model 2 produces the same result as Model 1.

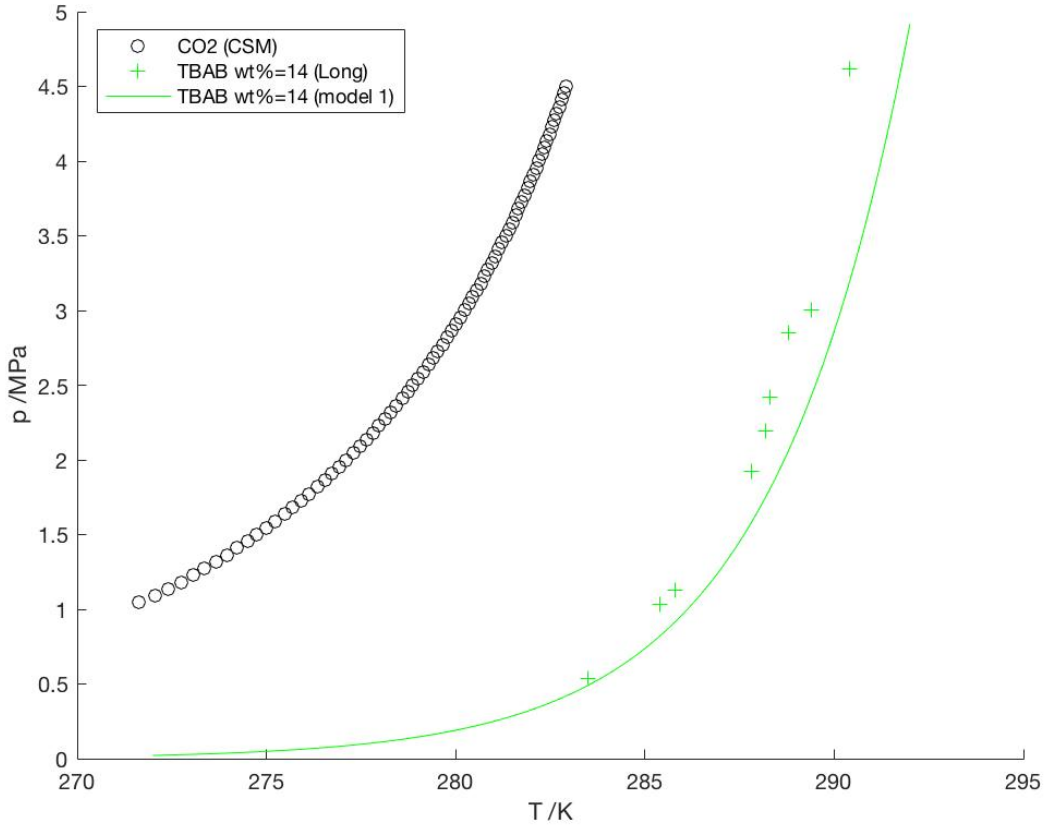

Figure C.8: CO_2/ TBAB phase equilibria. Note that Model 2 produces the same result as Model 1.

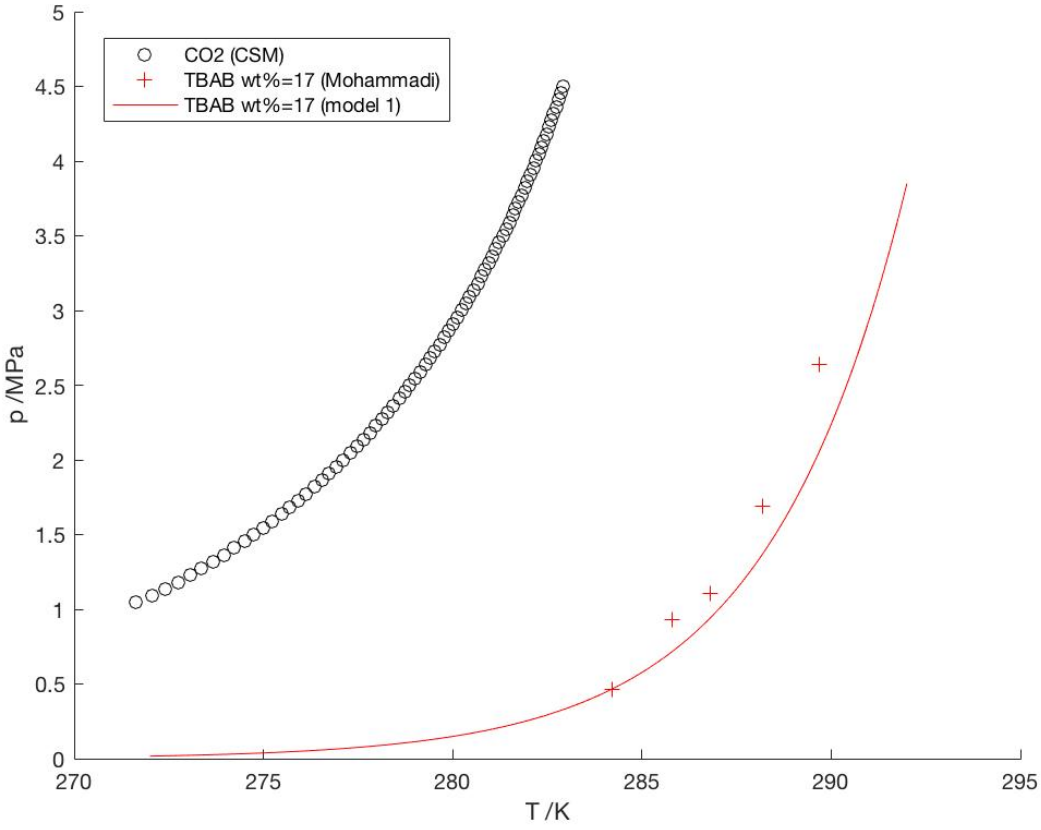

Figure C.9: CO_2/ TBAB phase equilibria. Note that Model 2 produces the same result as Model 1.

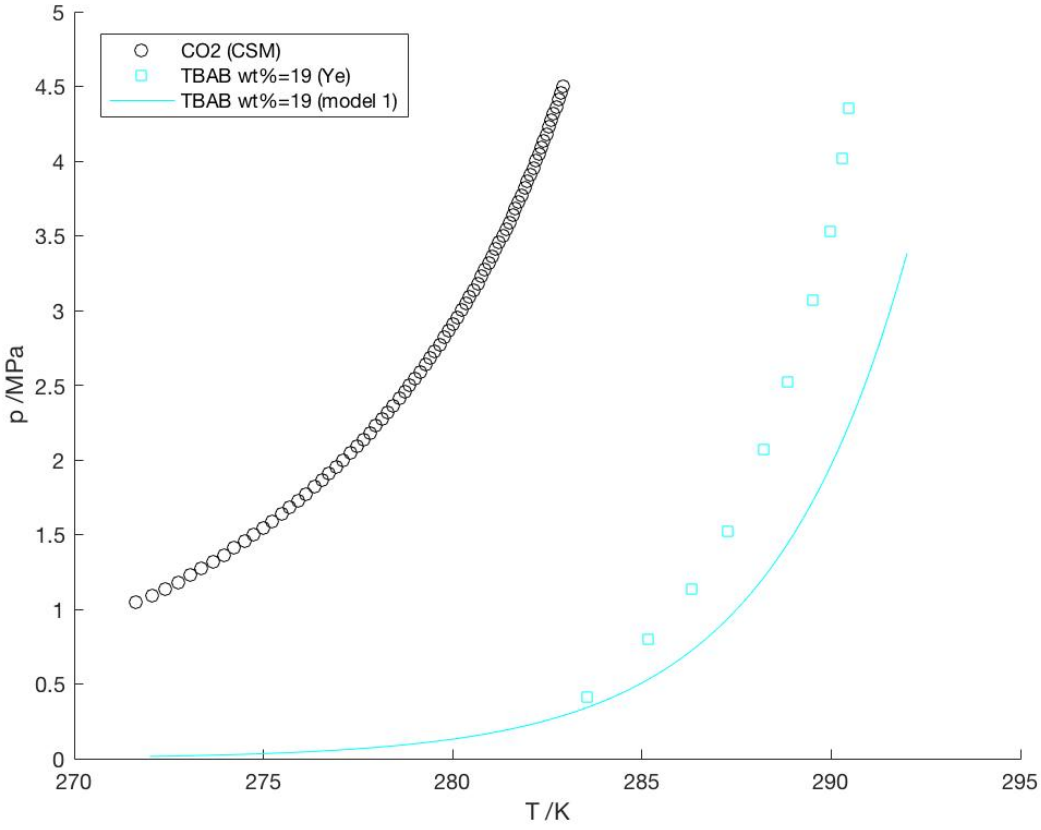

Figure C.10: CO_2/ TBAB phase equilibria. Note that Model 2 produces the same result as Model 1.

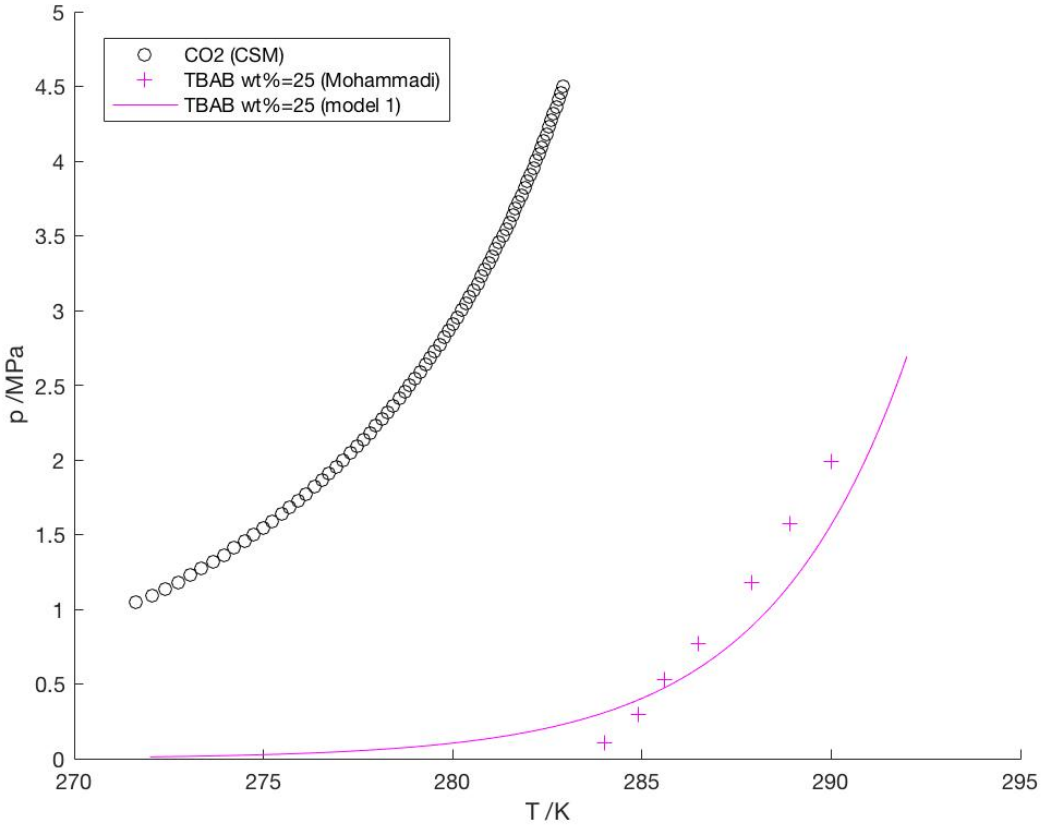

Figure C.11: CO_2/ TBAB phase equilibria. Note that Model 2 produces the same result as Model 1.

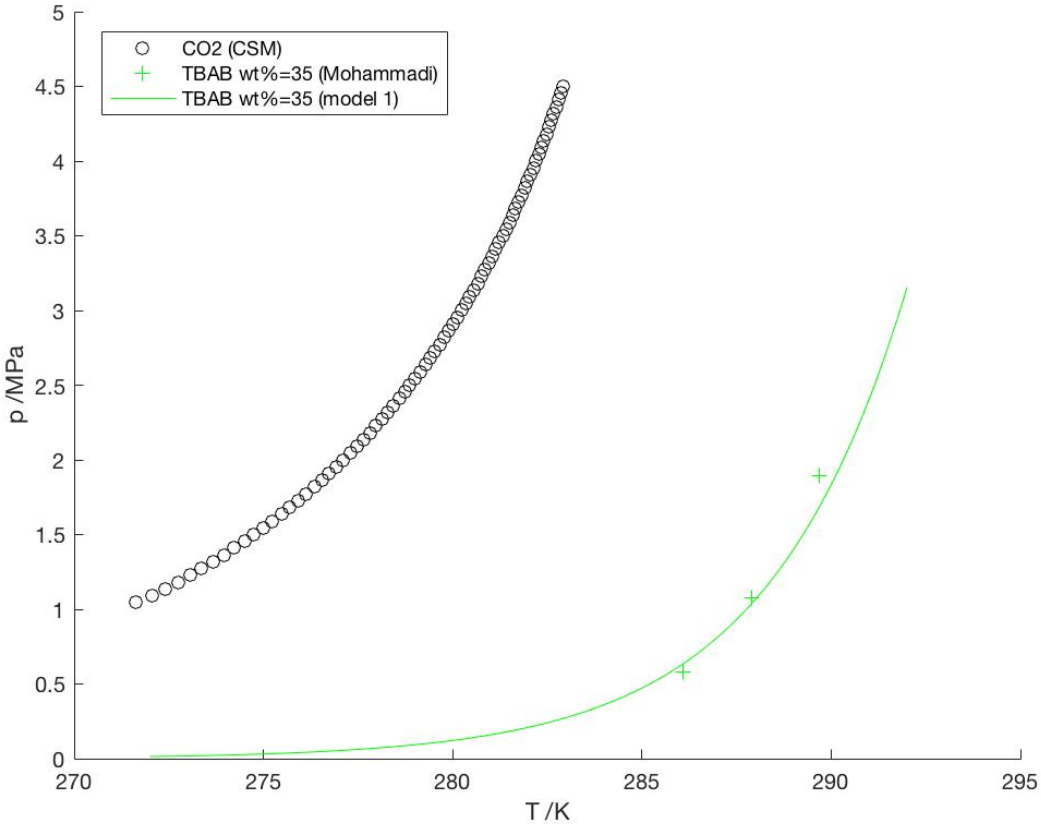

Figure C.12: CO_2/ TBAB phase equilibria. Note that Model 2 produces the same result as Model 1.

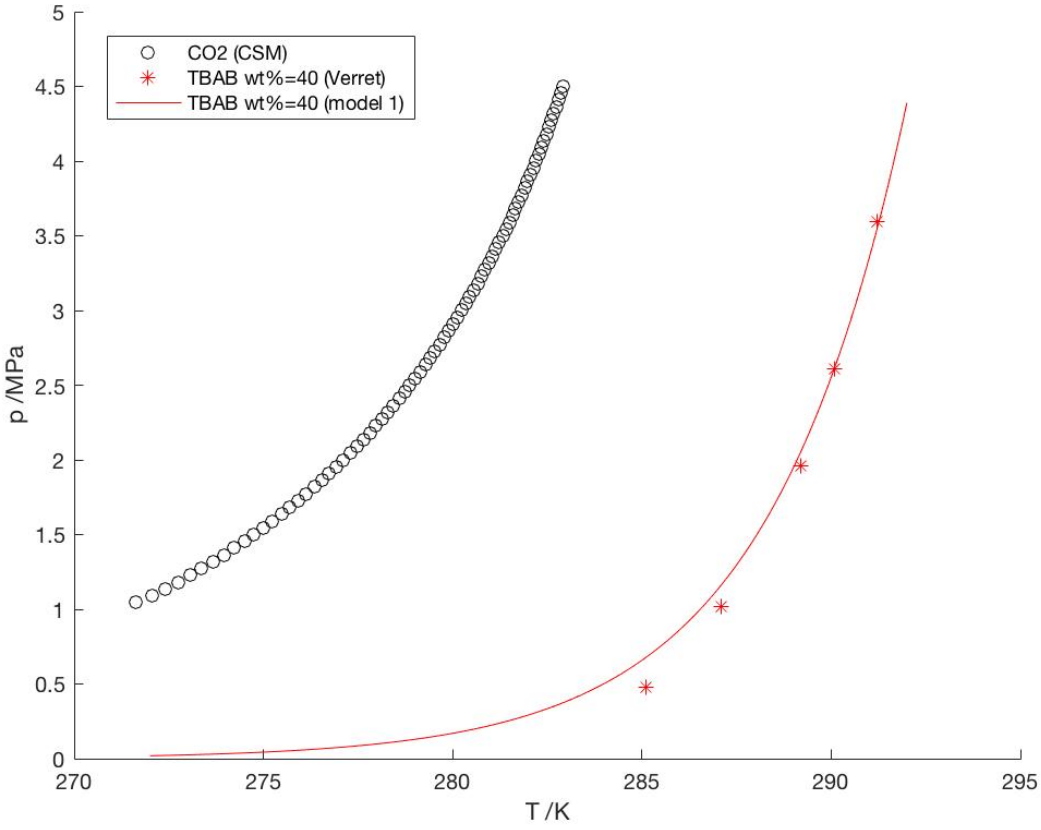

Figure C.13: CO_2/ TBAB phase equilibria. Note that Model 2 produces the same result as Model 1.

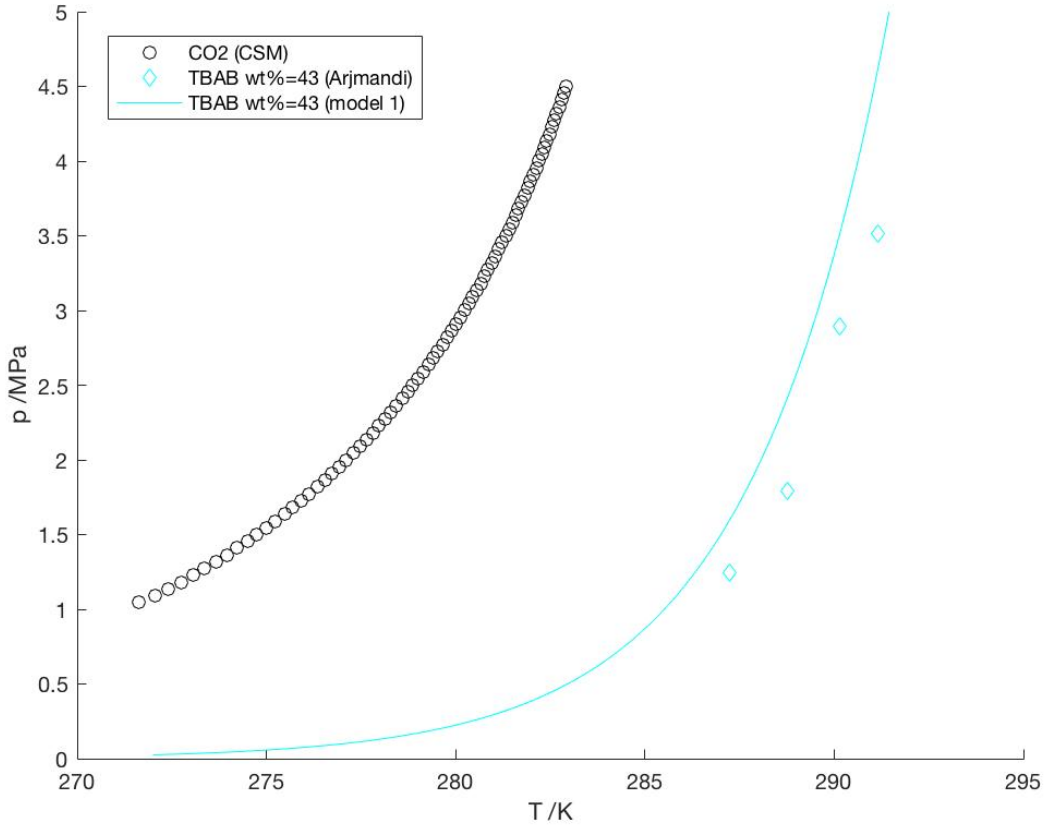

Figure C.14: CO_2/ TBAB phase equilibria. Note that Model 2 produces the same result as Model 1.

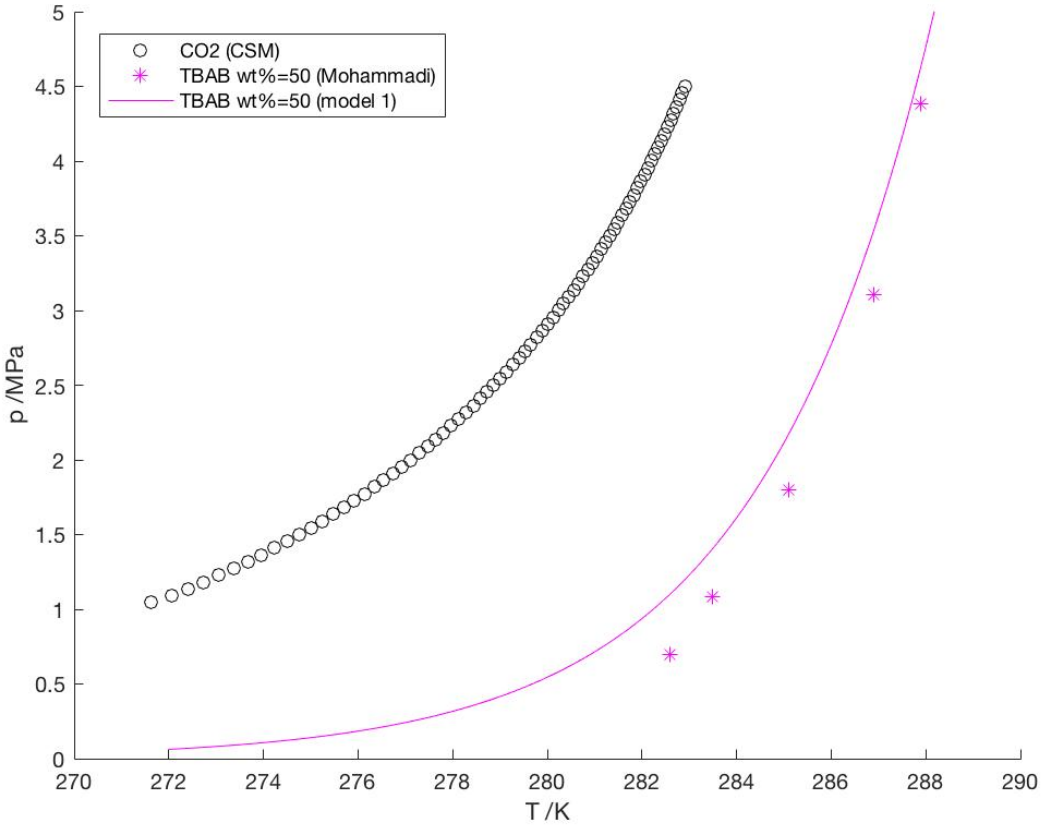

Figure C.15: CO_2/ TBAB phase equilibria. Note that Model 2 produces the same result as Model 1.

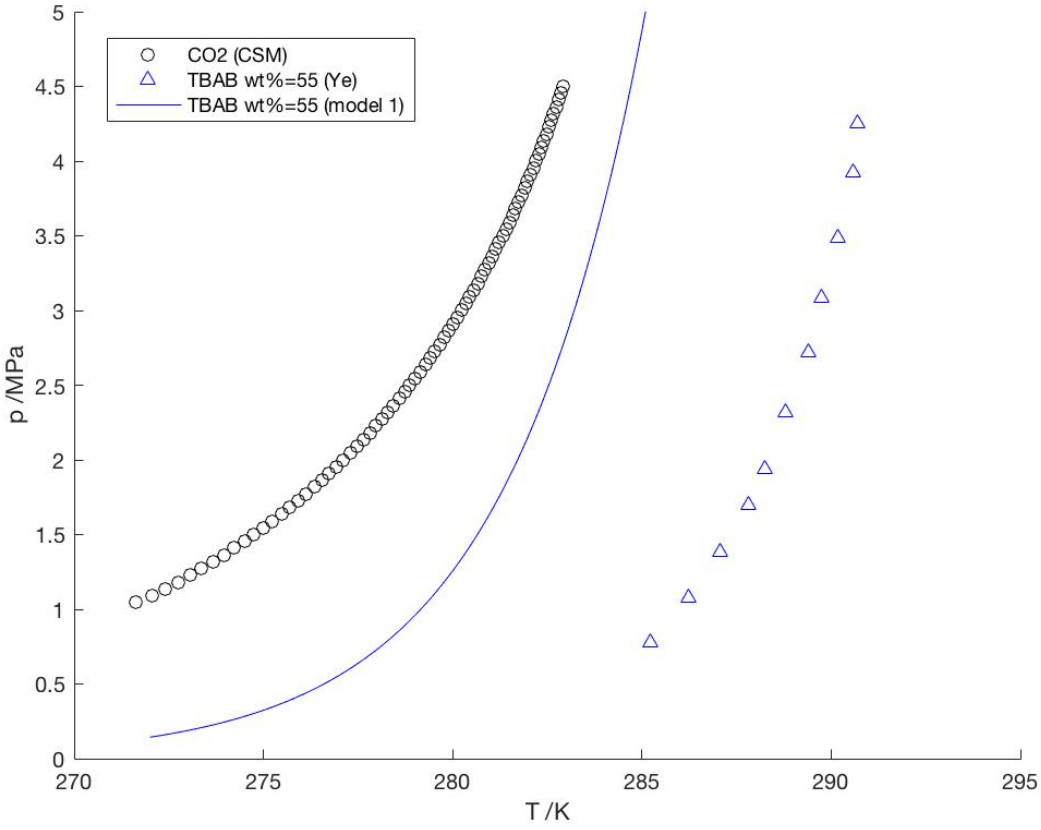

Figure C.16: CO_2/ TBAB phase equilibria. Note that Model 2 produces the same result as Model 1.

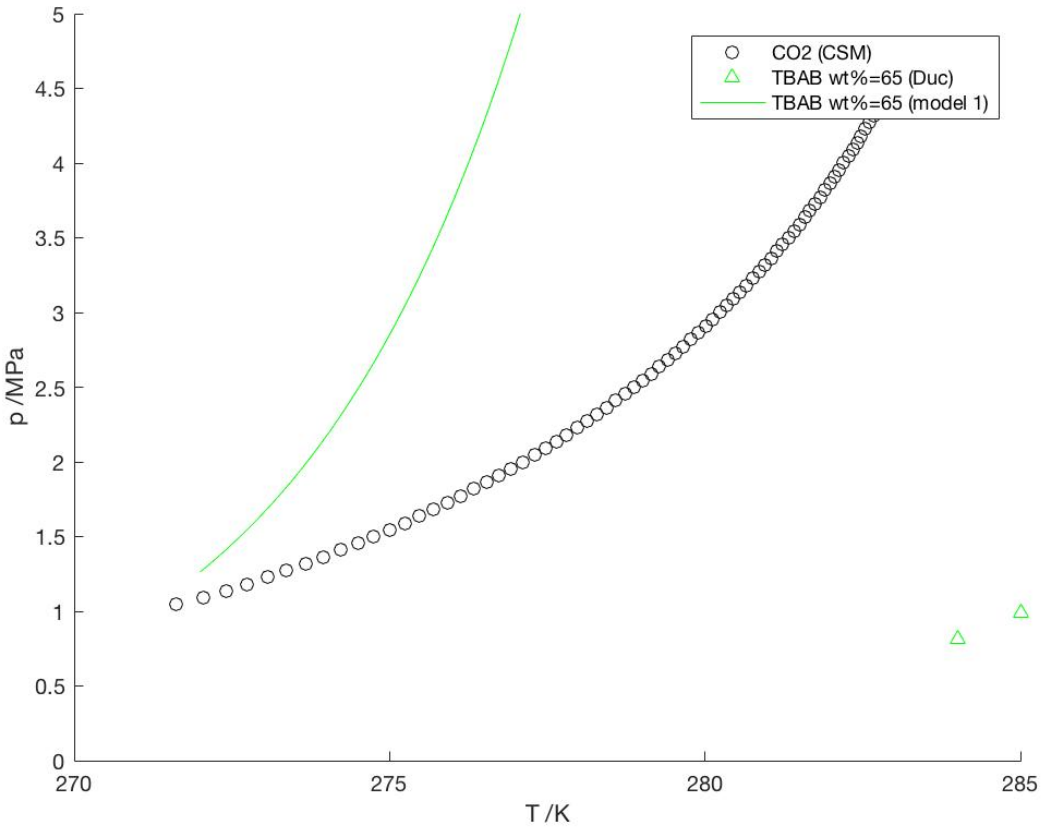

Figure C.17: CO_2/ TBAB phase equilibria. Note that Model 2 produces the same result as Model 1.

Bibliography

Adewumi, M. (2017). The hydrate problem.

Anres, S., Delaplace, T., Skivington, G., Mateen, K., Kusinski, G., et al. (2014). Deepstar 11901: Subsea low salinity injection water for increased oil recovery. In *Offshore Technology Conference*. Offshore Technology Conference.

Arjmandi, M., Chapoy, A., and Tohidi, B. (2007). Equilibrium data of hydrogen, methane, nitrogen, carbon dioxide, and natural gas in semi-clathrate hydrates of tetrabutyl ammonium bromide. *Journal of Chemical & Engineering Data*, 52(6):2153–2158.

Center for Hydrate Research CSM (2006). *User's guide for CSMGem*. Center for Hydrate Research Colorado School of Mines, version 1.00 edition.

Center for Hydrate Research CSM (2015). Software.
Retrieved from http://hydrates.mines.edu, Accessed: 2017-03-04.

Circone, S., Kirby, S. H., and Stern, L. A. (2005). Direct measurement of methane hydrate composition along the hydrate equilibrium boundary. *The Journal of Physical Chemistry B*, 109(19):9468–9475.

Corak, D. (2011). *Physicochemical evaluation of gas hydrate formation for water desalination - formation rates, hydrate amounts and heats of crystallization*. PhD thesis, University of Bergen.

Corak, D., Barth, T., Høiland, S., Skodvin, T., Larsen, R., and Skjetne, T. (2011). Effect of subcooling and amount of hydrate former on formation of cyclopentane hydrates in brine. *Desalination*, 278(1):268–274.

Dashti, H., Yew, L. Z., and Lou, X. (2015). Recent advances in gas hydrate-based co 2 capture. *Journal of Natural Gas Science and Engineering*, 23:195–207.

Dawe, R. (2003). Hydrate technology for transporting natural gas.

Deschamps, J. and Dalmazzone, D. (2009). Dissociation enthalpies and phase equilibrium for tbab semi-clathrate hydrates of n2, co2, n2+ co2 and ch4+ co2. *Journal of thermal analysis and calorimetry*, 98(1):113.

Duc, N. H., Chauvy, F., and Herri, J.-M. (2007). Co2 capture by hydrate crystallization–a potential solution for gas emission of steelmaking industry. *Energy Conversion and Management*, 48(4):1313–1322.

Garcia, M. and Clarke, M. (2014). Equilibrium conditions for tbab and tbac semiclathrates of xenon and argon. *Journal of Chemical & Engineering Data*, 59(11):3785–3790.

Gudmundsson, J. S. and Borrehaug, A. (1996). Natural gas hydrate-an alternative to liquefied natural gas? *Petroleum Review*, 50(592):232–5.

Henriet, J.-P. (1998). Gas hydrates: relevance to world margin stability and climate change. Geological Society of London.

Joshi, A., Mekala, P., and Sangwai, J. S. (2012). Modeling phase equilibria of semiclathrate hydrates of ch 4, co 2 and n 2 in aqueous solution of tetra-n-butyl ammonium bromide. *Journal of Natural Gas Chemistry*, 21(4):459–465.

Kamath, V. A. and Patil, S. L. (1994). Analogy between effect of inhibitors on hydrate equilibrium thermodynamics and hydrate decomposition kinetics. *Annals of the New York Academy of Sciences*, 715(1):463–467.

Kang, S.-P., Lee, J., and Seo, Y. (2013). Pre-combustion capture of co 2 by gas hydrate formation in silica gel pore structure. *Chemical engineering journal*, 218:126–132.

Kelland, M. (1994). Natural gas hydrates: energy for the future. *Marine pollution bulletin*, 29(6-12):307–311.

Kennett, J. P., Cannariato, K. G., Hendy, I. L., and Behl, R. J. (2003). *Methane Hydrates in Quaternary Climate Change: The Clathrate Gun Hypothesi*. Wiley Online Library.

Lachet, V. and Béhar, E. (2000). Industrial perspective on natural gas hydrates. *Oil & Gas Science and Technology*, 55(6):611–616.

Letcher, T. What are natural gas clathrate hydrates?
Retrieved from http://www.globalspec.com, Accessed: 10.10.16.

Li, S., Fan, S., Wang, J., Lang, X., and Wang, Y. (2010). Semiclathrate hydrate phase equilibria for co2 in the presence of tetra-n-butyl ammonium halide (bromide, chloride, or fluoride). *Journal of Chemical & Engineering Data*, 55(9):3212–3215.

Lin, W., Delahaye, A., and Fournaison, L. (2008). Phase equilibrium and dissociation enthalpy for semi-clathrate hydrate of co 2+ tbab. *Fluid Phase Equilibria*, 264(1):220–227.

Long, X., Wang, Y., Lang, X., Fan, S., and Chen, J. (2016). Hydrate equilibrium measurements for ch4, co2, and ch4+ co2 in the presence of tetra-n-butyl ammonium bromide. *Journal of Chemical & Engineering Data*, 61(11):3897–3901.

Mohammadi, A. H., Eslamimanesh, A., Belandria, V., and Richon, D. (2011). Phase equilibria of semiclathrate hydrates of co2, n2, ch4, or h2+ tetra-n-butylammonium bromide aqueous solution. *Journal of Chemical & Engineering Data*, 56(10):3855–3865.

Park, K.-n., Hong, S. Y., Lee, J. W., Kang, K. C., Lee, Y. C., Ha, M.-G., and Lee, J. D. (2011). A new apparatus for seawater desalination by gas hydrate process and removal characteristics of dissolved minerals (na+, mg 2+, ca 2+, k+, b 3+). *Desalination*, 274(1):91–96.

Petrowiki (2015a). Equations of state.
Retrieved from http://petrowiki.org, Accessed: 2017-05-03.

Petrowiki (2015b). Predicting hydrate formation.
Retrieved from http://petrowiki.org, Accessed: 2017-05-02.

PubChem (2005). Tetrabutylammonium bromide.
Retrieved from https://pubchem.ncbi.nlm.nih.gov, Accessed: 2017-04-28.

Qi, Y., Wu, W., Liu, Y., Xie, Y., and Chen, X. (2012). The influence of nacl ions on hydrate structure and thermodynamic equilibrium conditions of gas hydrates. *Fluid Phase Equilibria*, 325:6–10.

Roozeboom, H. (1884). Sur l'hydrate de l'acide sulfureux. *Recueil des Travaux Chimiques des Pays-Bas*, 3(2):29–58.

Roozeboom, H. (1885). Sur la dissociation des hydrates de l'acide sulfureux, du chlore et du brome. *Recueil des Travaux Chimiques des Pays-Bas*, 4(2):65–73.

Sigma-Aldrich. Tetrabutyalmmonium bromide.
Retrieved from http://www.sigmaaldrich.com, Accessed: 2017-05-15.

Sloan, E. and Koh, C. (2008). *Clathrate Hydrates of Natural Gases Third Edition*, volume 119. MARCEL DEKKER AG.

Sun, S. (2009). Dynamics research on natural gas storage and transportation by gas hydrates. In *Power and Energy Engineering Conference, 2009. APPEEC 2009. Asia-Pacific*, pages 1–4. IEEE.

Tretyakov, K. Clathrate desalination technology.

Undall, L. (2016). Desalination utilizing clathrate hydrates.

Verrett, J., Renault-Crispo, J.-S., and Servio, P. (2015). Phase equilibria, solubility and modeling study of co 2/ch 4+ tetra-n-butylammonium bromide aqueous semi-clathrate systems. *Fluid Phase Equilibria*, 388:160–168.

Wells, J. (2012). R-square: The coefficient of determination.
Version 1.4, Retrieved from https://se.mathworks.com, Accessed: 2017-06-01.

Ye, N. and Zhang, P. (2012). Equilibrium data and morphology of tetra-n-butyl ammonium bromide semiclathrate hydrate with carbon dioxide. *Journal of Chemical & Engineering Data*, 57(5):1557–1562.